Doctoral School of Chemical Engineering and Material Sciences
University of Pannonia

DOI:10.18136/PE.2019.729

MODIFICATION AND CHARACTERIZATION OF ADSORBENT MATERIALS AND CNTS FOR OIL SPILL CLEANUP FROM WATER

Written by

Nour Abdullah Ameen Aljammal

Supervisor

Dr. Juzsakova Tatjána, Associate professor

Submitted in partial fulfilment of the requirements for the degree of
Doctoral School of Chemical Engineering and Material Sciences

Veszprém, Hungary
2019

Modification and Characterization of Adsorbent Materials and CNTs for Oil Spill Cleanup from Water

Thesis for obtaining a Ph.D. degree in
The Doctoral School of Chemical Engineering and Material Sciences of the University of Pannonia.
Institute of Environmental Engineering

Prepared by: Nour Abdullah Ameen Aljammal

Supervisor: Dr. Juzsakova Tatjána, Associate professor

Propose acceptance (yes / no)

....
Associate prof. Dr. Juzsakova Tatjána

The candidate has achieved .... % in the comprehensive exam, Veszprém

....
Dr.
(Chairman of the Examination Committee)

As a reviewer, I propose acceptance of the thesis:

Name of reviewer: .... yes / no ....
(Signature)

Name of reviewer: .... yes / no ....
(Signature)

The candidate has achieved........... % at the public discussion

....
(President of UCDH)

Veszprém, 2019. ....

Modification and characterization of adsorbent materials and CNTs for oil spill cleanup from water

by
Nour Abdullah Ameen Aljammal

Supervisor:
Associate prof. Dr. Juzsakova Tatjána

Abstract

In this dissertation, two methods were implemented for expanding the environmental applications of two unique materials; namely the Jordanian zeolitic tuff (RZT) and multiwalled carbon nanotubes (MWCNTs). From their discovery until today, these materials have been widely investigated for several applications. While much work has been devoted to investigating the scope of their possible applications as adsorbents, enhancing their properties to be tailored to specific purposes, as oil adsorbents for oil spills remediation are still needed for the full potential of this class of materials.

The acquired knowledge of these materials and their characteristics have been essential for their application as adsorbents. The application of solid adsorbents for oil spills remediation has gained attention in recent times. This is due to the potential of this technology to minimize the danger of surface water spill or subsurface leakage of petroleum/petroleum derivatives. However, this requires the development of novel solid adsorbent materials with significant selectivity, large adsorption capacity, and fast adsorption coupled with excellent mechanical strength and the ability of regeneration.

This work aimed to develop advanced oil adsorbents for the removal of hydrocarbons from surface water. Chemical modifications of RZT and MWCNTs are manifested either in the backbone composing the underlying structure or in the functionalities exposed to the pore space and outer surface of the raw materials. Both approaches, microemulsification of MWCNTs and dealumination of RZT, are investigated in this dissertation. As the hydrophobic properties are the primary determinants of effective oil adsorbents, the hydrophobicity of RZT was modified via dealumination by single acidic treatment (TZT). Thus, the acid treatments markedly changed the composition and surface area of RZT so that the intrinsic properties of the RZT microporous structure come into effect. Further treatment of the dealuminated zeolitic tuff was achieved by microemulsion technique (μETZT). The microemulsion method was implemented to modify the surface structure of MWCNTs by attaching a hydrocarbon tail on its surface. Activated carbon was used as benchmark adsorbent for performance comparison.

The structural and surface chemistry properties of the prepared adsorbents were studied by different surface analytical techniques such as Brunauer-Emmett-Teller (BET) method, thermogravimetric analysis (TG), X-Ray diffraction (XRD), Raman-spectroscopy, microstructure and morphology using scanning electron microscopy (SEM), thermogravimetric analysis (TG) and Fourier-transform infrared spectroscopy (FTIR). The hydrocarbon removal efficiencies of the unmodified and functionalized sorbents were examined by using total organic carbon analyzer (TOC), gas chromatography (GC), and UV-Visible spectroscopy (UV-Vis) techniques. Different model hydrocarbon compounds were used for this investigation.

The experimental results revealed that microemulsion as a type of surface functionalization solved one main issue regarding MWCNTs functionalization as it proved to be beneficial for producing hydrophobic adsorbent with keeping the high crystallinity and uniformity of MWCNTs surface and without the need of additional functionalization and substitution steps to attach hydrocarbon side chains. Using kerosene as a hydrocarbon model compound, compared with raw MWCNTs, the maximum adsorption capacity of µMWCNTs increased by 63.5%. The adsorption capacity over zeolite-based adsorbents, enhanced by three- and four-fold for TZT and µETZT, respectively. Additionally, the outcomes indicated that the octane adsorption capacities of µETZT and µEMWCNTs reached up to 1.73 g/g and 6.07 g/g, respectively.

The kinetics experiments indicated that the capacities of µEMWCNTs, TZT, µETZT for the uptake of hydrocarbon increased when the sorption time increased. Pseudo-first order, pseudo-second-order, and intraparticle diffusion were examined for kinetic studies of toluene adsorption over the synthesized adsorbents. It was concluded that the kinetic data could be well described by the pseudo-second-order model with a high correlation coefficient.

Table of Contents

List of Tables

List of Figures

List of Abbreviations

List of Symbols

C	Intraparticle diffusion constant	g/g
C_o	Concentrations of adsorbate at the initial time	mg/l
C_t	Concentrations of adsorbate at time t	mg/l
C_f	Concentrations of adsorbate at final time t	mg/l
D_{av}	Average pore diameter	nm
k_1	Adsorption rate constant of the first-order model	1/min
k_2	Rate constant of second-order model	g/g. min
k_p	Intraparticle diffusion rate constant	g/g.min$^{0.5}$
M_o	The weight of the sorbent	g
M_p	Mass of adsorbed hydrocarbon	g
R^2	The values of the residual standard error	-
RE	Removal efficiency	%
q_e	Equilibrium Adsorption capacity	g/g
q_t	Adsorption capacity at time t	g/g
$S_{1.7\text{-}300}$	Pore volume having a diameter between 1.7 and 300 nm	cm^3/g
S_{BET}	Specific surface area	m^2/g
S_{BJH}	Surface area for pores	m^2/g
S_{micro}	The specific surface area of micropores (< 2 nm)	m^2/g
V_{micro}	Volume respectively of micropores (< 2 nm)	cm^3/g
λ	Absorbance wavelength	nm

List of abbreviations and acronyms

µEMWCNTs	Microemulsified multi-walled carbon nanotubes
µETZT	Microemulsified zeolitic tuff
BET	Brunauer-Emmett-Teller surface area determination method
BJH	Barret–Joyner–Halenda pore size distribution determination method
BTEX	Benzene, toluene, ethylbenzene and xylene
DTA	Differential thermal analysis
EDX	Energy Dispersive x-ray elemental analysis
FT-IR	Fourier transform Infrared Spectrometry
ITOPF	International Tanker Owners Pollution Federation Limited
IZA	International Zeolite Association
MWCNTs	Multi-walled carbon nanotubes
PTFE	Poly(tetrafluoroethylene)
RBM	Radial breathing mode

RE	Removal Efficiency
RZT	Raw zeolitic tuff
S	Sorption
SAS	Secondary-alkane-sulfonate
SEM	Scanning Electron Microscopy
SLES	Sodium-lauryl-ether-sulfate
TDS	Total dissolved solids
TGA	Thermogravimetric analysis
TOC	Total Organic Carbon
TZT	Treated zeolitic tuff
V	Volume
W	Mass of adsorbent
XRF	X-ray diffraction

Statement of Original Authorship

The work contained in this thesis has not been previously submitted to meet requirements for an award at this or any other higher education institution. To the best of my knowledge and belief, the thesis contains no material previously published or written by another person except where due reference is made.

Signature: __________________________

Date: __________________________

Acknowledgments

And for the pleasant task of acknowledging those who assisted in this thesis. No work such as this can be contemplated without the promise of advice and assistance from one's friends and colleagues, and I must first express my very deep sense of gratitude to my supervisor Dr. Juzsakova Tatjána and to Prof. Rédey Ákos, who more than anyone else has been responsible for this thesis coming to completion. This work owes much to Prof. Rédey Ákos, the moment we first talked about it in 2016, he seemed to have guessed my whole purpose, and ever since, he has never ceased to help its pursuit. I am most grateful for their unfailing support and help in a variety of ways.

I am also indebted to a number of my friends who have supported me all over the way. Dr. Balázs Zsirka and Dr. Viktor Sebestyén deserve special thanks for their extensive pieces of advice. One of the most pleasing aspects of my work has been the speed with which colleagues worldwide, some of whom I have never met, have promptly supported me, Prof. Igor Cretescu.

I acknowledge the financial support of this work through GINOP-2.3.2-15-2016-00016 project: Excellence of strategic R&D workshops: Development of modular, mobile water treatment systems and wastewater treatment technologies based on the University of Pannonia to enhance growing dynamic export of Hungary.

Finally, I want to express my appreciation for one person who unhesitatingly shared with me the details of this journey and sustained year after year the stresses radiating from me as the center of this activity, my Father. I also wish to thank my family for their patience during the trying ordeal of thesis preparation, a word of apology for the many occasions on which I was forced to neglect them while working on this thesis.

Chapter 1: Introduction

This chapter outlines the background of oil spills and their remediation technique in section 1.1. The context and purposes of this research are elaborated in section 1.2. Section 1.3describes the significance and scope of this research and provides definitions of terms used.

1.1 BACKGROUND

Oil spillage has always been seen as ubiquitous and central in several areas of the conventional and contemporary environment's scientific interest. The world witnessed several oil spills accidents, which resulted in massive contamination of the water bodies including the oceans, seas, lakes, and rivers (Aguilera et al., 2010; Chang et al., 2014; Peterson et al., 2003; Toyoda and Inagaki, 2000).

Oil spills are considered serious environmental catastrophes since they result in both immediate and long-term ecological and environmental damages (Peterson et al., 2003; Toyoda and Inagaki, 2000). Moreover, oil contamination of the soils and geological layers threaten the underground water reservoirs. Since the oil products contain toxic/phytotoxic compounds, in particular, aromatic hydrocarbons, heteroatom-containing compounds and occasionally heavy metals such as, e.g., arsenic, the contamination of the waters exhibit high risks for the healthy and safe water supply (Ahmaruzzaman, 2011; Annunciado et al., 2005). As a consequence of the massive oil spill of about 210 million gallons in the Gulf of Mexico on 22nd April 2010 caused by the explosion at the Deep-water Horizon oil rig, both the accidental and deliberate releases of oil during production, transportation, and storage became a worldwide concern.

Different types of oils and petroleum fractions exhibit different properties; therefore, the environment and ecosystems are influenced in several ways (Liu and Kujawinski, 2015). The light oils and light petroleum fractions present major hazards as those can ignite or explode. Moreover, many light petroleum fractions, such as gasoline, kerosene, and diesel, are considered to have toxic potential, as well. The light petroleum fractions can kill animals or plants after contact, and they are dangerous to human beings who breathe their vapours. The destructive effects of spilled oil on ecosystems and the long-term influence of environmental pollution alert for urgent solutions to improve the existed technologies for oil pollution cleanup.

Due to the recent increase in oil contamination of water, the repercussions of oil exposure on the environment have become an environmental concern. Thus, the treatment of oil-contaminated water is of top priority for many organizations (EPA, 2018, 2015; WHO, 2008). One of the most challenging decisions that oil spill responders face during a spill is evaluating the trade-offs accompanying with choosing the most appropriate remediation technique. Therefore, the type of spilled oil along with the propagation speed of the oil on the water surface influenced by water temperature, and weathering processes such as; atmospheric temperature, wind, and flow directions are very significant aspects of guiding the companies and authorities to decide on the pre-eminent remediation techniques. For example, burning as a remediation technique can be used for the spilled oil with a high percentage of volatile compounds, while this method must be avoided if the spilled liquid is heavy oil, which burns poorly.

On one hand, every effort should be made to prevent spilled oil from spreading, as removing oil from sand, rocks, and vegetation is difficult and costly. However, if it happened, then a combination of several remediation techniques must be used as a first-class and second-class intervention. Regardless of the effectiveness of the modern technologies used as a practical approach for petrochemical wastewater treatment (Guodong et al., 2015; Sepehri and Sarrafzadeh, 2018), the researchers keep looking for an efficient, environmentally friendly and cost-effective technology for oil spill remediation over large areas such as adsorption.

In some cases, primary remediation technique such as manual removal via shovels and rakes can be used to remove the majority of heavy oil spilled or bituminous cuts as main remediation technique as this method has the advantage of minimizing waste generation but is labour intensive and relatively slow; thus, additional remediation technique is needed, as adsorption. It is, however, not always easy to decide what is the best combination for efficient spill removal. Nevertheless, it is believed that adsorption can play a vital part in the remedial-actions combination. Adsorption can be used as (i) primary oil recovery for very small and limited oil spills in sea and spills from tankers. Or (ii) as an integrated technique for another remediation process in which the sorbent can be used to clean up the final traces of oil spills on water surfaces or land (Fingas, 2016). Several factors influence the selection of appropriate adsorbents such as availability, cost, safe use, and regeneration of the adsorbent materials. Many other parameters governed by the structure of the adsorbents play a vital role in the cleaning process such as hydrophobicity (oleophilic properties), porosity, suitable pore size, and surface area. Adsorbents with the high surface area have proved to be highly efficient and versatile materials for oil removal from the water surface. Nonetheless, a small number of materials meet all these requirements for selectivity, adsorption capacity, adsorption rate, and recyclation.

1.2 CONTEXT AND PURPOSES

Adsorption is believed to be a simple, cheap, and effective technique for the removal of hydrocarbons from emulsified water. However, the synthesis of adsorbents with superior oil sorption performance remains a great challenge. Moreover and as mentioned earlier that despite the many exciting and compelling recent developments on CNTs and clay minerals applications as adsorbents, sorption on a large scale is still in an immature phase. There is already a very considerable literature on the application of adsorbents for hydrocarbons removal from oil-contaminated water, and no doubt, its growth is set to continue. Hence, the novelty of this study arises from the possible enhancement of hydrophobic properties for natural zeolites and CNTs materials easily and cost-effectively. Since the rapid development in sorbent materials and innovative cyclic adsorption processes has become an essential separation process in many environmental applications. At the outset, there would seem to be two different classes of question demanding attention, to justify the novelty of this work, on one hand, the reason behind selection above addressed adsorbents, and discern what kind of pre-treatment and functionalization may enhance their adsorptive properties.

The reasoning behind the selection of these two adsorbents stemmed solely from the outcome of a deep literature review of the existing oil adsorbents. Both adsorbents the multi-walled carbon nanotubes MWCNTs and natural zeolite have a unique structure and high specific surface area in addition to exceptional mechanical properties, rapid sorption rates, high sorption capacity, and engineered surface chemistry. All this structural diversity has underscored its potential in water remediation processes, although fewer examples exist.

CNTs as a new class of carbon-based adsorbents as it believed to hold remarkable positions in adsorptive materials for various reasons. For one thing, they provide chemically inert surfaces for physical adsorption, as their high specific surface areas measure up to those of activated carbons (ACs).

Clay mineral as zeolitic tuff was selected as one of the available outstanding porous material with crystalline aluminosilicate structure with several microporous and cavities of numerous sizes at regular intervals. Much interest has been shown for zeolites due to the controllable level of aluminium/silicon, and it is potential for numerous applications such as synthesis of the water softener. Zeolites' sieving properties, functioning at the molecular level, and their exceptional chemical, thermal and hydrothermal stability advocate that these porous materials may have technological potential as adsorbents in separation and purification processes in aqueous media. Furthermore, the availability of natural zeolites in many countries such as China, Jordan, Turkey, the United States, with considerable deposits, provides low-cost treatment such as the ion-exchange process. According to the U.S. Geological survey in 2019, the world's annual production of natural zeolite approximates 1,100,000 tons (U.S. Geological Survey, 2019). Further significant developments via chemical modification on zeolites and CNTs can enhance their adsorptive properties. Based on the literature review, there is an incentive to develop cost-effective and high performance natural and carbon-based adsorbents for second stage removal of hydrocarbon from water (after mechanical treatment). Knowledge gaps for this purpose were identified as follows (i) natural and carbon-based adsorbents have not been adequately developed and characterized for removal of hydrocarbon from water and (ii) implications of this work concerning physico-chemical properties of adsorbents are not extensively elucidated.

It is noteworthy that at the time of compiling this thesis, no book had been published to date, which proposes an easy and cost-effective way for the preparation and characterization of highly hydrophobic adsorbents. Therefore, this work has attempted to provide a detailed account of the preparation of highly hydrophobic adsorbents with a particular emphasis on the microemulsion of CNTs and dealumination of zeolitic tuff as a state of the art modification techniques. To this end, the thesis has been sub-divided into nice chapters.

1.3 SIGNIFICANCE, SCOPE, AND DEFINITIONS

This investigation aims to develop an effective, low cost, flexible, sustainable, and environmentally friendly adsorbent as a potential method for adsorbing hydrocarbons from oil-contaminated water. The efficiency of both adsorbents for the removal of several model hydrocarbons was further investigated by studying further physico-chemical characteristics of the proposed adsorbents. The main parameters that influence hydrocarbon's adsorption abilities are considered; thus, the main aims of the thesis can be given as follows:

- To modify the surface of both adsorbents to increase the hydrophobic properties,
- To characterize both raw and modified forms, to determine whether the selected treatment improves its selectivity properties or adsorption capacity,
- Sorption models are to be studied to determine the exact mechanism of the sorption,
- To identify the factors that affect the performance of adsorbents and affect the rate of adsorption,
- To determine the applicability of several kinetic models, pseudo-first-order, second-order and intraparticle diffusion isotherms and to estimate the parameters characterizing the performance of the batch process

Chapter 2: Literature Review

This chapter begins with a historical background for oil spills (section 2.1) and reviews literature on the following topics: remediation techniques (section 2.2); particular focus on adsorption as promising remediation technique (section 2.3); and introduction for the main sorbents used in this thesis including carbon-based adsorbent namely carbon nanotubes (subsection 2.3.1) and natural zeolite-based adsorbent (subsection 3.2.2).

2.1 HISTORICAL BACKGROUND

Crude oil spills in lands and seas have triggered an interest in devising environment-friendly and economical methods to clean up oil contaminations; Table 1 presents the oil spill cases, which had been registered as a massive disaster. Moreover, tanker spillage also considered as the primary source for water contamination, as over the last 49 years, statistics for the frequency of spills higher than seven tones from tankers show a marked downward trend as illustrated in Figure 1 (ITOPF Limited, 2019)

Table 1: The 13 largest oil spills in history (Moss, 2010).

Case	**Date**	**location**	**Amount ($m^3 \times 10^3$)**
The Torrey Canyon	1967	Scilly Isles, U.K.	49-136
The Sea Star	1972	Gulf of Oman	133.63
Amoco Cadiz	1978	Portsall, France	261.2
Atlantic Empress	1979	Trinidad and Tobago	340.69
Ixtoc 1 Oil	1979	Mexico	529.96
Castillo de Bellve	1983	Saldanha Bay	299.05
Nowruz Oil Field	1983	Persian Gulf, Iran	302.83
Kolva River	1983	Russia	317.97
Odyssey	1988	Nova Scotia, Canada	154.07
Exxon Valdez	1989	Alaska	201.01
M/T Haven Tanker	1991	Genoa, Italy	170.34
Arabian Gulf	1991	Kuwait	1438.46-1968.41

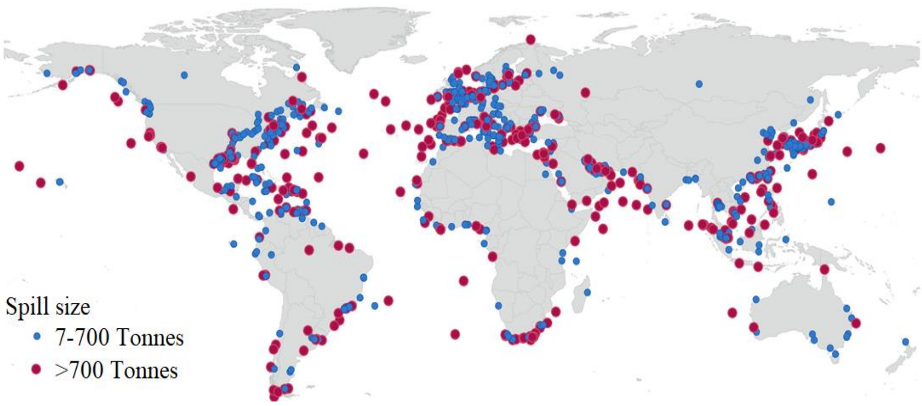

Figure 1: Location of spills >7 tonnes from 1970 to 2018 (ITOPF Limited, 2019)

Scientists' efforts of describing the ecological danger of oil spills and how such hydrocarbons affecting the environment and human beings have now reached a sophisticated level; leading not only to the formation of new remediation technologies but also in developing existing technologies from several disciplines (e.g., physical chemistry, materials chemistry), where chemistry plays an indispensable role in solving this serious problem. Several techniques have been reported in spill response. Nevertheless, the effectiveness of each technique is influenced by several aspects, just as the properties and the amount of spilled oil, location, and time of the year. Several kinds of research and projects have investigated a large number of experiments to assess the efficiency of different cleanup techniques. On a broader basis, oil spill removal methods are divided into three main categories:

(i) Mechanical recovery. Where oil is contained in an area using a boom or natural barriers and removed using skimmers, gravity separation (Zhang et al., 2015). Flotation methods (dissolved air, column flotation, electro, and induced air) (Wang et al., 2010); ultra and microfiltration, reverse osmosis (Jian et al., 1999), filtration (ultra and micro) (Gryta et al., 2001); various flotation methods (Gapingsi et al., 2017) (dissolved air, column flotation, activated sludge treatment (Tong et al., 2013), membrane bioreactors (Gu et al., 2014; Masuelli et al., 2009; Shang et al., 2012), various materials such as skimmers, solidifiers dispersants are used.

(ii) Non-mechanical recovery where chemical countermeasures, basically dispersants, burning or bioremediation are used to degrade or disperse the oil layer, sorption, biological treatment, chemical coagulation (Fu and Cao, 2011), electro-coagulation and coalescence and adsorption (De Gisi et al., 2016; Hyung-Mln and Cloud, 1992; Nwadiogbu et al., 2016) .

(iii) Manual recovery. In which oil is removed using simple hand tools and techniques such as pails, shovels, or nets (Olalekan et al., 2014).

As there is no general method which can be commonly applied to completely remove the oil from contaminated sites, the proficiency of each remediation technique requires information about the (i) composition of the crude oil/petroleum products and weather conditions, leakage quantity, sensitivity of the location and the toxicity of the chemicals. However, the cleanup of heavy crude oil is challenging. The weathering or evaporation of volatiles may produce solid or tarry oil. The remediation of medium crude oil spills is more difficult than the heavy crude oil and tends to infiltrate into porous media while the light crude oil (volatile oil) spreads rapidly on solid or water surface and penetrates porous surface (Ornitz and Champ, 2002).

2.2 REMEDIATION TECHNOLOGIES

As hinted earlier, oily water is usually treated by different physical, chemical, and biological procedures, various technologies for oil spill clean-up methods are illustrated in Table 2 (Behnood et al., 2013; Fingas, 2016; Jameel et al., 2011). However, using one of these conventional treatment technologies is not sufficiently compelling to remove the suspended/emulsified oil from water. Thus, an environmentally and cost-effective spill response may require a combination of clean-up methods (Ivshina et al., 2015). Most of the conventional treatment technologies have several drawbacks, such as high operational cost and low efficiency to remove the suspended/emulsified oil from water (Ahmaruzzaman, 2011). Therefore, many precautions must be considered when selecting the appropriate remediation method. Knowing the precise information of the oil spills is crucial in choosing a suitable remediation combination. For example, if the oil spill is fresh, burning could be a fast solution, but the emissions of the toxic combustion products will create additional environmental severe problems (Fritt-Rasmussen and Brandvik, 2011). Another example can be given, the usage of dispersants which considered one of the best way to remove oil from water surface, nevertheless the dispersants have harmful toxins of their own and can concentrate left-over oil toxins in the water, where they can kill fish and migrate great distances. Therefore, each of the many available oil remediation techniques addresses a somewhat different aspect of the problem.

Table 2: Oil clean-up techniques

Method	Example
Physical	Skimming and booming Wiping with an adsorbent material Mechanical removal Low-pressure flushing washing Stripping Dispersants
Chemical	Demulsifiers Gelling agents, solidifiers Surface film chemicals In situ burning
Natural	Natural attenuation
Biological	Bioremediation Phytoremediation

Accordingly, the new technologies for removal of oil from oil-impacted areas should take into consideration the efficiency of any remediation method that varies with oil type, time, and location of the spill in addition to weather conditions of the spill’s place. It is worthy of mentioning that one method alone is not sufficient to remove spilled hydrocarbons up to the desired level, for example, Department of Environmental Quality in Wyoming permitted the water discharge into a dry ravine if the water contains less than 10 ppm oil in water (Doyle, D.H., Brown, 1997). A crucial possible complication during the selection of remediation process is the existing of aliphatic, alicyclic and aromatic compounds in oil-contaminated water; therefore a combination of various remediation techniques have to be used together to achieve the acceptable level of hydrocarbon in the treated water (i.e., 20 ppm or less oil in water). These techniques may perform differently if it is implemented individually, but when applied together, thorough water treatment can be achieved. Because of this, attention has turned to the adsorption as supportive technique.

Among physical techniques, the adsorption is a commonly used method (Al-Jammal et al., 2019; Al-Jammal and Juzsakova, 2017; Kong et al., 2015). Adsorption is a potential remediation technique for hydrocarbon contaminated water (Alaa El-Din et al., 2017; Bandura et al., 2017), owing to their outstanding hydrocarbon removal efficiency, the possibility of regeneration, eco-friendliness, availability, and ease of applicability as well as economic feasibility (Ahmaruzzaman, 2011; De Gisi et al., 2016; Hyung-Mln and Cloud, 1992). Sorbents are commonly manufactured in particulate form for distribution over an oil slick or as sheets, rolls, pillows, or booms (Fingas, 2016). Moreover, sorbents can be used as (i) primary oil recovery for very small and limited oil spills in sea and spills from tankers or (ii) as a backup form as integrated technique for other remediation process in which the sorbent can be used to clean up the final traces of oil spills on water or land (Fingas, 2016). This highlights the necessity for efficient adsorbents and rational design for such treatment (Al-Jammal and Juzsakova, 2017; Kong et al., 2015; Teas et al., 2001).

2.3 ADSORPTION

Before studying the adsorption as one of the oil remediation techniques, some prior knowledge has to be presented. Adsorption term was coined by the German physicist Heinrich Kayser in 1881 (Swenson and Stadie, 2019). Adsorption usually takes place when a fluid exposed to a porous material surface. At that moment, unsaturated and unbalanced molecular forces will emanate the interaction between the solid surface and the fluid. The solid surface tends to make the balance between the two surfaces and the boundary layer by attracting and holding on the fluid molecules on its surface and pores. Therefore, a higher concentration of the gas or liquid in the adjacent vicinity of the solid surface than in the bulk gas or vapour phase facilitates the penetration of this fluid into the porous material (Bansal and Goyal, 2005). Adsorption remains distinguished from absorption by its limitation to the surface or interface of the sorbent; upon diffusion beyond the interface into the bulk of the sorbent (Swenson and Stadie, 2019). Generally, sorbent materials can act either by adsorption or, less commonly, by absorption. In this context, the discussion will be on adsorbents as solid material and oil/water as the adsorbate. In adsorption, the oil is preferentially attracted to the surface of the material, whereas absorbents incorporate the oil or other liquid to be recovered into the body of the material, as illustrated in Figure 2. While absorption process allows the oil to penetrate pore spaces in the solid material body as, shown in Figure 3 (Erdem et al., 2004). The majority of products available for oil spill response are adsorbents; few are true absorbents.

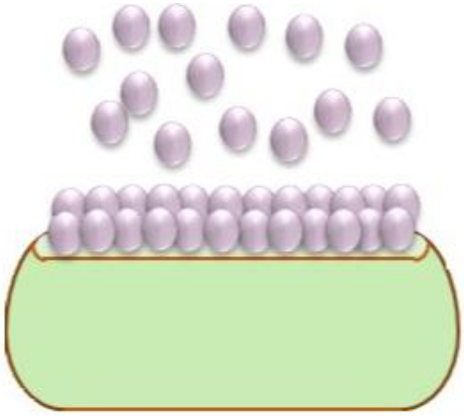

Figure 2: Illustration of the adsorption process in which atoms, ions, or molecules are adhering to the surface of the adsorbent

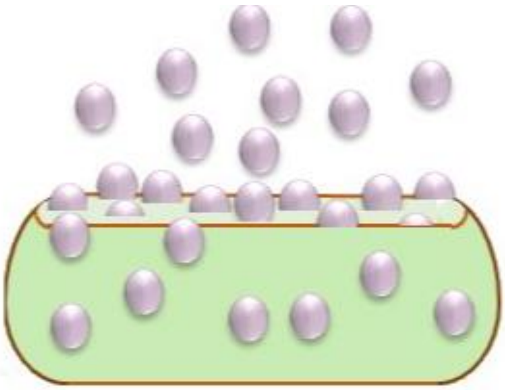

Figure 3: Illustration of the absorption process, in which atoms, ions, or molecules entering the volume of the absorbing substance

Many parameters governed by the structure of adsorbents play a vital role in the separation process. The specific surface area, pore size, pore size distribution, and surface chemistry features of the sorbent are crucial factors that must be taken into consideration for sorbent's selection/design in research and development work (De Gisi et al., 2016). The hydrophobicity of the sorbents is also an essential feature since the sorbents should preferentially adsorb the hydrocarbons on their surface and must not adsorb the water (Deschamps et al., 2003; Hyung-Mln and Cloud, 1992; Kong et al., 2015; Nguyen et al., 2012). Additionally, high carbon or oxygen content bears some essential relation to the potential of adsorbent, but of lesser interest than other properties. In general, the main characteristics of both adsorbents and oil types must be considered when choosing adsorbents for cleaning up oil spills. The suitable adsorbents must have the following aspects (De Gisi et al., 2016; Gedik and Imamoglu, 2008):

(i) **Rate of absorption:** The absorption of oil is faster with lighter oil products. Once absorbed, the oil cannot be released. Effective with light hydrocarbons (e.g., gasoline, diesel fuel, benzene).

(ii) **Adsorption capacity/** Oil recovery (mass of pollutant adsorbed onto adsorbent per adsorbent's mass) in a wide range of adsorbate concentrations. This feature related to adsorbents high porosity, uniform molecular-sized channels, and large specific surface area.

(iii) **Rate of adsorption**: The thicker oils adhere to the surface of the adsorbent more effectively.

(iv) **Low cost of acquisition** and does not introduce additional pollution into the environment, minimal waste generation

(v) **Ease of application**: Sorbents may be applied to spills manually or mechanically, using blowers or fans. Many natural organic sorbents that exist as loose materials, such as clay and vermiculite, are dusty, difficult to apply under windy conditions, and potentially hazardous if inhaled.

It must be an attempt to adjust some crucial techno-economic data of the adsorption process to carry out scale-up experiments with possible economic analysis and perspectives of the use of green adsorbents (Guodong et al., 2015). However, there are indeed very narrow and somewhat limited numbers of materials that meet all the role adsorbents' requirements in terms of selectivity, sorption capacity, sorption rate, and recyclability.

To date, the synthesis of adsorbents with superior oil sorption performance remains a significant challenge. Several sorbents such as activated carbon, polymeric resins, agricultural wastes, fly ash, and zeolites have been used for water clean-up (Abdelwahab et al., 2017; Cretescu et al., 2015). Furthermore, the removal of hydrocarbons from surface water has been widely studied by adsorption over powdered activated carbon (PAC) and deposited carbon (DC) (Kong et al., 2015; Nguyen et al., 2012). Many studies and real application proved that the efficiencies of such sorbents are outstandingly good (Carmody et al., 2007; Maulion et al., 2015). However, the efficiency (adsorption capacity) of each adsorbent is subject to several parameters such as: (i) the contact time; (ii) the ratio of sorbents to the oil-water emulsion, (iii) the type of surface modification of sorbents and more importantly (iv) hydrophobic properties (Ceylan et al., 2009; Nguyen et al., 2012; Site, 2000).

Several researchers classified the sorbents into three categories as (i) synthetic polymers (polyurethane, polypropylene, polyethylene, etc.), (ii) natural fibre materials (agricultural wastes) (Husseien et al., 2009), and (iii) inorganic minerals (bentonite, vermiculite, etc.) (Chen et al., 2016; Duong and Burford, 2006; Gui et al., 2011; Tu et al., 2016; Zou et al., 2010) and carbon-based adsorbents (Dettmer et al., 2000). However, there are several drawbacks related to the conventional sorbents, e.g.: (i) their slow decomposition (Gui et al., 2011), (ii) high water uptake and low adsorption capacity towards the hydrophobic organic contaminants (Moura and Lago, 2009; Rajakovi and Rajakovi, 2008), (iii) clogging of pores which decrease the efficiency of the adsorbents (Suresh Kumar et al., 2017; Syuhada et al., 2017). All these drawbacks have triggered the development of innovative new super-hydrophobic and super-oleophilic adsorbents to overcome their limited application for oil spill remediation; additionally, it provoked many companies and research centres to further investments in research and developments to develop an outstanding adsorptive material for large scale applications (Chen et al., 2016; Duong and Burford, 2006), see Table 3.

Table 3: Adsorbents types and their properties

Adsorbent Type	Advantages	Drawbacks
(i) Natural fiber materials and organic Adsorbent (Green Adsorbents)		
Agricultural sources residues as lignin (Naseer et al., 2019); activated carbons after pyrolysis of agricultural sources (Abdul Khalil et al., 2013), natural fiber materials such as cotton fibers (Wang et al., 2013), corn stalk (Wang et al., 2016) and nonwoven wool (Radetić et al., 2003).	• Environmentally-Friendly (from abundant natural sources, • Biodegradable, non-toxic and low-cost materials	• Low sorption capacities and are mostly hydrophilic • Cost-potential makes them competitive • One of the disadvantages of the plant origin sorbent is its high-water absorption, which resulted in the loss of the sorbent buoyancy
(ii) Synthetic Adsorbent		
Synthetic polymers; such as polyethylene and butyl rubber polyurethane (Ceylan et al., 2009), polypropylene (Teas et al., 2001).	• The synthetic polymers are widely used due to their hydrophobic and oleophilic characteristics.	• The synthetic polymers have very slow degradability, which makes them an environmental concern. • They are not naturally occurring as mineral products
(iii) Inorganic minerals		
Perlite, graphite, vermiculites, sorbent clay and diatomite (Adebajo et al., 2003), vermiculite (Adebajo et al., 2003), exfoliated graphite sepiolite (Bayat et al., 2008) and zeolites (Al-Jammal et al., 2019).	• The high adsorption capacity of 3.5–4.0 g petroleum/g sorbent Can be regenerated.	• Having a porous structure for these materials can actively absorb water that can be considered as its disadvantage, sensitivity to fouling and susceptibility to ageing processes
(iv) carbon nanotube adsorbents		
CNTs, copolymer consisting of modified multi-walled carbon nanotube (MWCNT) (Gupta and Tai, 2016) and magnetic carbon nanotube sponges (Gui et al., 2013)	• Exceptional one-dimensional structure and large specific surface area. • Outstanding oleophilic and hydrophobic nature	• Poor solubility and process ability restrict their applications. • Also, because of very fine particle size, working with this material is too difficult so that it is limited to laboratory-based studies

In this work, the focus will be given to carbon-based adsorbent (MWCNTs) and inorganic adsorbents (zeolitic tuff) since they have generated a lot of attention as outstanding types of adsorbents due to their exceptionally high adsorption capacity for oil-water separation. Both materials have had exceptional success in academic applications, most notably in water treatment and petrochemistry, where the raw and modified forms of CNTs and zeolites have found widespread use, and have been pervasively studied in both academic and industrial laboratories. Their success cannot be assigned to a single cause, but rather to a number of favourable factors, which will be presented in the following subsections of this chapter.

2.3.1 Carbon nanotube-based adsorbents

Nowadays, carbon-based adsorbents are in the focus of researchers for water/oil separation. Such as carbon aerogels (Zou et al., 2010), carbon coatings (Gupta and Tai, 2016), activated carbon (Maulion et al., 2015; Zhu et al., 2013), graphene or carbon nanotubes (CNTs) coated sponges, sponges (graphene foams) (Sultanov et al., 2017), porous carbon nanoparticles and carbon fiber (Zhu et al., 2013). All these materials have been widely investigated for water filtration, water/oil separation, oil-spill clean-up, wastewater treatment, gas separation and purification (Gupta and Tai, 2016; Ihsanullah et al., 2015).

CNTs in its several forms, such as (i) single-walled carbon nanotubes (SWCNTs) and multi-walled carbon nanotube (MWCNTs), have generated a lot of attention as a new type of adsorbent due to their exceptionally high adsorption capacity. Since the introduction of the carbon nanotubes (CNTs) in 1991 had earned a significant interest due to their exceptional properties and stability (Golnabi, 2012). Those materials have a unique structure and high specific surface area in addition to exceptional mechanical properties, rapid sorption rates, high sorption capacity, and engineered surface chemistry (Ci et al., 2007; Gui et al., 2010). All this structural diversity have underscored their potential in water remediation processes (Khosravi and Azizian, 2015; Pham and Dickerson, 2014). It is believed that the properties of CNT-water interface to be similar to those of the graphite-water interface. The latter is known to be strongly hydrophobic (Allen et al., 1999). Despite the many exciting and compelling recent developments on CNTs applications as adsorbents, sorption on a large scale is still in an immature phase, and the literature is somewhat coy in dealing with their functionalization.

To draw a concrete strategy for rationalizing the synthesis and implementation of CNTs as an adsorbent, it is important to understand their structure to find a suitable and effective way of modification to enhance their properties.

Carbon nanotubes are cylindrical bodies, and each wall consists of carbon atoms bound by covalent links (Kaushik and Majumder, 2015). In practice, SWCNTs and MWCNTs are distinguished. The SWCNTs are graphite layers of cylindrical shape with diameters vary from 0.4 to 2 to 3 nm, and their length is normally of the micrometer range (Eatemadi et al., 2014). On the other hand, MWCNTs consists of several single-walled CNTs located concentrically, in which case the graphite cylinders are at a distance of 0.35 nm from each other. It should be noted that the inner diameter of MWCNTs diverges from 0.4 nm up to a few nanometres depending on the number of layers, while the outer diameter differs typically from 2 nm up to 20 to 30 nm (Eatemadi et al., 2014; Samadishadlou et al., 2018). In the case of MWCNTs, the concentrically cylinders layers are fixed by van der Waals bonds (Saifuddin et al., 2012).

The functionalization of CNTs surfaces was envisioned by many researchers to enhance their chemical properties (Jeon and Chang, 2011). A wide range of functional groups can be used to decorate CNTs' bodies, as being composed of backbone, functionality can be attached to the backbone, or/and their pores' environment (Figure 4). Functionalizing the raw MWCNTs imparts a wealth of properties that would not otherwise be possible with current MWCNTs, this tunable feature of CNTs/MWCNTs places them as a good candidate for scientific research. The surface modification of the CNTs can be performed by attaching functional groups via covalent links or by van der Waals bonds (noncovalent links) (Le et al., 2013; Meng et al., 2009). The key approaches for the modification of CNTs falls into three categories: (i) the covalent attachment of chemical groups onto the π -conjugated skeleton of CNTs; (ii) the non-covalent adsorption or wrapping with various functional molecules; and (iii) the endohedral filling of their empty inner cavity (Wu et al., 2010).

The first category allows access to a much wider range of CNTs' functionalization techniques since in covalent modification, the desired functional group is attached to the sidewall or the ends of the carbon nanotubes (Karousis and Tagmatarchis, 2010), while in the case of non-covalent modifications, van der Waals force and π-π interactions play an important role. It is worth mentioning that the non-covalent tuning of

CNTs is preferable for the enhancement of interfacial properties of the CNTs as it avoids the destruction of CNTs' structure (Jeon and Chang, 2011) Figure 4. However, the most prominent interactions are between aliphatic C-H donors and aromatic π -acceptors and interactions between aromatic C-H donors and aromatic π -acceptors.

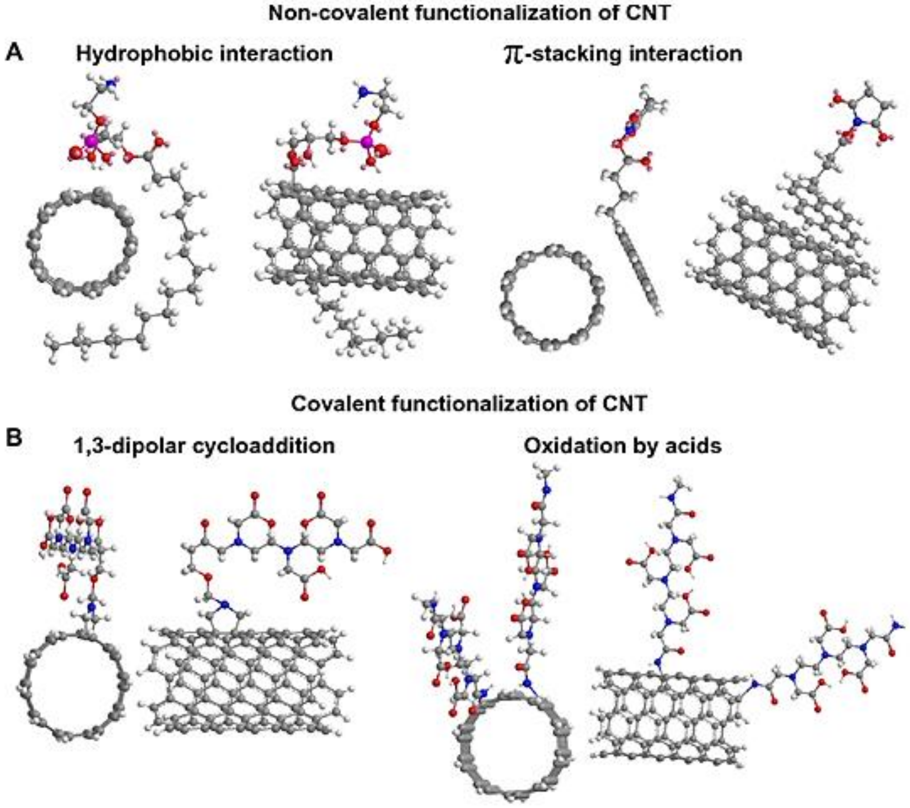

Figure 4: Modes of CNTs functionalization (Kim and Kotagiri, 2014)

Commonly, the functionalization of CNTs performed by attaching tailored chemical functionalities onto the *sp*^{2} carbon framework; such as OH, COOH, NH_2 or many other groups that can promote the CNTs dispersion in a wide variety of solvents and polymers and enabling their use in a wide range of applications (Hirsch, 2002). The lack of innovation in CNTs as adsorbents stems from several sources; one of them is to find a simple and easy way of functionalization. The type of functionalization of CNTs has to be chosen with a view to the intended use as a successful enhancement of CNTs' properties depends on the effective outer/inner surface modification. A convenient way of entering the detail of this subject is by summarizing the possible way of functionalization. Figure 5 illustrates some of the main covalent surface chemistry for the CNT functionalization.

For example, fluorinated CNTs used as an efficient metal-free catalyst for the destruction of organic pollutants in catalytic ozonation (Wang et al., 2018). Another example is coating the CNTs with polyurethane, which has been widely used as a recyclable oil sorbent from oil-contaminated water, with high oil absorption capacity and outstanding reusability (Wang and Lin, 2013).

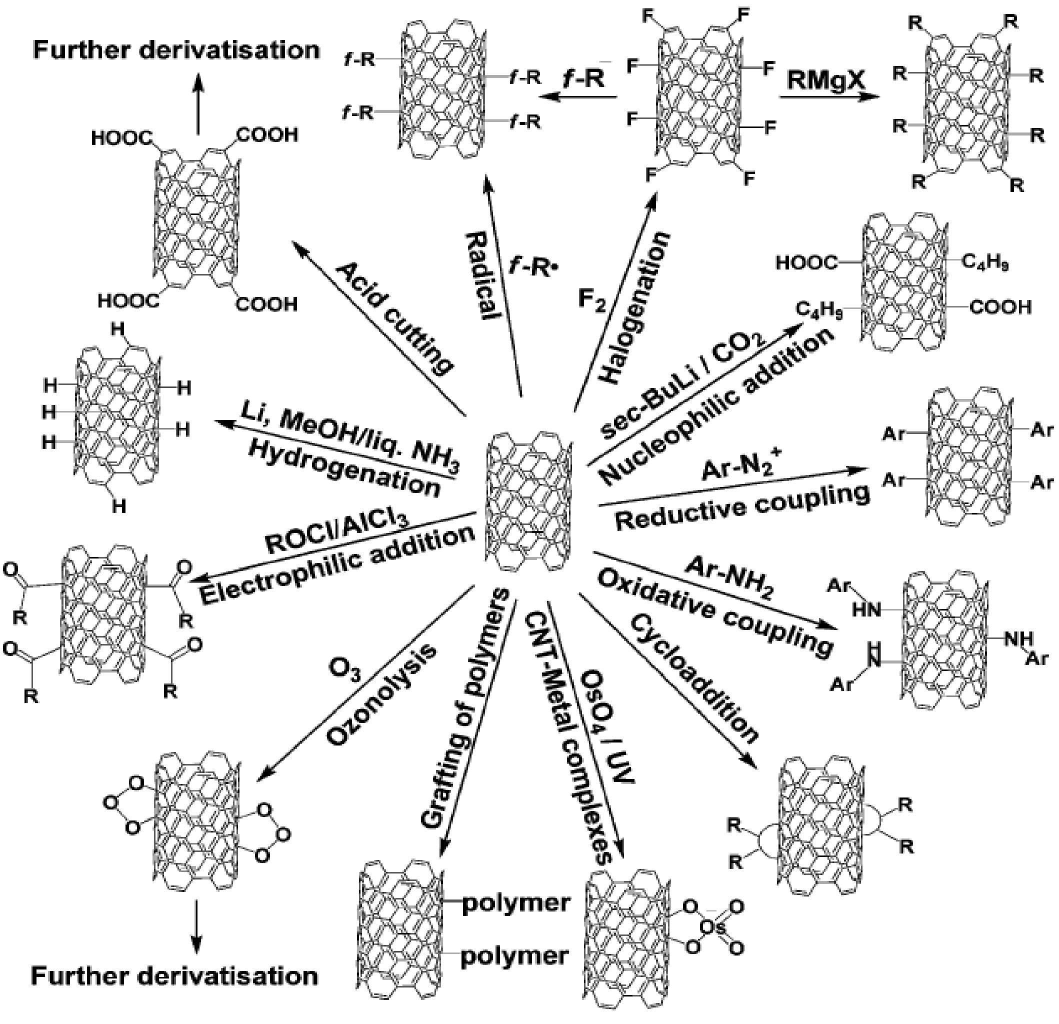

Figure 5: Surface functionalization of CNTs (Wu et al., 2010)

In the field of oil-water separation, the hydrophobic character of adsorbent is one of the main criteria for choosing the functionalization method. Functionalization varies in difficulty but often adds a few steps to the preparation and substitution on MWCNTs surface. Lau et al. prevailed to develop superhydrophobic CNTs forests by modifying the surface of vertically aligned nanotubes with a PTFE coating (Lau et al., 2003). Sun et al. used by p-phenylenediamine to functionalize the CNTs surface (Sun et al., 2014). Several preparations were also made in which hydrophobic properties were present in a laudable level to obtain its positive influence on oil separation (Ge et al., 2013; Gui et al., 2013; Lee et al., 2010).

2.3.2 Zeolite based adsorbents

One of the earliest applications of natural zeolites is to tackle the problem of wastewater treatment (Margeta et al., 2013). This class of porous materials occur in nature and have been known for almost 250 years as aluminosilicate minerals. The discoveries revealed several types of zeolites, such as faujasite, mordenite, offretite, ferrierite, erionite, and chabazite (Weitkamp, 2000). The term‘zeolite ‘dates to late 1756 in which the Swedish mineralogist Baron Cronstedt in 1756 primed a quantum leap in understanding and investigating this material (Mastinu et al., 2019). Zeolite was created from two Greek words meaning ζε´ω (zéo)“ to boil”and λiθος (lithos) “ stone,” which refers to certain silicate minerals that force out water when heated (Fuoco, 2012). Georges Friedel took the early lead through some studies to prove that zeolite is similar to an open sponge-like framework, after having observed the occlusion of various liquids such as benzene by dehydrated zeolites. The outstanding progress in research and development of this porous material has been outlined since the 1950s (Auerbach, 2003; Kesraoui-Ouki et al., 1994).

After briefly recalling the history of this discovery of zeolites, it is essential to know the structure of the zeolite. Zeolites are microporous crystalline aluminosilicates having a uniform pore structure and exhibiting ion-exchange behavior (Weitkamp and Puppe, 1999). Zeolite's structure characterized by a framework of linked TO_4 tetrahedra (T = tetrahedral atom, e.g., Si, Al) with O atoms connecting neighbouring tetrahedral as shown in Figure 6. Each tetrahedron has either aluminium or silicon atom in the middle, and oxygen atoms at the corners, the tetrahedral are linked together through their corners in a three-dimensional arrangement (Auerbach, 2003). Their pore volumes are typically between 0.10 and 0.35 cm^3 g^{-1} and pore sizes, typically ranging from 0.3 to 1.0 nm.

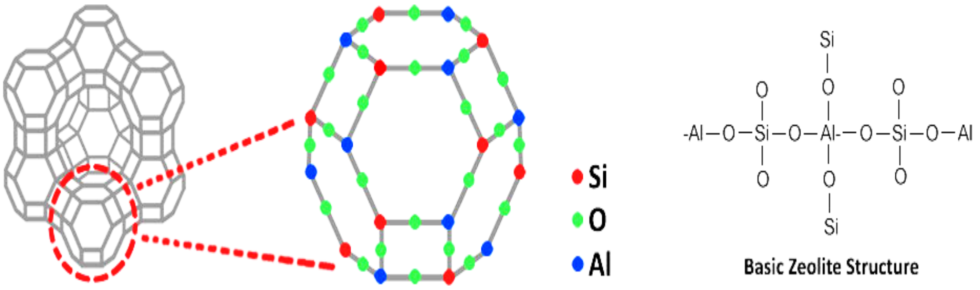

Figure 6: Framework and extra- framework in zeolite

This strong framework, in combination with the preference for the formation of rigid cages, renders zeolite highly robust porous materials, thus setting them apart from other clay minerals.

For a completely siliceous structure, a combination of TO_4 (T = Si) units in this fashion lead to silica (SiO_2), which is an uncharged solid. Upon incorporation of Al into the silica framework, the +3 charge on the Al makes the framework negatively charged, and the presence of extra framework Al requires inorganic and organic cations to compensate for the negative framework charge, within the structure yielding framework electrical neutrality (Auerbach, 2003). The basicity of ion-exchanged zeolites arises from the framework's negative charge. Therefore, the moderately high aluminium content of zeolite results in a substantial framework negative charge (Davis, 2003; Lercher et al., 2008). The chemical composition of zeolite can hence be represented with the following formula: Extra framework cations, framework, and adsorbed phase; $A^{m+}_{y/m}.\left[(SiO_2)_x.(AlO_2)_y{}^{-}\right].nH_2O.$

Where *A* is the cation with charge *m*, (x+y) number of tetrahedra per crystallographic unit cell, and x/y is the so-called framework silicon/aluminium or simply Si/Al ratio (Weitkamp, 2000). The source of negative charge on the framework of zeolite is related to the Si/Al ratio and the quantities of ion-exchanged cations such as K^+, Na^+, and Mg^{2+}, which exist in cavities of zeolites (Munthali et al., 2015). It is well known that the negative charge of a zeolite not localized on one tetrahedron but is distributed over the entire framework of oxygen ions. The density of negative charge is naturally higher close to the aluminium tetrahedral (Roberge et al., 2002). It is worth mentioning that the possibility to manipulate the total charge of zeolite by chemical modification, synthesis, and post-synthesis can result in a huge range of hydrophilic/hydrophobic properties of this material. This fact allow zeolite to be used in several applications as diverse as adsorption, catalytic reactions.

Based on several studies on zeolite, zeolites can be successfully used in a wide range of application as catalysts and adsorbents, due to their well-defined structures, characterized by the compositional Si/Al ratio, framework topology and distribution of framework Al atoms in zeolites (Lami et al., 1993). Main properties of zeolites like high adsorption capacity, ion exchangeability, molecular sieve properties, shape selectivity, catalyzing action, thermal stability and resistance in different chemical atmospheres brings researcher's attraction to zeolites, in addition of low cost that enhance the availability for large application (Li et al., 2017; Shaw et al., 2016; Weitkamp et al., 2004). Adsorbents derived from natural materials like zeolite are promising candidates in the field of environmental remediation (De Gisi et al., 2016; Li et al., 2017). Those are widely used as effective adsorbents in water and wastewater treatment (Wang and Peng, 2010). However, the composition and source of the zeolite have a profound effect on the properties and subsequent applications. According to the International Zeolite Association (IZA) Structure Commission, zeolites can be categorized in relation to the Si/Al ratio; i.e. low silica zeolites (Si/Al = 1-2), medium silica zeolites (Si/Al = 3-10) and high silica zeolites (Si/Al ≥ 10) (Csicsery, 1986).

2.3.2.1 "Low" and "intermediate" silica zeolite adsorbent

Generally, natural zeolite minerals (for example, phillipsite, chabazite) have been assessed as appropriate agents for environmental clean-ups (Noor-Ul-Amin, 2014; Reeve and Fallowfield, 2018). Chen was the first researcher who suggested the utilization of hydrophobic molecular sieves to remove hydrocarbons from the water surface (Chen, 1976). Few works on the application of natural zeolitic materials in hydrocarbon sorption have been investigated (Bandura et al., 2015a; Muir and Bajda, 2016).

Bandura and co-workers conducted a review on the published works related to zeolite as oil adsorbent, and they concluded that the adsorption capacities of the zeolite group were in the range of 0.6 to 1.2 g/g. This variation is due to the difference in the structure and surface area of the used zeolite. In particular, synthetic zeolites exhibited higher sorption capacities for oils, while lower values of sorption capacities were obtained using natural zeolites (Bandura et al., 2017).

The modified synthetic zeolites also show high efficiency for BTEX removal, and those can be efficiently used in as many as four adsorption cycles (Vidal et al., 2012). In a study on $LaFeO_3$ doped acid-modified natural zeolites, it was suggested that the use of this material could be a promising heterogeneous photocatalyst for dye degradation in wastewater treatment (Phan et al., 2019).

2.3.2.2 "High" silica zeolite

Over the years, research is progressively concentrating on hydrophobic pure-silica or high silica-containing zeolites as a feasible alternative for activated charcoal for the sorption of organic pollutants (such as volatile organic compounds). This kind of zeolite surpassing that of all other classes of porous zeolite in several properties such as hydrophobicity. High silica zeolites have a unified structure with a defined pore size of 0.2-0.9 nm and a high specific surface area (Küntzel et al., 1999). This type of adsorbents represents a privileged class of adsorbents for the removal of organic pollutants from water surfaces (Jiang et al., 2018). The hydrophobic/organophilic character of high silica content zeolites has been long recognized (Flanigen, 1980) and are widely used as effective adsorbents in water and wastewater treatment (Wang and Peng, 2010). As a salutary example, the synthetic high silica-containing zeolite Y has succeeded in removing 89% of organic contents from wastewater (Hosseini Hashemi et al., 2019). Their sieving properties, operating at the molecular level, and their excellent chemical, thermal and hydrothermal stability suggest that these materials may have technological potential as adsorbents in separation and purification processes in aqueous or wet media. Hence, silicates display a high degree of hydrophobic-organophilic properties and are capable of adsorbing hydrocarbon molecules from the contaminated water.

It has been an article of faith in zeolite chemistry that aluminium/silicon content or (Si/Al) should be manipulated for the synthesis of material with specific properties. Different research groups have verified that the SiO_2/Al_2O_3 ratio increases in various zeolites as the excess alkalinity decreases. It is worthy of mentioning that the degree of hydrophobicity of zeolites is directly dependent on their aluminium content or in their Si/Al ratio. Thus, one of the clearest desirable traits to modify zeolite is to manipulate this ratio. A straightforward way to achieve this is via dealumination/desilication of zeolite. However, the reduction of the aluminium content in zeolite will result in a reduction of its ionic charge and thus will decrease the zeolite polarity.

Consequently, the hydrophobicity of the framework will be enhanced by shifting zeolites' adsorption affinity toward nonpolar molecules, like hydrocarbon, instead of polar substances like water (Malik et al., 2012). In contrary to the "low" and "intermediate" silica zeolite, the surface of zeolite with high silica content approaches a more homogeneous characteristic with an organophilic/ hydrophobic selectivity (Flanigen, 1980; Maesen and Marcus, 2001)

Zeolites with high silica content are generally synthesized via direct synthesis or by thermochemical framework modification of zeolites using the dealumination process (Lutz, 2014; Maesen and Marcus, 2001; Roberge et al., 2002). The term "dealumination" refers to the removal of aluminium from zeolite frameworks by chemical reactions resulting in lattice deficiencies Figure 7. Several dealumination processes have been developed over the years, such as (i) silylation process (Bokhoven et al., 2000; Campbell et al., 1996); (ii) modification with silicon hexafluoride (Ferey, 2002; Peixoto et al., 2003) (iii) chelating agents (Kerr, 1968); (iv) treatment with mineral or organic acids (Barrer and Makki, 1964; Jones et al., 2001); and (v) by steaming (Boveri et al., 2006; De Lucas et al., 1997). However, in its general use, it relates to a more complex process comprising the incorporation of other elements, especially of silicon into the transient framework vacancies left temporarily by the release of aluminium (Beyer, 2002).

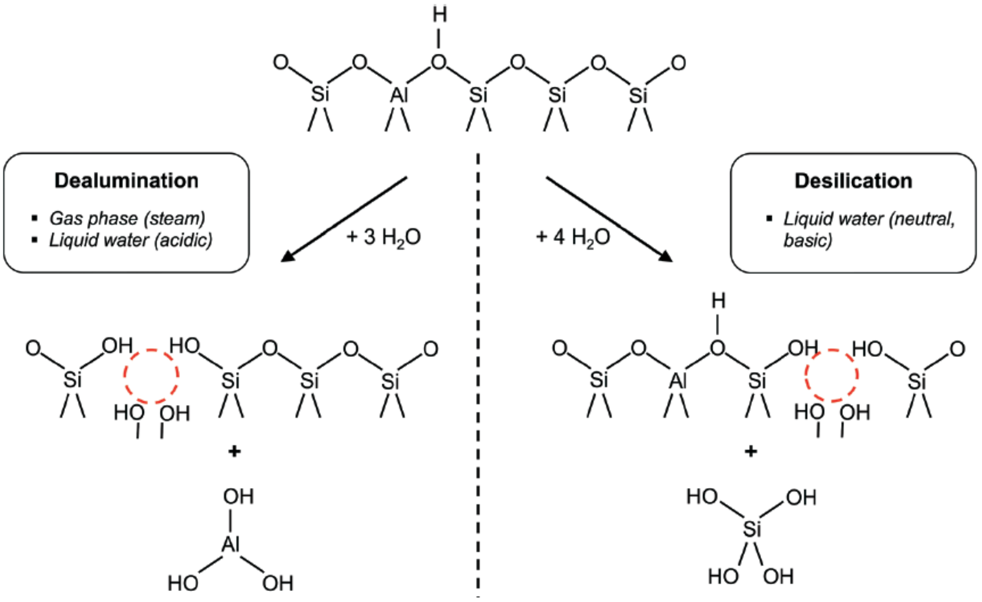

Figure 7: Dealumination hydrolysis reactions (left) and desilication hydrolysis reactions (right) (Gounder, 2014)

Dealumination of zeolites could result in creating defects within the framework. Thus, it gives rise to significant variation in the surface area and micropore volume of the dealuminated zeolites. One could argue that not all zeolites have a similar structure, and dealumination may exhibit a very different behavior towards the various dealumination methods, and this is verified by several researchers (Csicsery, 1986; Müller et al., 2000). These modifications appear to be promising in the case of clay minerals and zeolites, for example, organo-clays and organo-zeolites display higher sorption performance to organic compounds in water media than the raw materials. This conclusion has been anticipated to some extent by many researchers who worked with zeolite (Yonli et al., 2012; Zhu et al., 2015).

Chapter 3: Research Design

This chapter describes the design adopted by this research to achieve the aims and objectives stated in section 1.3 of Chapter 1, which summarized the modification and synthesis of the novel, inexpensive adsorbents that will reduce the cost associated with oil spills remediation. Section 3.1 discusses the methodology used in the functionalization of adsorbents' surface to enhance its hydrophobic properties, the stages by which the functionalization was implemented. Section 3.2 outlines the used materials and applied procedure for the preparation and analysis of the synthetic solutions used as a model sample for contaminated water. Section 3.3 details all characterization techniques and justifies their use. Finally, section 3.4 lists all the instruments used to determine the potential of adsorbent in terms of their adsorption capacities.

3.1 METHODOLOGY

For synthesis: the hydrophobic properties of zeolite were enhanced by two methods (i) dealumination (via acidic treatment) and (ii) dealumination followed by microemulsification. While the hydrophobic properties of MWCNTs were enhanced by microemulsion only. Simple impregnation was used to modify the hydrophilic/hydrophobic features for both adsorbents.

In the case of zeolite, the Si/Al ratio plays a crucial role in determining the hydrophobic properties of the zeolites. The main aim of dealumination processes is to increase this ratio by the removal of aluminium from zeolite frameworks, which in turn results in lattice deficiencies, while microemulsion was implemented to directly, decorate the surface of MWCNTs or TZT with a chain of hydrocarbon to enrich their hydrophobic properties and to increase the oil uptake capacity from the water. The prepared adsorbents were examined in batch experiments at fixed hydrocarbon-water emulsion volume and an appropriate amount of adsorbent. The resulting solution was tested to investigate the amount of remaining hydrocarbon after adsorption.

3.2 MATERIALS

3.2.1 Carbon nanotubes based adsorbents

Raw (commercial) and modified MWCNTs were used for the experiments. Commercial grade MWCNTs were purchased from Timesnano Ltd. (TNNF-6 type, China). From now on, commercial MWCNTs are referred to as untreated or raw carbon nanotubes. The purchased MWCNTs had a length of 5-20 µm; and 10-20 nm outer average diameter with a purity of > 95 and a specific surface area of 120 m^2/g.

3.2.2 Zeolite based adsorbents

Jordanian zeolitic tuffs are located at Jabal Aritayn (30 km North-East of Azraq), Tal Alshahba (20 km East of Al Safawi), Tal-Rimah (35 km North-East of Al Mafraq) and other small deposits can be found in the South Jordan (Tell Burma, Tell Juhaira and Wadi El-Hisa) and in central Jordan (Makawer, Al-Zara, Wadi Heidan, and Wadi Al-Walah). The used sample in this work was obtained from Tall Hassasn deposits, Jabal-Arityan, the southern part of Jordan. Usually, this kind of zeolitic tuff contains mainly Phillipsite-K mineral [$(K, Na)_2\ Al_8Si_8O_{16}.4H_2O$], forsterite, chabazite-K, quartz, hematite, and sanidine. The chosen sample has a SiO_2/Al_2O_3 ratio of 2.5. Table 4 illustrates the properties of Tell Hassan RZT (Yasin et al., 2015).

Table 4. Properties of Tell Hassan RZT

Properties	**Values**
Water absorption	8.53-10.8 %
Colors	grey, grey to brown
Unit weight	1010 kg/m^3
Specific gravity	1.56-1.80 g/cm^3
Void ratio	17.54
Pulse Velocity	3333-3564 (m/sec)
Surface abrasion	27-28
T.D.S	1250-1500 (mg/L)
Elongation	11.09
Flakiness	22.59

3.2.3 Commercial adsorbents

Commercial activated carbon adsorbents were used as benchmark adsorbent for the sake of comparison. AquaCarb activated carbons were purchased from EVOQUA Water Technology Co. as it has a high microporous structure of coconut shell-based carbon, and it has excellent volatile organic carbon (VOC) removal capacity; moreover it exhibits a higher adsorption capacity than coal-based carbon for surface water treatment. Such adsorbents have a density varying between 460 and 470 kg/m^3 with a total surface area of 1100 m^2/g with a mean particle size of 1.2 mm, and it is commonly used in industrial water and wastewater treatments (Chemvioncarbon, 2018). The adsorption capacities of synthesized adsorbents were compared with commercially available activated carbon adsorbents, namely, Norit GAC 1240EN and Aquacarb 207C.

3.2.4 Chemicals and methodology

3.2.4.1 Dealumination of zeolitic tuff

Hydrochloric acid of analytical grade (37%) (Sigma Aldrich) was used for the pretreatment of raw zeolitic tuff. The raw zeolitic tuff (RZT) was crushed, ground, and sieved to obtain particles with 26-μm average particle size. After sieving, the precursor has been subjected to several processes, including washing RZT several times with distilled water to remove all soluble salts and dried in an oven at 105 °C for 4 h. The dried RZT was treated with diluted hydrochloric acid (16%), and the mixture was stirred with a magnetic stirrer at room temperature for at least 24 h. The treated material was then filtered by using a 0.41-μm filter paper (Whatman 41) to remove the aqueous yellowish acidic solution formed during the reaction of the dilute hydrochloric acid and associated minerals. The colour of RZT slightly changed; this change occurs due to the extraction of associated material and impurities. If the process does not proceed to completion of the required Si/Al ratio, a series of acidic treatments or use of stronger acidic concentration are suggested. This procedure, " dealumination via acid," is especially effective with the clay minerals. It is, therefore, at first sight, somewhat surprising that it has not been used more widely to prepare hydrophobic adsorbents.

3.2.4.2 Microemulsion, chemicals, and preparation

Raw MWCNTs and dealuminated/treated zeolitic tuff (TZT) and were treated by microemulsion according to the procedure described by Dantas and co-workers (De

Castro Dantas et al., 2001). In this method, saponified coconut oil (mostly lauric acid, $CH_3(CH_2)_{10}COOH$, with some myristic acid, $CH_3(CH_2)_{12}COOH$), used a surfactant. Coconut oil was saponified by standard procedure ASTM D-5558/1995 (ASTM International, 1995) to form $CH_3(CH_2)10COO^-Na^+$. After saponification, 10 m % of the surfactant was added to 25 m % of the aqueous phase (deionized water). The mixture was then mixed with 40 m % of the co-surfactant (isoamyl alcohol, 99 % P.A.) and 25 m % of the oil phase (n-octane). It is must be noted that the choice of the oil phase is another element to control microemulsion nature.

The mixture can be prepared in one-step by simply mixing the constituents as this is a matter of no importance, due to the spontaneous formation of microemulsions. Thus, the sequence of the addition of the components is not considered a critical factor for the preparation of the microemulsion, and of course, mixing time effects the latter process as it can influence the period needed for microemulsion to reach the equilibrium phase. However, this time will increase if the co-surfactant is added to the organic phase since its higher solubility in this phase will prevent the diffusion in the aqueous phase (Vandamme, 2002).

To prepare microemulsified adsorbents, 10 g of adsorbents and 20 cm^3 of microemulsion were mixed and then dried at 65 ^oC for 48 h. The same procedure was followed to prepare µMWCNTs adsorbents.

3.3 CHARACTERIZATION OF THE ADSORBENTS

The physico-chemical properties of the adsorbents were examined using several characterization techniques to obtain information about the structural, chemical and surface properties of the prepared adsorbents such as X-ray diffraction (XRD), Fourier transform infrared spectrometry (FT-IR), Brunauer–Emmett–Teller (BET) method, scanning electron microscopy (SEM), energy dispersive X-ray (EDX), X-ray fluorescence (XRF), thermogravimetric analysis (TGA) and Raman spectroscopy.

3.3.1 X-ray diffraction (XRD) measurements

X-ray diffraction (XRD) was used as a standard procedure to investigate the phase composition of the raw and modified adsorbents. XRD patterns were recorded at room temperature over 4-70° 2θ angular range with a scan of acquisition speed of 0.02°/sec by a Phillips PW3710 diffractometer equipped with a Cu Kα source ($\lambda = 1.5406$ Å) and operated at 50 kV, 40 mA.

For zeolite-based adsorbent: a sample of 3 g was crushed and pressed into an aluminium sample holder then inserted into the X-ray diffractometer. Each sample was measured for 1 h.

For MWCNTs based adsorbents: Even though MWCNTs is considered as a non-crystalline material, its periodic structure results in distinct X-ray diffraction peaks (Oddershede et al., 2007). The identification of the phases in the samples was carried out at room temperature over 4-70° 2θ angular range with a scanning acquisition speed of 0.02 ^{o}/sec.

3.3.2 X-ray fluorescence (XRF) measurements

X-ray fluorescence (XRF) was used conventionally to determine the elemental concentrations of the zeolite-based adsorbents. The samples were dried, ground to small particle size, and homogenized before XRF analysis. The sample powder was placed in the sample cup (diameter 32 mm x depth 14 mm) sealed by polypropylene film. A hand-held XRF X-MET 5100 analyzer (Oxford Instruments, UK) was used with a silicon drift detector (SDD) for in-situ qualitative analysis of elements ranging between Mg and U, between atomic number 12 and 92, respectively. Ten elements (Al, Si, P, S, Cl, K, Ca, Ti, Mn, Fe) were monitored and analyzed in samples. Each sample was scanned three times for 60 s.

3.3.3 Fourier transform infrared spectrometry (FT-IR) measurements

Fourier-transform infrared (FTIR) spectroscopic measurements were carried out by using a BRUKER Vertex 70 type spectrometer with a Bruker Platinum ATR adapter on the ground samples without additional sample manipulation. The spectra were recorded in the range between 400 and 4000 cm^{-1} at a resolution of 2 cm^{-1} at room temperature with a DTGS detector by averaging 512 scans.

3.3.4 Raman spectroscopy measurements

Raman spectroscopy provides information on the structure of the prepared MWCNTs adsorbents. A Bruker RFS 100/S FT–Raman spectrometer equipped with Nd: YAG laser (1064 nm, operated at 30mW) and liquid nitrogen-cooled Ge-diode detector was used in this study. The spectra were recorded by the co addition of 2048 scans with a resolution of 2 cm^{-1}.

3.3.5 Brunauer–Emmett–Teller (BET) measurements

The pore volume and pore size distribution measurements for both adsorbents were carried out by using ASAP 2000 Micromeritics equipment. For zeolite-based adsorbent, the specific surface area, pore-volume, and pore size distribution in the micropore (1.7–2 nm), mesopore (2–50 nm), and the macropore (50–100 nm) diameter ranges were determined by nitrogen adsorption/desorption isotherms. Samples with a weight of 0.5–1.0 g were outgassed in vacuum at 105 °C before using it for the experiments. Pre-treatment of each sample was stopped when the vacuum reached a value of less than 10 µmHg.

The surface areas of the samples were determined by the BET (Brunnauer–Emmett–Teller) method from the corresponding nitrogen adsorption isotherms. The pore size distribution and volume values were calculated from the nitrogen desorption isotherms using the BJH (Barret–Joyner–Halenda) model. The BET specific surface area of the MWCNT and µEMWCNT samples were determined at -196 °C with nitrogen sorption/desorption, the samples were outgassed for 8 h at 300 °C before the measurements to remove the adsorbed moisture and contaminations from the surface.

3.3.6 Scanning electron microscopy (SEM) and energy dispersive X-ray (EDX) measurements

The surface morphology and chemical composition of MWCNTs and µEMWCNTs samples were investigated by Philips XL 30 ESEM scanning electron microscope combined with Energy Dispersive X-ray (EDX) analyzer. An accelerating voltage of 20 kV was used for the analyses. The magnifications of 100x and 300x allow to obtain the images in a 100 and 200 µm scale, respectively. The powder samples were fixed on a carbon holder by double-sided adhesive tape then samples were studied in vacuum 900 µHg (1.2 mBar).

Records were taken on the particle surface, and simultaneous quantitative and qualitative electron probe microanalyses were carried out. The elemental analysis on specimen surface was performed in the so-called spot mode. In this case, the diameter of the microprobe beam was about 20 nm. The spot mode analysis was carried out for 3 points of the same sample. The average concentration of the elements was determined by using surface area scanning mode. In this case, the electron beam penetrated to about 1.6–2.1 μm sample layer depth.

3.3.7 Thermogravimetric analysis (TGA) measurements

Thermogravimetric (TG) and differential thermal analysis (DTA) measurements were carried out in a Derivatograph-C type thermoanalytical instrument (Hungarian Optical Works, Hungary). The samples were heated in an open ceramic crucible with 5 °C/min heating rate in a static air atmosphere.

The thermal stability of the prepared adsorbents was obtained from thermogravimetric analysis (TGA) as it can measure the changes in the physical and chemical properties whilst increasing temperature constantly. Moreover, the grafting rate of microemulsion on adsorbents' surfaces was estimated using the difference of the mass loss between raw and modified material during the thermal treatment.

3.4 OIL ADSORPTION TESTS

The adsorption capacities were evaluated using several methods such as (i) classical standard (i) Westinghouse method, (ii) Total organic carbon (TOC) analyzer, (iii) gas chromatography (GC), and (iv) ultraviolet-visible spectroscopy (UV-Vis). Selection of analysis technique depends on the type of hydrocarbon model (octane- n-C_8H_{18} 95 %, decane- n-$C_{11}H_{24}$, 99 %, dodecane- n-$C_{12}H_{26}$, 99 %, toluene- C_6H_5-CH_3, 99.5 % and kerosene)

3.4.1 Feedstock solution preparations and adsorption tests

Typical hydrocarbons present in produced/spilled oil-contaminated water include aliphatic, alicyclic, and aromatic compounds. Accordingly, several hydrocarbon models were used for the adsorbents examination. It is worth mentioning that each hydrocarbon model was treated and analyzed with a suitable technique. Table 5 presents a summary of the performed experiments.

Table 5: Summary of the performed batch experiments

Method/oil	Carbon con. (mg C/L)	Batch vol.(ml)	Adsorbent wt.,g	
			Zeolite based	CNTs based
Classical method				
Toluene (C_6H_5-CH_3)	anhydrous, 99.8%	-	1.5	1.5
Octane (n-C_8H_{18})	anhydrous, ≥99%	-	1.5	1.5
Dodecane (n- $C_{12}H_{26}$)	anhydrous, ≥99%	-	1.5	1.5
Undecane (n-$C_{11}H_{24}$)	anhydrous, ≥99%	-	1.5	1.5
Kerosene (n-C_{10}-C_{16})	-	-	1.5	-
Distilled water	Pure	-	1.5	-
TOC				
Octane (n-C_8H_{18})	475-500	100	0.5	0.01
Undecane (n-$C_{11}H_{24}$) +SAS and SLES)	500	100	0.5	0.01
GC[1]				
Kerosene (n-C10-C16)	560	250	1	0.01
Undecane (n-$C_{11}H_{24}$)	500	250	-	0.01
UV-Vis				
Toluene	450-550	100	1	0.01

3.4.2.1 Adsorption protocol of kerosene - water solution

The commercially available kerosene (EU number: 649-423-00-8, MOL Co.) was further purified. The obtained kerosene cut contained only alkanes from C_{10} to C_{16}, and it was used for the preparation of kerosene-water mixtures. The kerosene cut had a boiling point range of 174–287 °C, with a density of 0.800 g/mL. The solutions were prepared in a glass flask by adding 175 µL kerosene to 250 mL distilled water, resulting in a kerosene solution with a carbon concentration of 560 mg/L. The model solutions were mixed for 10 min using magnetic stirrer followed by adding the adsorbent in an amount of 100 mg. Then the solutions were kept under continuous mixing for an additional 30 min at room temperature. The adsorbent was separated from the solution with S1 porous glass filter having a pore size of 100–160 µm. The filtered water solution was taken for the extraction step, to prepare the sample for the determination of

---

[1] Higher volume used due to extra extraction step needed before GC analysis

hydrocarbon content by gas chromatographic (GC) method according to Hungarian Standard MSZ 1484-7 (MSZ, 2009).

3.4.3.1 Adsorption of pure hydrocarbon - water solutions

The stock hydrocarbon-water solution was prepared by using as model hydrocarbon; undecane, octane, toluene, and dodecane in range of 450-550 mg C/L. Distilled water and surfactants (sodium salt of secondary-alkane-sulfonate (SAS) or sodium-lauryl-ether-sulfate (SLES) solution was prepared. About 5 m % surfactant calculated for the hydrocarbon content was added into the hydrocarbon-water mixture to stabilize the emulsion. The solutions were kept closed and shaken at a speed of 600 rpm for 1 h. Then, the solutions were kept under sonication for 5 min before use.

TOC and UV-Vis analysis were carried out at fixed hydrocarbon-water emulsion volume (100 mL) containing hydrocarbons, while GC analysis was carried out with 250 ml. Adsorbents were added at optimum dosage, whereas all experiments were conducted at room temperature. The model solutions were mixed for 10 min using magnetic stirrer followed by adding the adsorbent in an amount of 100 mg.

The dosage of zeolite-based adsorbent was varied from 0.03 to 1 g to find the optimal value for maximum removal of hydrocarbon from water. Regarding carbon-based adsorbent, only 10 mg dosage of MWCNTs adsorbent was used to examine the MWCNTs and µEMWCNTs adsorption capacities. The samples were agitated using a mechanical shaker at a fixed agitation speed of 300 rpm.

3.4.4 Instruments and protocols used for the analysis of hydrocarbon concentration measurements in water

The following analytical techniques were used to determine the hydrocarbon removal efficiency of the adsorbents from hydrocarbon-water mixtures:

- Classical Westinghouse method of absorbability;
- Total organic carbon analyzer (TOC);
- UV-visible spectroscopy (UV-Vis); and
- Gas chromatography (GC).

3.4.4.1 Classical Westinghouse method of adsorption

Naturally, primary attempts to investigate the hydrocarbon adsorption from the water had employed the simplest classical method. The classical Westinghouse method of absorbability developed by Muir and co-workers (Muir and Bajda, 2016) was used for this purpose. This test based on oil recovery/ water uptake at room temperature (25±2 ^{o}C) to indicate the performance of sorbents. The adsorption test consisted of adding drops of hydrocarbon compounds to the dry zeolite sample with a known weight (1.5 g) until the point of maximum saturation was reached. The moment when the next drop of hydrocarbon compound flowed over the sorbent (i.e., the liquid was not absorbed) was considered to be the end of the experiment. As the deep cavities are filled, molecules have to diffuse through a large number of intercrystalline pores to find suitable empty cavities. Once the cavities are filled, then molecules being adsorbed in cavities near the outer surface. It is to be noted that, in this test, pure hydrocarbons were used instead of the hydrocarbon-water model. The sorption percentage was determined by comparing the weights of the samples before and after the sorption of hydrocarbon compounds.

3.4.4.2 Protocol for samples analysis via total organic carbon analyzer (TOC)

The hydrocarbon concentrations were measured by using a combustion type TOC analyzer (Elementar, model Vario TOC SELECT; detection range of 4 mg/L to 40 000 mg/L). Initially, all the glassware was washed with 2 % nitric acid and ethanol to remove all the impurities and to avoid any further adsorption of dust or particles from the air. Three samples from the treated solution were taken for the initial concentration measurements, and average values are reported here. For final concentration measurement, 40 mL samples were taken at each time interval for TOC measurement. At each test, the system was calibrated using an appropriate IC (inorganic carbon) and TC (total carbon) standard solutions. For quality control, blank samples, as well as TC and IC samples, were also tested. All the experiments were performed in triplicate, and the average values are reported. The measured values were all within the range of ± 3%.

3.4.4.3 Protocol for samples analysis via UV-Vis spectrophotometric

Toluene was selected as a model hydrocarbon for the UV-Visible spectroscopic studies since this technique is suitable for the identification of aromatic hydrocarbons in water.

The ultraviolet-visible spectrophotometry (UV-Vis) using a deuterium lamp can be used for the determination of the aromatic hydrocarbon content of water samples. Nicolet Evolution 500–UV-Visible double beam spectrometer (Thermo Electron Co.) with 1 cm quartz cuvette was used with measuring a range of 230-400 nm wavelength and equipped with single photomultiplier to detect the aromatic hydrocarbon content of the waters. The preparation of the model toluene-water mixture was the same as given earlier. The surfactant was used in 5% to stabilize the hydrocarbon-water emulsion. After 30 min of running the adsorption test, the adsorbent was separated by filtration, and the organic phase (aromatic hydrocarbon) was extracted from the filtrate by cyclohexane (99.99%, Reanal Ltd.), and the extract was dried over sodium sulfate. Quartz cuvette was used for spectrometric investigation of the obtained sample.

3.4.4.4 Protocol for samples analysis via gas chromatography (GC)

The liquid samples were analyzed by Agilent, GC 7890A type Gas Chromatograph with a J&W HP-5 type capillary column (30 m x 0.320 mm, 0.25 µm film thickness). Flame-ionization detector (FID) was used for the analysis. As mentioned earlier, the determination of hydrocarbon content by gas chromatographic (GC) method was carried out according to Hungarian Standard MSZ 1484-7 (MSZ, 2009).

It is worthy of mentioning that the samples needed some treatment steps before performing GC analysis. Therefore, before the extraction with hexane, 1-chloro-octadecane standard was added to the sample to determine the recovery efficiency of the hydrocarbons. The kerosene-water solution was extracted two times, with 15 mL hexane. The collected hexane fraction was dried with Na_2SO_4 powder. The blank solution was prepared in the same method without adding adsorbent. Kerosene standard was prepared by dissolving 175 µL kerosene in 25 mL hexane to determine the manipulation efficiency of the kerosene–water sample. An internal/injection standard was added to the 25 mL hexane solution, and an aliquot of 2 µL was injected into the gas chromatograph. An injection standard, 1,4-dichlorobenzene, was used for control of the GC analysis.

In the next two chapters, the results obtained from characterization and adsorption tests of carbon nanotube-based adsorbents and zeolite-based adsorbents will be presented.

The results and discussion will be given as per the type of adsorbents (i) carbon nanotube-based adsorbents and (ii) zeolite-based adsorbents. The final conclusions will be presented in Chapter 8.

Chapter 4: Results of MWCNTs based adsorbents

The detailed results of physico-chemical characterizations of the synthesized adsorbent, adsorption experimental results, and outcome of carbon residue analysis are presented and discussed in this chapter.

4.1 CHARACTERIZATION RESULTS OF CARBON-BASED ADSOEBENTS

The formation of a new kind of bond, not present in the raw MWCNTs material was confirmed by FT–IR spectroscopy, while thermal analysis (thermogravimetric analysis (TGA) gives information whether the surface functionalization was successful or not. XRD helped to determine the crystalline structure of the prepared adsorbent. The incorporation of new elements was assessed by means of energy-dispersive X-ray spectroscopy (EDX) and scanning electron spectroscopy (SEM).

4.1.1 Results of the SEM and TEM investigations

The TEM and SEM images of the raw MWCNTs are given in Figure 8, Figure 9, and Figure 10, as provided by the manufacturer.

Figure 8: The transmission electron microscopic (TEM) record of the MWCNTs (By courtesy of the MWCNTs manufacturer)

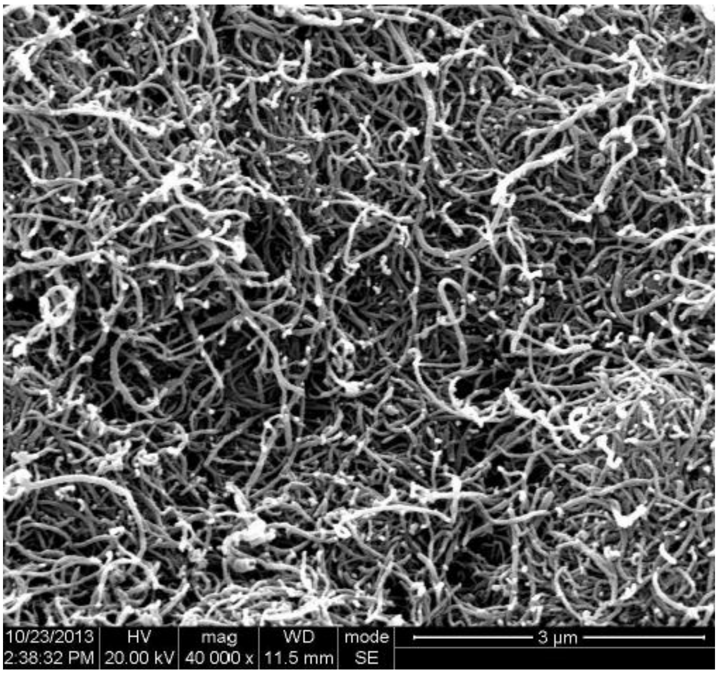

Figure 9: The scanning electron microscopic (SEM) record of the MWCNTs (by courtesy of the MWCNTs manufacturer)

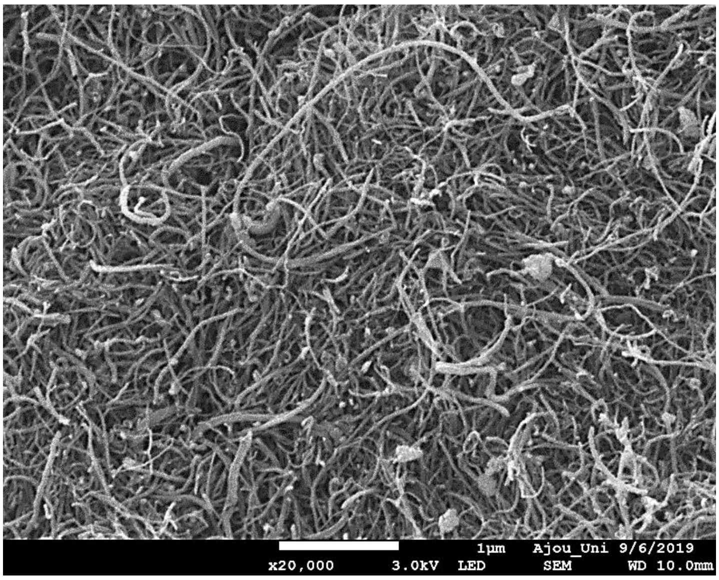

Figure 10: The scanning electron microscopic (SEM) record of the MWCNTs

Based on Figure 8-Figure 10, it can be seen that the MWCNTs are molecular size tubes, which are approximately 10,000 times thinner than the human hair. The MWCNTs consist of rolled-up sheets, in which case the primary building units are hexagonal carbon formations. Figure 9 illustrates the MWCNTs without contamination. The SEM record taken by the author (Figure 10) were in consistent with the one offered by the manufacturer. SEM and TEM analyses revealed interesting morphological features in the Timesnano MWCNTs as it had a mixture of smooth-walled nanotubes with continuous hollow cores that were mainly bundles and ropes that can individually be seen. For µEMWCNTs, Figure 11 b and d showed that microemulsification created thicker tubes. High magnification SEM images of this sample show the individual thicker tubes, which are attributed to the oil/water interface, which essentially acts as a site for the tubes' walls to aggregate and coalesce.

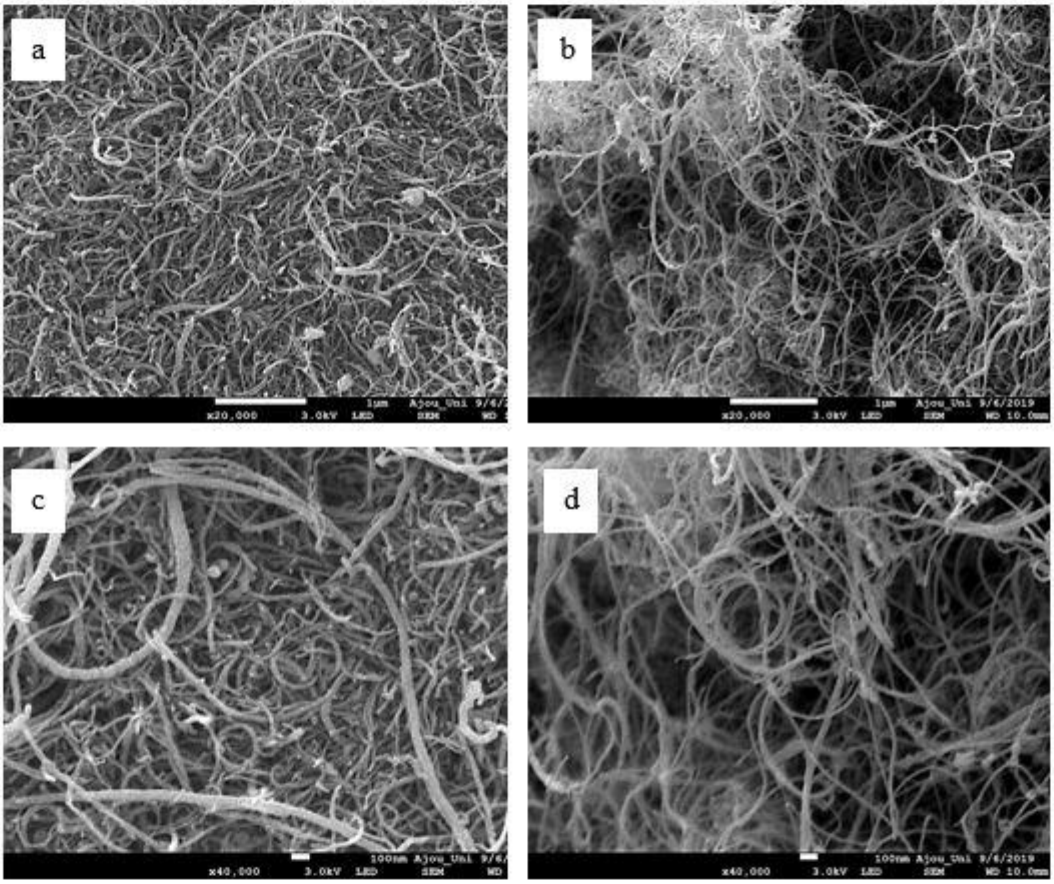

Figure 11: The scanning electron microscopic (SEM) record of the (a) Raw MWCNTs, (b) µEMWCNTs at magnification: x 20.000 and (c) Raw MWCNTs, (d) µEMWCNTs at magnification: x 40.000

4.1.2 Results of the morphological measurements

The specific surface areas and pore size distributions of samples MWCNTs and µEMWCNTs were studied and are presented in Table 6. In the case of the MWCNTs sample, the measurements were carried out at 30 and 160 °C as well, and it was concluded that no significant difference could be observed between the samples, which were pre-treated at different temperatures. This means that the pre-treatment temperature does not influence the pore size distribution and the specific surface area. It can be seen that there is a significant decrease in the BET specific surface area of the modified sample compared to the original one as it was ~155-156 m^2/g MWCNTs and for µEMWCNTs reached up to 98 m^2/g.

Table 6: Nitrogen adsorption results of samples MWCNTs and µEMWCNTs

Sample and Pre-treatment temp.	**S_{BET} (m^2/g)**	**S_{BJH} (m^2/g)**	**S_{micro} (m^2/g)[2]**	**$S_{1.7-300}$ (cm^3/g)[3]**	**S_{micro} (cm^3/g)[4]**	**D_{av} (nm)**
MWCNTs, 30 °C	155	159	14.7	0.7781	0.0067	13.1
MWCNTs, 160 °C	156	158	15.2	0.6847	0.0069	12.5
µEMWCNTs, 65 °C	98	110	0	0.7026	0	18.3

It was concluded that the pore structure did not change significantly by the functionalization of the MWCNTs. The BJH specific surface area of the µEMWCNTs was 110 m^2/g, while the BJH specific surface area of the untreated MWCNTs was 158 m^2/g. As a result of the surface treatment/functionalization, the pore volume of the µEMWCNTs decreased, and the pore diameters increased (Figure 12). In the case of the untreated samples, the pore diameter of the MWCNTs was 12-13 nm, while the pore diameter of µEMWCNTs was 18.3 nm. In addition to this, it was also observed that the micropores have disappeared after the microemulsion treatment (Figure 12 and Figure 13). This can be attributed to the attached hydrocarbon chain, which covered

---

[2] The specific surface area of micropores (< 2 nm)

[3] Pore volume according to Barrett, Joyner and Halenda (BJH) theory for pores having a diameter between 1.7 and 300 nm

[4] Volume respectively of micropores (< 2 nm)

the MWCNTs surface. The smallest pores (~2.7 nm) are filled with the compounds used during the functionalization of the MWCNTs.

As a consequence of the surface treatment/functionalization, the pore volume of the µEMWCNTs decreased, and the pore diameter increased. BJH pore distribution plot shows two maxima at ~2.7 nm and at ~40 nm in the mesoporous region, which can be attributed to inner and outer pore diameters. Li et al. (Li et al., 2004) observed a little bit higher inner pore diameter for MWCNTs (3.3 - 3.5 nm), and it can be due to the openings between the walls of the MWCNTs that are formed when they twist together tightly. Pores having a width between 20-60 nm are present in a higher amount in the investigated samples (Figure 13).

The BET and BJH surface areas for all investigated samples are quite similar, indicating the uniform occurrence of tubular pores in the carbon nanotubes before and after the microemulsion modification (Table 6). These results show good agreement with the published work related to the characterization of MWCNTs from a different manufacturer (Birch et al., 2013). The adsorption and desorption isotherms of the MWCNTs and µEMWCNTs are shown in Figure 14.

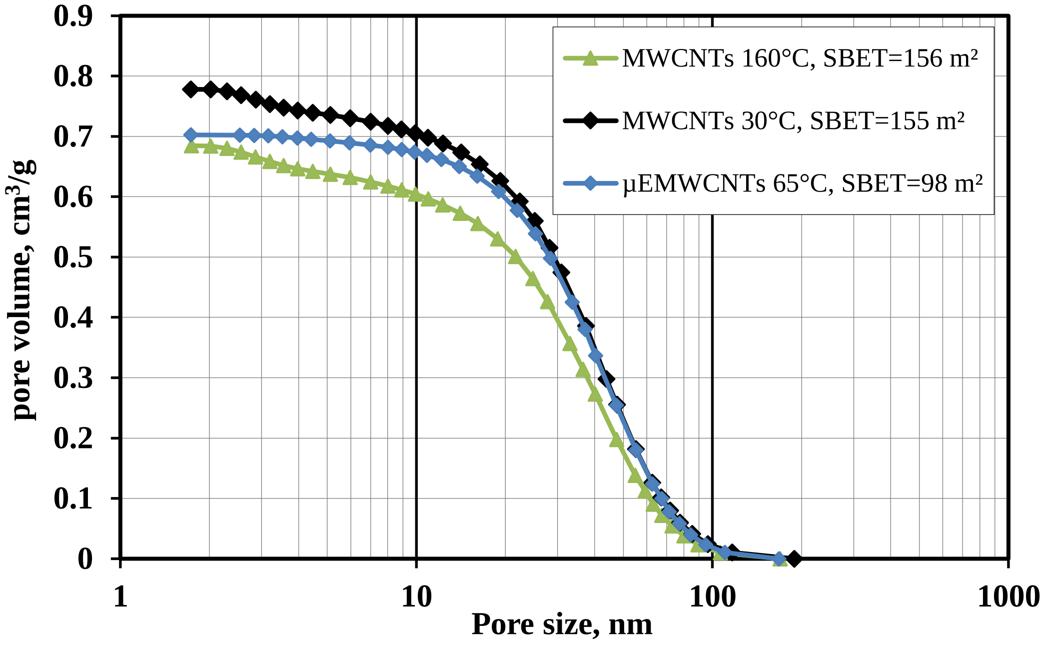

Figure 12: Cumulative mesoporous volume distribution of MWCNTs

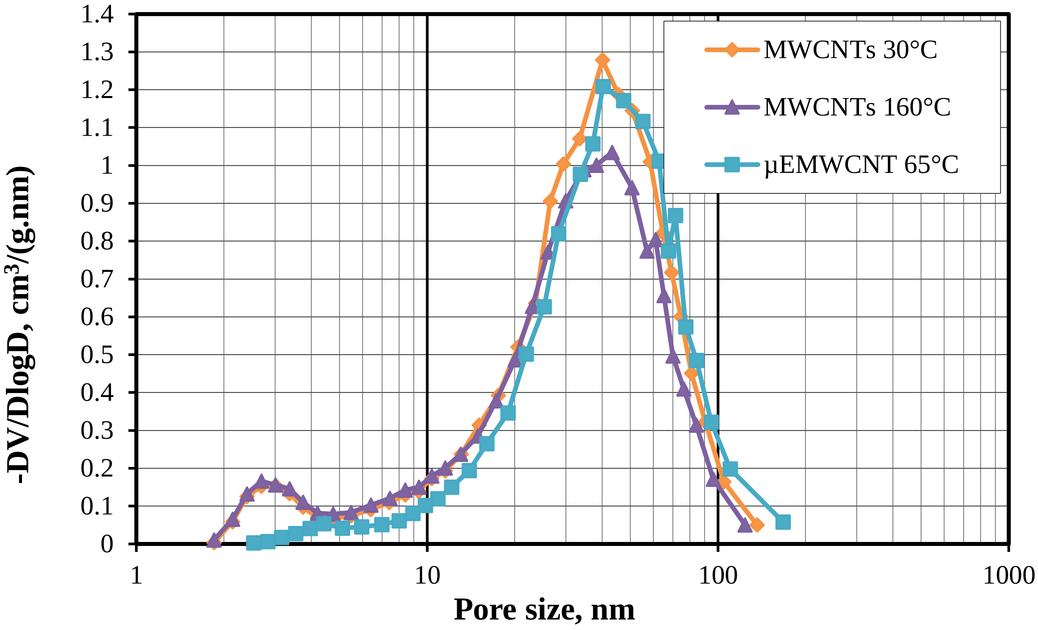

Figure 13: Logarithmic pore volume distribution of MWCNTs calculated based on the BJH theory

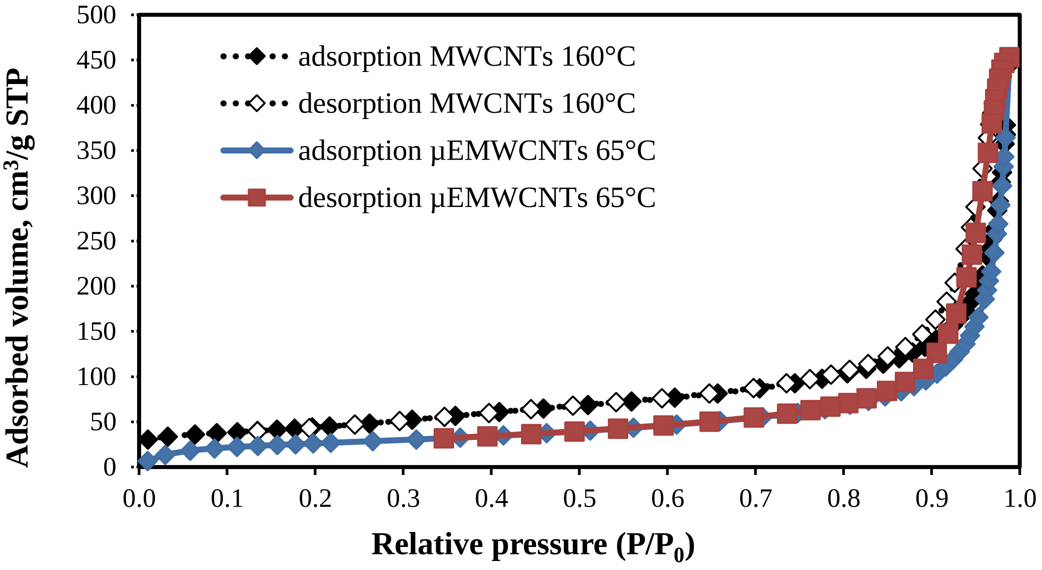

Figure 14: Adsorption and desorption isotherms of MWCNTs

All samples exhibited an IV type of isotherms (Sing, K et al., 1985). The presence of a hysteresis loop of type HI is an indication of capillary condensation and presence of meso- and macropores of regular shape (Sing, K et al., 1985). Also, it is an indication of the existence of non-capped pores of carbon nanotubes (Gheorghiu et al., 2014).

The observed weight losses of the MWCNTs sample at 30 °C and 160° C pre-treatments under vacuum were 0.21 and 0.32 m %, respectively. A similar mass loss value was observed for µEMWCNTs at pretreatment at 65 °C under vacuum. The mass loss is an indication of the desorption of the adsorbed gases/components from the surface of the sample. This result is in agreement with the results of the thermoanalytical investigations listed in Section 4.1.4, where mass losses up to 200 °C temperature were less than 0.5 m % for both samples, and the decomposition of MWCNTs started above 500 °C.

4.1.3 Results of the XRD investigations

X-ray diffraction investigations were carried out on the MWCNTs and the µEMWCNTs samples to determine the crystalline structures of the carbon nanotubes.

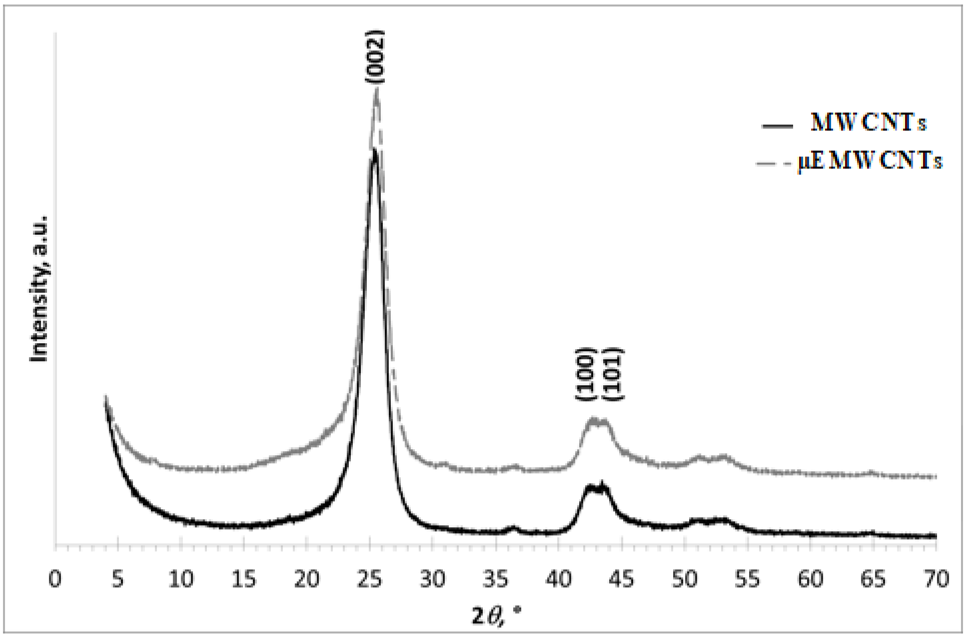

Figure 15: XRD patterns of MWCNTs and µEMWCNTs samples

As can be seen in Figure 15, two main characteristic peaks at 2θ = 25.3° and ~ 43° can be observed. MWCNTs can be formed from rolled graphene sheets with their interlayer distance similar to that of graphite ($d_{(002)=}$0.335nm) (Yusa and Watanuki, 2005).

The most intensive peak appears at $2\theta = 25.3°$, and it can be attributed to (002) plane of the single graphene layer of hexagonal structure with a d-spacing interlayer distance of 0.352 nm (Ovejero et al., 2006). This graphene sheet distance remains almost the same, even in the case of µEMWCNTs ($d_{(002)} = 0.350$ nm). The second main peak with two maxima at 2θ ~ 43° is observed for both samples, and it can be due to the reflections of the diffraction sheet of the nanotubes (100) and (101). This peak shows the reflection within the graphene hexagonal layer (Rebelo et al., 2016).

4.1.4 Thermoanalytical investigations

The composition of the µEMWCNTs was determined by elemental analysis and thermal analysis using a combined TG-DTG-DTA technique. The measurements were carried out in argon flow to determine the thermal stability, purity of MWCNTs, and to investigate the effect of emulsification. The decomposition curves of MWCNTs and µEMWCNTs are given in Figure 16, while the mass loss data are summarized in Table 7.

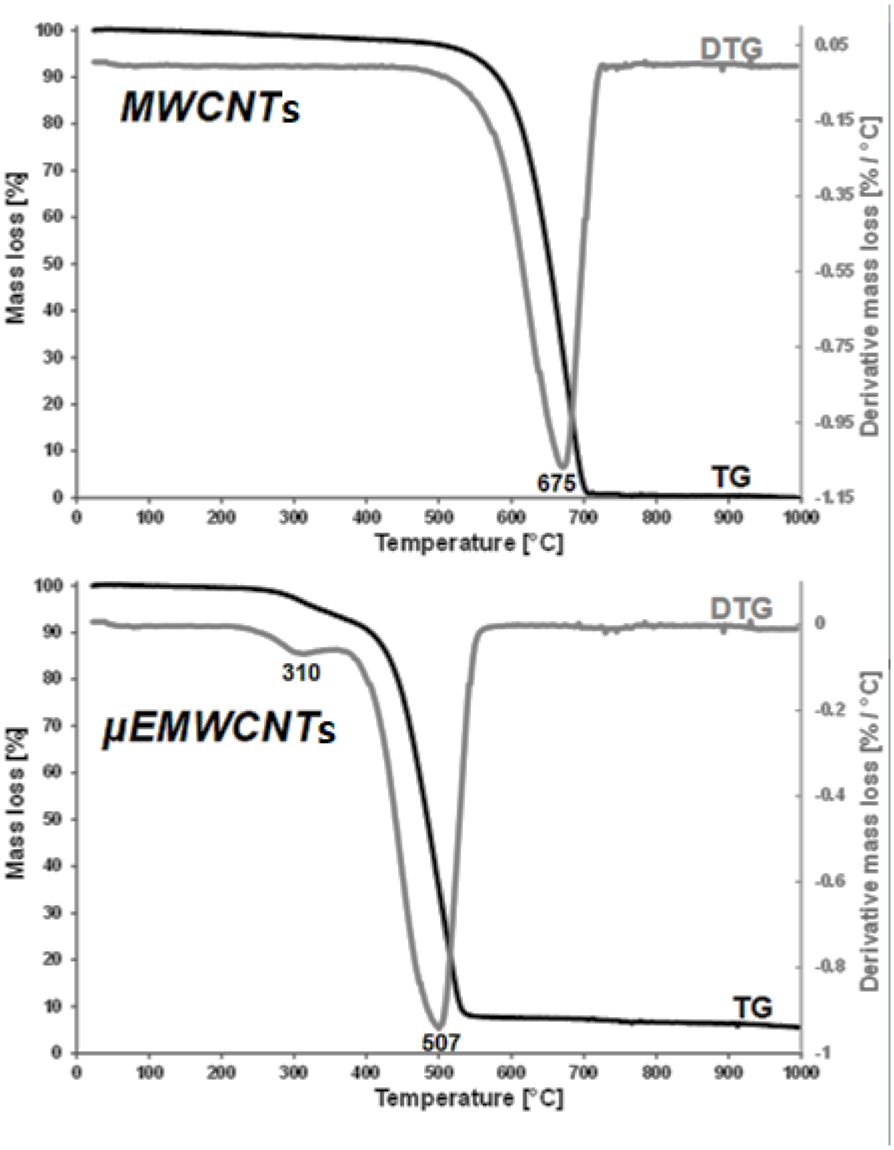

Figure 16: TG and DTG curves of samples MWCNTs and µEMWCNTs

In Figure 16, a single major mass loss step (480-720 °C, Δm= -96.59 m %) is observed for the MWCNTs sample, which is typically in the decomposition temperature range of MWCNTs (Lehman et al., 2011). At 1000 °C, the total mass loss of 100 % indicates that there is no metal catalyst residue present in the sample used during the production of MWCNTs by the CVD method (Hirsch, 2002).

Two major mass loss steps can be observed on the DTG curve for the µEMWCNTs. The step between 200 °C and 376 °C can be attributed to the loss of adsorbed myristic and lauric acid (Δm= -7.04 m %). The decomposition of the µEMWCNTs can be observed between 376 and 575 °C (Δm= -84.89 m %) (Table 7). The significant decrease in the decomposition temperature indicates a functionalized surface and/or the structural defect sites in the µEMWCNTs sample (Lehman et al., 2011). Up to 1000 °C, the overall mass loss is 94.49 m %, while the residual mass is 5.51 m %. This latter figure can be explained due to the presence of pollutants introduced during the microemulsion modification.

Table 7: Mass loss data of samples MWCNTs and µEMWCNTs during thermoanalytical studies

Sample	**T_{start} (°C)**	**T_{max} (°C)**	**T_{end} (°C)**	**Mass loss step**	**Reason of step**
MWCNTs	24	-	200	0.49	Water desorption
	480	675	720	96.59	MWCNTs decomposition
	720	-	1000	0.79	Loss of residual carbonaceous
	Sample mass: 4.276				Total mass loss: 100%
µEMWCNTs	22	-	200	0.36	Water/adsorbed microemulsion desorption
	200	310	376	7.04	Adsorbed microemulsion de-
	376	507	575	84.89	MWCNTs decomposition
	575	-	1000	2.20	Impurities of the coconut oil
	Sample mass: 4.428				Total mass loss: 94.49 %

4.1.5 Raman spectroscopic measurements

Raman spectroscopy can be expediently used for the determination of characteristic features of carbon nanotubes. The Raman spectra of MWCNTs are well interpreted and are usually used for the interpretation of the more complicated MWCNTs.

The radial breathing mode (RBM, between 120 and 350 cm^{-1}) corresponds to the radial expansion-contraction of carbon atoms in the radial direction. The D-band (around 1350 cm-1) is typical for graphite-like materials and stems from the presence of structural defect sites. The G-band (around 1600 cm^{-1}) indicates the tangential vibrations of carbon atoms. The overtone of D-band (G' band) can be found around 2600 cm^{-1} and is indicative of the long-range order in the structure (Dresselhaus et al., 2005; Lehman et al., 2011). The Raman spectra of MWCNTs and µEMWCNTs are given in Figure 17.

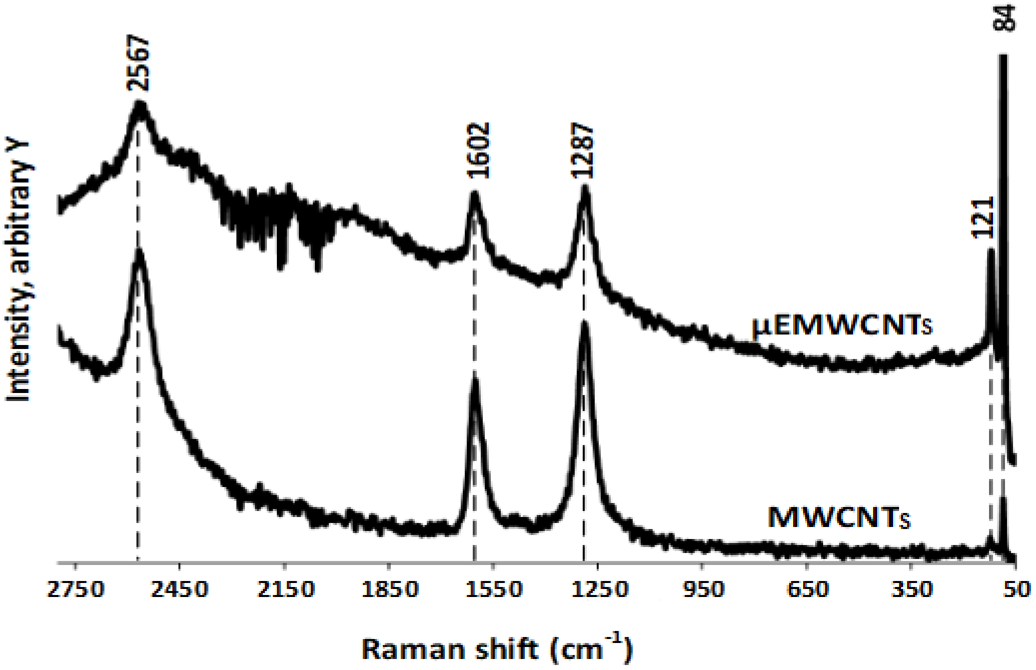

Figure 17: The Raman spectra of samples MWCNTs and μEMWCNTs

The well-separated D-band (1287 cm^{-1}), G-band (1602 cm^{-1}), and G’ band (2567 cm^{-1}) can be observed in the Raman spectra, which are characteristic of tubular CNTs. The 121 cm^{-1} vibrations can be attributed to the radial breathing mode. The peak positions remain unchanged after modification. The structural quality and purity of CNTs are usually estimated using the D/G bands intensity ratios. However, the G-band intensity is sensitive to carbon impurities, while the G’/D intensity ratios could be more accurately used for quality and purity assessment (Dileo et al., 2007). The calculated I_D/I_G and $I_{G'}/I_D$ values of MWCNTs were 1.32 and 1.31, while for the μEMWCNTs, the ratios were 1.01 and 1.28, respectively. The decreasing intensity ratio values indicate a slightly increased disorder/impurity in the MWCNTs structure as a result of microemulsion modification. The μEMWNTs exhibited significant changes in the CH bending vibrations as compared to the raw MWCNTs, demonstrating the existence of intermolecular CH-π interactions between the carbon nanotubes and lauric/miristic acid.

4.1.7 FT-IR spectra measurements

The changes in the surface functional groups of μEMWNTs after toluene adsorption were also confirmed by FTIR spectra through the changes in the positions of some the peaks as well as the appearance of some new peaks. Fig. 10 shows the FT-IR spectra of µEMWNTs before and after toluene adsorption with different groups. For the µEMWNTs, the bands in the range of 1630–1400 cm^{-1} can be assigned to the C=C groups in aromatic rings, and it can be attributed to the π–π interactions that developed between cyclic organic pollutants and the sheets of the µEMWNTs (Al-ghouti and Al-degs, 2011). In a detailed description, the aromatic ring of toluene act as electron-acceptor and the carboxylic oxygen-atom of the µEMWNTs surface act as electron-donor and this proof the chemisorption adsorption for the uptake of toluene by µEMWNTs (Pourzamani et al., 2015). In addition, the spent µEMWNTs spectra shows new bands at 2910 and 2980 cm^{-1} in the carbon-hydrogen region, as a consequence of microemulsion modification and toluene adsorption. The bands at 2910 and 2980 cm^{-1} are assigned to -OH stretch from carboxylic groups (-COOH and -COH) (Pourzamani et al., 2015). In fact, FTIR revealed the non-polar nature of surface functional groups of the fresh µEMWNTs, as spent µEMWNTs spectra display a new peak in the range of around 3400-3500 cm^{-1} wavelength that was absent in the spectra of fresh µEMWNTs, this peak is related to O-H stretch.

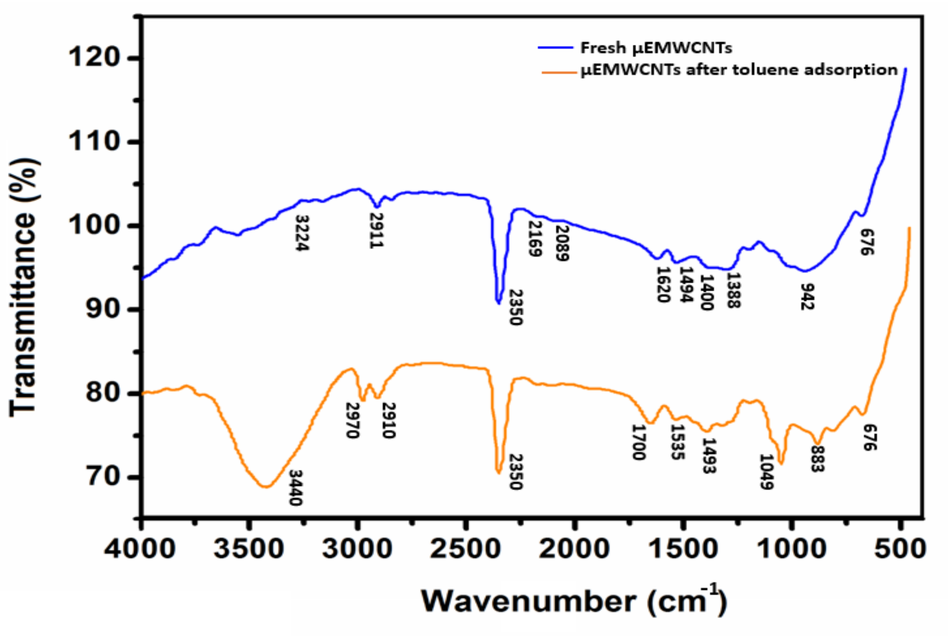

Figure 18. Fourier transform infrared spectra of samples fresh µEMWCNTs and spent µEMWCNTs.

4.2 ADSORPTION TEST RESULTS

4.2.1 Performance evaluation of µEMWCNTs by classical Westinghouse method

Table 8 summarizes the Westinghouse sorption results. The sorption (S) in %, was calculated based on the (Eq. 1).

$$S = \frac{M_p}{M_o} \times 100\% \quad (1)$$

Where, M_p: a mass of adsorbed hydrocarbon, g; and M_o: the weight of the sorbent, g. It can be concluded that the µEMWCNTs sample exhibited higher sorption capacity than the MWCNTs in all tested hydrocarbon models, which can be attributed to the enhanced hydrophobicity of MWCNTs and thus high sorption capacity for the µEMWCNTs was measured. For example, when the n-octane model was used, the sorption capacity of µEMWCNTs reached 6.07 g/g while the MWCNTs exhibited lower sorption capacity reaching up to 4.64 g/g.

Table 8: Sorption of different hydrocarbons over samples MWCNTs and µEMWCNTs (g adsorbate/g adsorbent)

Model hydrocarbon/Water	**Sample**	**Sorption (g/g)**
Octane	MWCNTs	4.64
	µEMWCNTs	5.77
Dodecane	MWCNTs	5.16
	µEMWCNTs	5.93
Undecane	MWCNTs	4.67
	µEMWCNTs	5.83
Toluene	MWCNTs	4.67
	µEMWCNTs	5.68
Water	MWCNTs	2.48
	µEMWCNTs	-

Based on the obtained results, it can be observed that water cannot be adsorbed on the µEMWCNTs due to the strong hydrophobicity of this material and adequate attached adsorption sites. These results are in accord with the previous results obtained by Liu and co-workers (Liu et al., 2015). It was shown that the functionalization technique used was efficient in modifying the MWCNTs' interactions with the adsorbate and can create more adsorption sites with high oil uptake capacity.

4.2.2 Performance evaluation of µEMWCNTs via by TOC analysis

During the TOC investigations, undecane-water mixtures were used to investigate the hydrocarbon removal efficiency from the water. Surfactants (SAS and SLES) were used to stabilize the hydrocarbon-water emulsion. Table 9 summarizes the results regarding the hydrocarbon removal from water over the MWCNTs and µEMWCNTs. The removal efficiency was calculated as per Eq.2:

$$RE\ (\%) = \frac{(C_i - C_f)}{C_i} * 100 \quad (2)$$

Where

C_i: initial concentration of metal ions (mg/L),

C_f: final concentration of the contaminant in the solution at equilibrium (mg/L).

Based on the experimental results, it can be concluded that the µEMWCNTs is suitable sorbent for the removal of paraffin hydrocarbons from water.

Table 9: n-$C_{11}H_{24}$ removal efficiency of MWCNTs determined by TOC

Materials	n-$C_{11}H_{24}$ RE (%)	Adsorption capacity (g/g)
SLES+ C_{11}+MWCNTs	32 ± 5	1.6
SLES + C_{11}	79 ± 5	3.95
SAS+ C_{11} +MWCNTs	33 ± 5	1.65
SAS+	83 ± 5	4.15

Based on data presented in Table 9, it can be observed that the µEMWCNTs exhibit higher undecane removal efficiency in comparison with the untreated MWCNTs. No significant difference can be observed between using surfactants SLES and SAS in the undecane removal experiments, which means that the surfactants functioned as it was expected.

4.2.3 Performance evaluation of µEMWCNTs by GC results

Undecane and kerosene were used as hydrocarbon model to study the hydrocarbon removal efficiency over raw and microemulsified MWCNTs, and the results were compared with that of obtained over commercial activated carbons. The measurement data are presented in Table 10.

The higher undecane removal efficiency of 94% was achieved over µEMWCNTs sorbent as compared to MWCNTs (57%). Kerosene removal from water by adsorption method was around 35 % in the presence of MWCNTs. By using µEMWCNTs, this value increased up to 96%; however, it is higher than that of obtained over the widely used commercial Chemviron Carbon sorbent (55%). The lower hydrocarbon removal efficiency was obtained over Norit GAC 1240EN activated carbon sorbent (27%) from the two commercial activated carbon sorbents.

Table 10: Undecane and kerosene removal efficiencies over MWCNTs, µEMWCNTs, and commercial activated carbon sorbents

Sample	**Carbon conc. (mg C/ l)**	**RE (%)**	**Adsorption capacity (g/g)**
	Undecane (n-$C_{11}H_{24}$)		
Blank/Initial	500	0	
MWCNTs	214	57 ± 5	2.86
µEMWCNTs	30	94 ± 5	4.7
	Kerosene (n-C_{10}-C_{16})		
Blank/ Initial	560	0	
MWCNTs	352	35 ± 5	2.08
µEMWCNTs	22	96 ± 5	5.38
Chemiviron Carbon	240	55 ± 5	3.2
Norit GAC 1240EN	399	27 ± 5	1.61

4.2.4 Performance evaluation of µEMWCNTs by UV-Vis spectrophotometric

As mentioned in para 3.4.4.3, toluene was selected for the UV-Vis spectrophotometric studies since the toluene concentration change can easily be followed by UV-Vis spectrophotometry (Reichenbächer and Einax, 2011). The results of UV-Vis spectrophotometric investigations are summarized in Figure 19 and in Table 11.

The change in the toluene concentration is proportional to the absorbance. The toluene removal efficiency from the toluene-water mixture over MWCNTs and µEMWCNTs can be investigated. According to the literature (Reichenbächer and Einax, 2011), the characteristic peak of toluene in hexane appears at 269 nm.

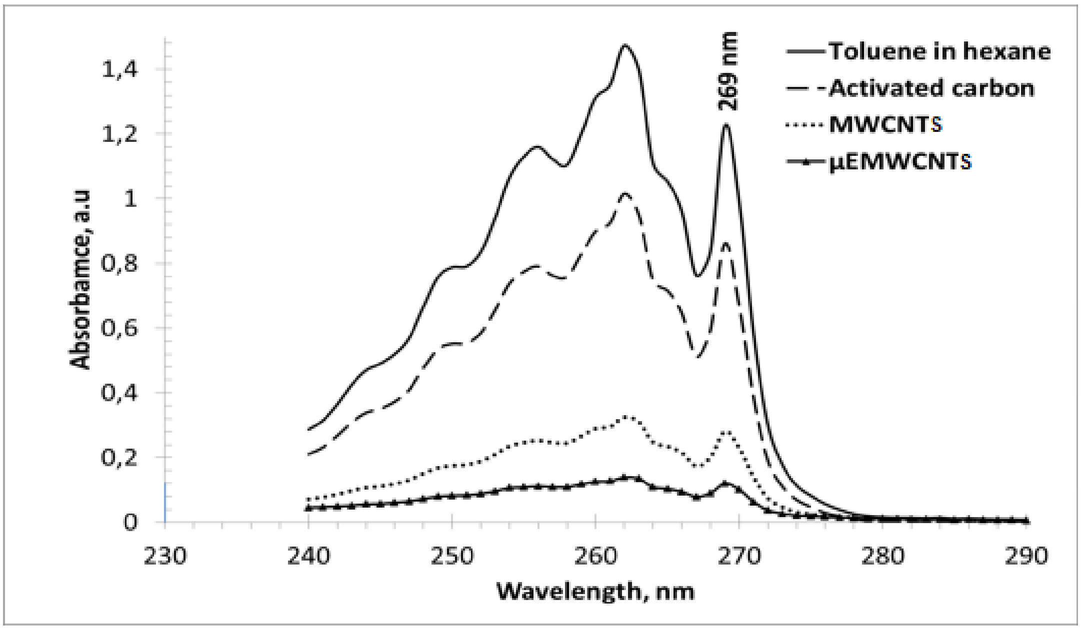

Figure 19: UV-Vis spectrophotometric results for MWCNTs and µEMWCNTs

The toluene in hexane was used only as a reference curve to illustrate the identification of the toluene. It can be seen in Figure 19, and in Table 11 that the toluene concentration decreased significantly after treatment over µEMWCNTs (the peak at 269 nm decreases) in comparison with MWCNTs and activated carbon. Not only toluene peak is reduced, however, the peak areas of impurities in the range of 240-278 nm decrease as well.

Table 11: UV-Visible spectrophotometric results over samples MWCNTs and µEMWCNTs form the removal of toluene

Sample	**Abs.** **λ : 269 nm**	**C_f (mg C/L)**	**RE (%)**	**q_e (g/g)**
Blank	1.23	500	-	
Activated carbon (Chemviron)	0.86	350	30	1.5
MWCNTs	0.28	114	77 ± 7	3.86
µEMWCNTs	0.12	49	90 ± 7	4.51

Based on the experimental results, it can be concluded that the µEMWCNTs proved to be more efficient for the removal of toluene from the toluene-water mixture (90%) in comparison with the untreated MWMCNTs (77%). It can be seen in Figure 19 that the removal efficiency of the activated carbon (Chemviron) did not approach that of the µEMWCNTs since it achieved a removal efficiency up to 30% only; however, it is to be noted that over activated carbon not only the toluene but the water adsorbs as well (McCallum et al., 1999).

4.2.5 Kinetic studies over µEMWCNTs

Series of adsorption batch tests were performed at different adsorption time and room temperature to investigate the equilibrium sorption capacity of toluene over µEMWCNTs. In each run, 10 mg of µEMWCNTs were added in a 100 ml toluene-water stock solution, with a carbon concentration of 500 mg C/L. The solutions were mixed by a magnet mixer at 300 rpm, as mentioned in section 3.4.3.1.

The main objective of the equilibrium studies was to determine the maximum capacity of µEMWCNTs towards toluene removal under the studied conditions and accordingly to make a comparison with raw MWNCTs. Figure 20 shows the adsorption kinetics of toluene; the uptakes reached equilibrium at approximately 60 min. The adoption capacity can be calculated according to the Eq. 3

$$Q = \frac{(C_i - C_f)xV_S}{W_{ads}} \quad (3)$$

Where C_i and C_f (mg/l) are the concentrations of adsorbate at initial and at time t (min), respectively, W (mg) is the mass of adsorbent, and V (ml) is the volume of the mixture.

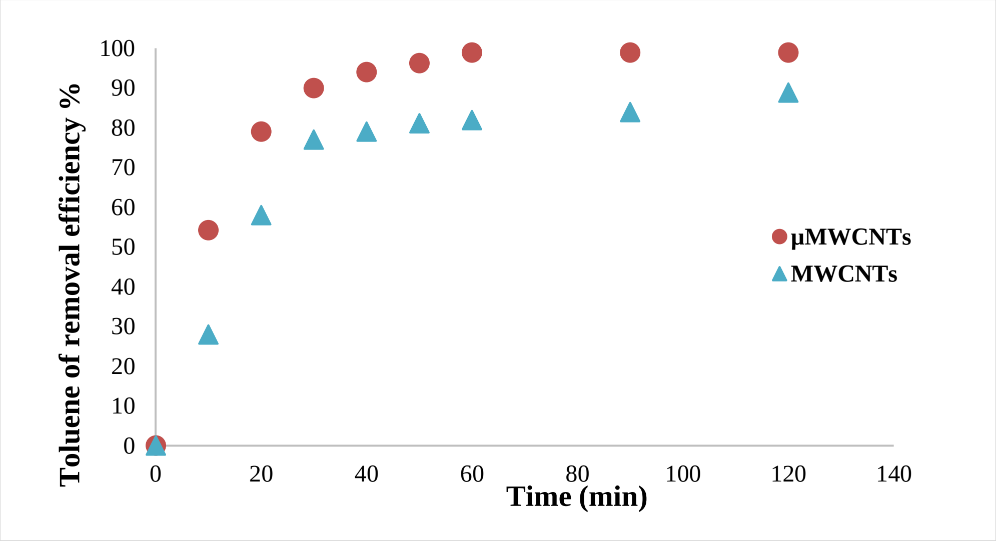

Figure 20: The change in toluene removal efficiency of over µEMWCNTs and MWCNTs in the function of contact time

It can also be indicated from Figure 20 that the adsorbed amounts of toluene increase rapidly with time and then reach equilibrium in about 60 min. At this time, the µEMWCNTs maximum uptake for toluene is 4.99 g/g, which is higher than that of raw MWCNTs 4.05 g/g (see Appendix A). The higher adsorption capacity of toluene by µEMWCNTs compared to MWCNTs can be attributed to the enhanced hydrophobic properties of µEMWCNTs.

It is essential to be able to expect the rate at which oil is removed from aqueous solutions to scale up the adsorption process. To present an equation representing kinetic adsorption, three mechanisms; pseudo-first-order and pseudo-second-order equations (Wu, 2007; Xiao et al., 2018) and intraparticle diffusion (Lv et al., 2018) were taken into consideration (Eq. 4, 5, 6 respectively).

Pseudo 1st order: $\ln(q_t - q_e) = \ln(q_e) - k_1 t$ (4)

Pseudo 2nd order: $\frac{t}{q_t} = \frac{1}{k_2 {q_e}^2} + \frac{t}{q_e}$ (5)

Intraparticle diffusion: $q_t = k_p t^{1/2} + C$ (6)

Where q_e (g/g) is equilibrium uptake, k_1 (1/min) is the adsorption rate constant of 1st order model, k_2 (g/g. min) is the rate constant of 2nd order model, k_p (g/g.min$^{0.5}$) is the intraparticle diffusion rate constant, and parameter, C is a constant expressed in (g/g).

Table 12, in conjunction with Figure 21-23, summarize the models applied for the analysis of kinetics data and the correlation coefficients (R^2) for each model obtained by nonlinear regression analysis for toluene adsorption by µEMWCNTs. Moreover, it must be emphasized that there is a statistical issue in the usual method employed in the literature to estimate adsorption kinetics. Especially, first and second-order laws, thus the experimental results for q_e, must be compared for their abilities to represent the real adsorption capacity q while complying with the condition $R^2 > 0.8$ (Simonin, 2016).

Table 12: Kinetic parameters of the pseudo 1st order, pseudo 2nd, and intra-particle diffusion models for toluene adsorption by µEMWCNTs

Parameter	**Pseudo-first order model**			
Toluene	k_1 (min^{-1})	q_e , cal (g/g)	q_e , exp (g/g)	R^2
	0.0456	1.3169	4.9445	0. 8519
	Pseudo-second order model			
	k_2 (min^{-1})	$q_{e,}$ cal (g/g)	q_e , exp (g/g)	R^2
	0.0303	5.2854	4.9445	0.9976
	Intraparticle diffusion			
	k_p (mg/g min$^{0.5}$)	C (g/g)		R^2
	0.4366	1.2925		0.5831

Figure 21 shows a plot of the linearized form of the pseudo-first-order model for the initial 40 minutes. However, the experimental data diverge significantly after 40 minutes. It can be observed from Figure 22 that correlation coefficients for the linear plots of t/qt against time from the pseudo-second-order rate law are greater than 0.995. This suggests that this sorption system is not a first-order reaction or intraparticle diffusion model. In Table 12, one can notice that optimum adjustment is obtained with k_2 because it gives a value for $q_{e;\,cal}$ that is in slightly better agreement with $q_{e;exp}$. Thus, the pseudo-second-order model is the best-correlating model. These results based on the assumption that the rate-limiting step may be chemical sorption or chemisorption involving valency forces through sharing or exchanging of electrons between sorbent and sorbate. This provides the best correlation of the data. This conclusion, in agreement with several adsorption studies, stated that the pseudo-second-order model provides the best correlation for several systems (F. Elkady, 2017; Ho and Mckay, 1999).

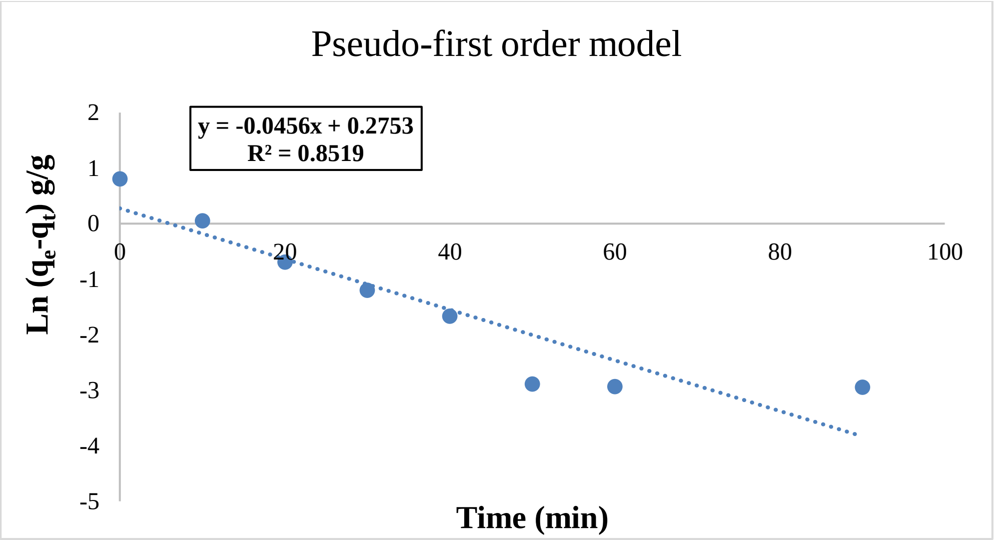

Figure 21: Adsorption kinetics of toluene over µEMWCNTs, pseudo 1st order plot

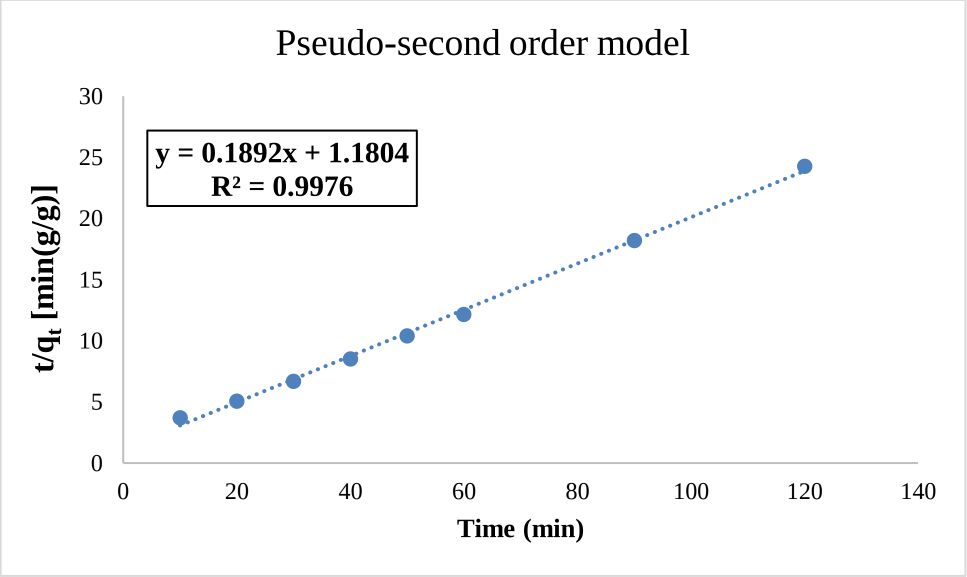

Figure 22: Adsorption kinetics of toluene over µEMWCNTs, pseudo 2nd order plot

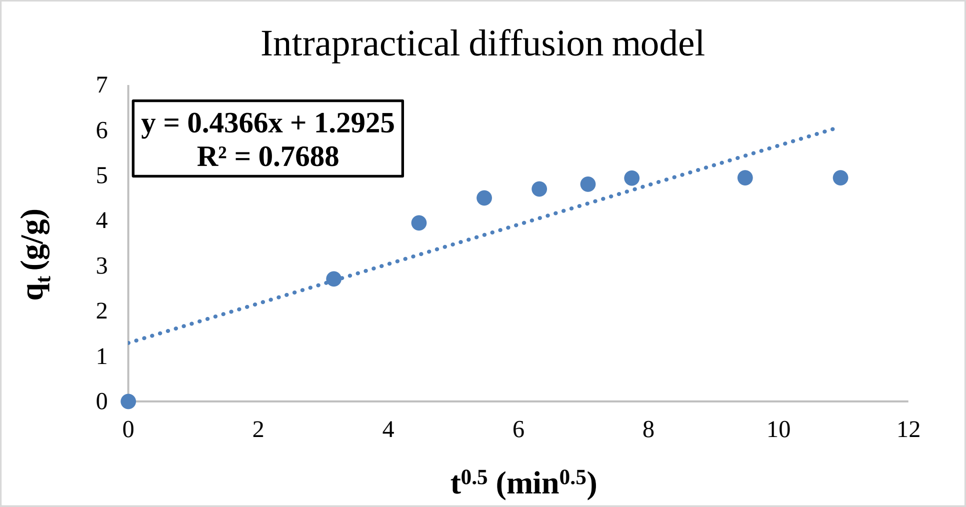

Figure 23: Adsorption kinetics of toluene over µEMWCNTs, intraparticle diffusion plot

The effect of temperature on the adsorption rate of toluene over µEMWCNTs was investigated at 25 and 60 ^{o}C. Figure 24 presents the effect of temperature on adsorption capacity value. At higher temperature (60 ^{o}C), the maximum adsorption capacity was reached in a shorter time (40 min), while at 25 ^{o}C, it reached the maximum value 60 min. Moreover, the 40 min adsorption capacity at 25 and 60 ^{o}C was 4.811 and 4.97 g/g, respectively. The effect of changing the temperature on the equilibrium capacity of the µEMWCNTs is attributed to the reduction of solution viscosity at a higher temperature, which in turn, will increase the rate of diffusion of toluene across the external boundary layer and in the internal pores of the µEMWCNTs.

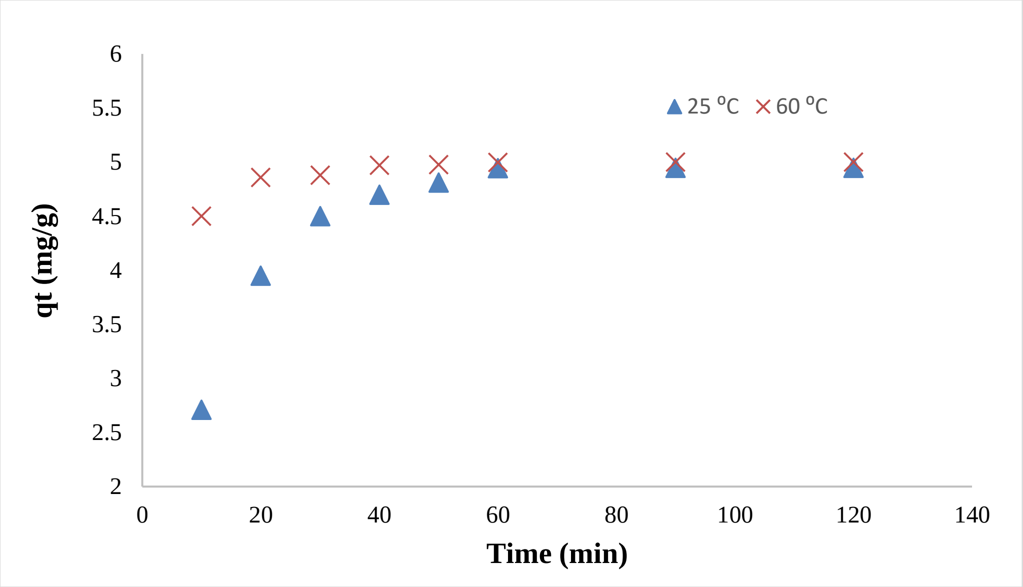

Figure 24: Kinetic analysis of temperature effect (µEMWCNTs = 10 mg/in 100 ml toluene-water solution 500 mg C/L)

Chapter 5: Discussion of the results obtained over MWCNTs

There has not been a report of synthesizing oil adsorbent from MWCNTs by means of microemulsification. Fewer than fifty examples exist of CNT based nanocatalyst constructed using microemulsion technique. Microemulsion modification was used to increase the hydrophobic properties of MWCNTs. Microemulsion is defined as thermodynamically stable solutions, macroscopically homogeneous due to the dispersion of two immiscible fluids by the aid of surfactant, and it contains at least three components, specifically a nonpolar phase (often, oil), a polar phase (frequently, water), and a surfactant (Malik et al., 2012) (Figure 25).

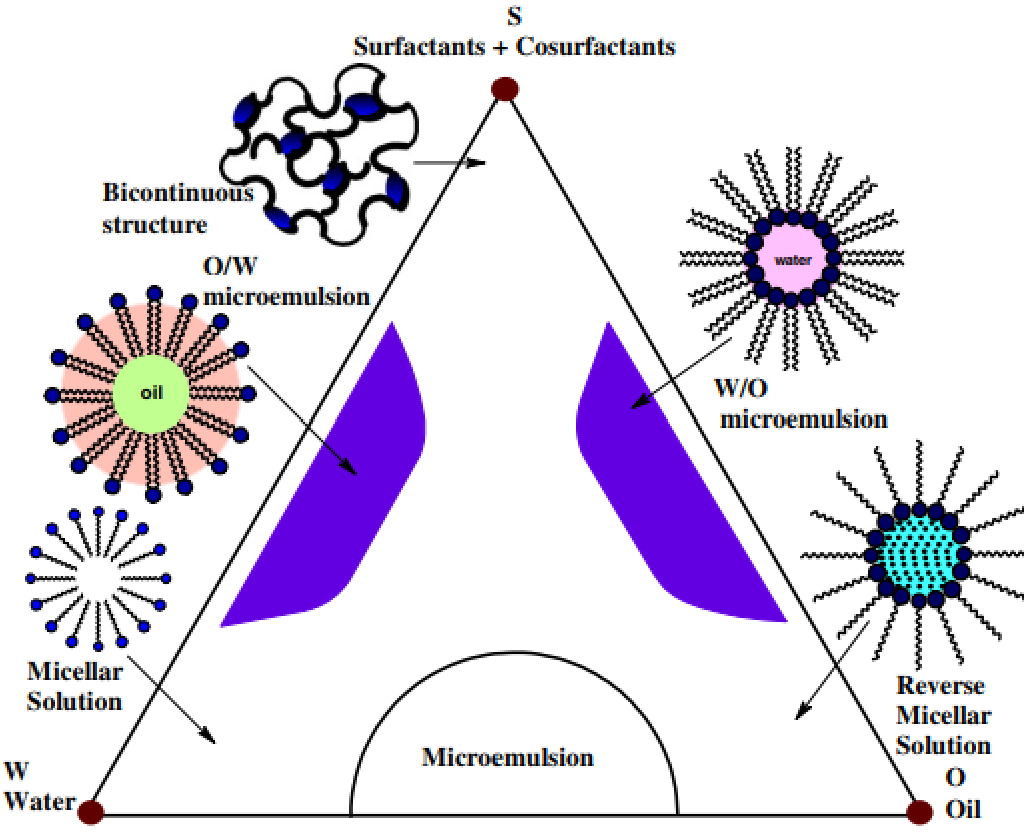

Figure 25: Hypothetical phase regions of microemulsion systems (Malik et al., 2012)

The µEMWCNTs, which are decorated with the surfactant molecules, have two distinct parts. The hydrophilic polar head likes to come into contact with an aqueous phase and the nonpolar hydrophobic tail as it resists interactions with the aqueous phase (Figure 26).

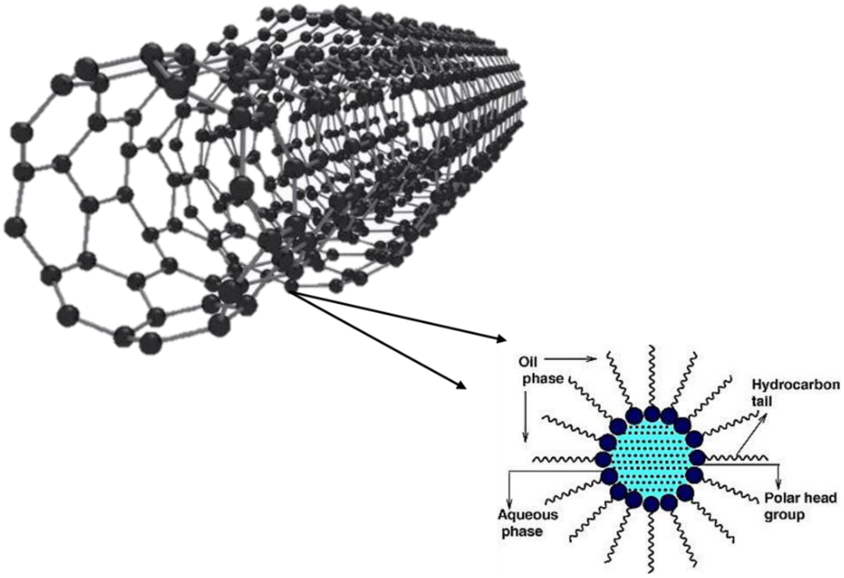

Figure 26: Illustration for µEMWCNTs and the droplet of the microemulsion

Raw and functionalized MWCNTs have been used to study the hydrocarbon adsorption from water. Different surface analytical techniques were used to study the changes in the structure of the MWCNTs after emulsification treatment and to correlate those changes with the adsorption results. The morphological studies revealed that the microemulsification resulted in a decrease in the specific surface area of MWCNTs by 36% and reduction of the pore volume by 9 %. This result proves the successful incorporation of functional groups into the MWCNTs' pores. However, the average pore size increased from 13.1 nm (MWCNTs) to 18.3 nm (µEMWCNTs). The thermogravimetric studies showed that during microemulsification treatment fatty acid esters (esterified miristic acid and lauric acid) were incorporated in 6.8% onto the surface of the MWCNTs, which influences the heat stability of the carbon nanotubes.

The structural analysis was carried out by XRD technique, and the surface investigation was performed by Raman spectroscopy. It can be stated that the MWCNTs have a crystalline structure, and this structure is preserved after the functionalization. The Raman spectroscopic studies confirmed the interaction between the MWCNTs and the functional groups of the fatty acid esters used for the modification.

It is necessary to examine briefly the mechanisms by which such hydrocarbon are formed, and what interactions they exhibit. Different mechanisms can be considered during organic chemical and MWCNT interactions, such as (i) hydrophobic interactions; (ii) π–π bonds, and (iii) electrostatic interactions, (v) hydrogen bonding and mesopore filling (Das et al., 2018). The sorption mechanism is supposed to be different for different types of organic chemicals (such as polar and nonpolar chemicals). π- π interactions are a type of non-covalent interaction that involves π systems. Kar and coworkers have investigated the nature of interactions between aromatic systems and CNTs, their findings so far have demonstrated that π–π stacking configurations are more strongly bound than CH---π analogues (Kar et al., 2008). From this perspective, the controlled noncovalent functionalization of MWCNTs using microemulsion offered the possibility of attaching the hydrocarbon chain using van der Waals and π-π stacking forces with only minor perturbations of the electronic network of the tube.

In this context, toluene was chosen as a model hydrocarbon to propose an adsorption mechanism. The adsorption affinity of toluene by µMWCNTs increases by -C=O and aromatic π- π bonds and/or by aromatic $–OK^+$ substitution. The sorption of the toluene on the surface of the µEMWCNTs can be given, as depicted in Figure 27. It should be noted that the mobility of adsorbed toluene on the tube surface can be considered in terms of rotating, tilting, and sliding. Interestingly, the suggested mechanism in this study has found to be in good agreement with the earlier adsorption mechanisms of organic pollutants on MWCNTs suggested by Pourzamani and co-workers (Pourzamani et al., 2015).

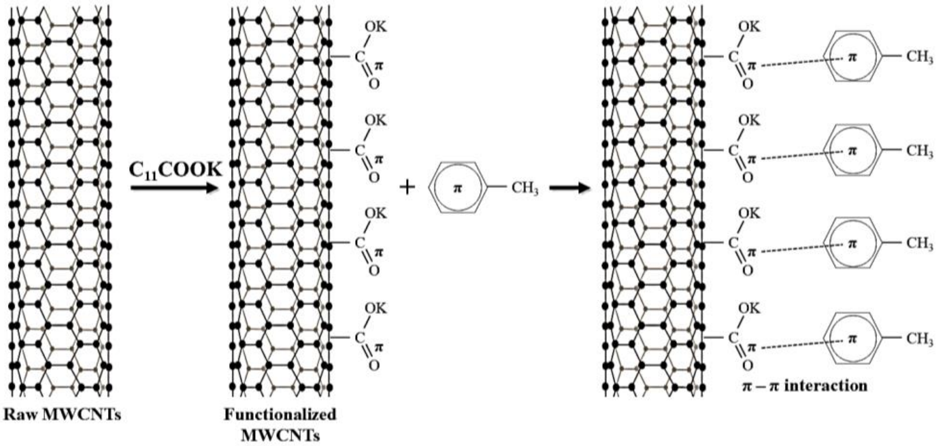

Figure 27: The mechanism of the surface functionalization and sorption of toluene over µMWCNTs

Once again, however, the way in which the adsorption mechanism is proposed remains quite unclear. Due to the possibility of several interactions occurrence at one time, depending on the type of hydrocarbon and the type of functional group on the MWCNTs surface. The principal observation from all experimental studies of hydrocarbon molecules and fragments occupy clearly defined sites on adsorbent surfaces. In essence, the noncovalent interactions of saturated and unsaturated hydrocarbons such as cation−π, $\pi - \pi$, and CH$\cdots\pi$ with carbon nanomaterials is ubiquitous and vital in explaining several hydrocarbon adsorption mechanisms.

Within this framework, toluene removal efficiency by UV-Vis over µMWCNTs supported the notion that the microemulsification is a suitable method for enhancement of the adsorption capacity of pristine MWCNTs. By using toluene as a model hydrocarbon, the removal efficiency of µMWCNTs was enhanced to reach up to 90%; these results are in line with the outcome of the TOC measurements. Kinetic studies show that adsorption of toluene obeys a pseudo-second-order model. The adsorption capacity of µMWCNTs increased by increasing the temperature.

Undecane used as another hydrocarbon to investigate the potential of µMWCNTs as hydrocarbon adsorbent. Based on the adsorption tests carried out by TOC, a significant increase in undecane adsorption was observed from 32% to 79-83% as a consequence of the surface modification. It is worthy of mentioning that the values obtained for hydrocarbon removal efficiencies by TOC and GC measurements are in harmony with each other. The obtained results confirm that the MWCNTs could earn a significant potential in hydrocarbon depollution control of waters.

Chapter 6: Results of zeolite-based adsorbents

This chapter presents the results obtained from characterization techniques used to study the physio-chemical properties of zeolite-based adsorbents. Moreover, the results obtained from adsorption tests are given, as well.

6.1 CHARACTERIZATION RESULTS OF ZEOLITE-BASED ADSORBENTS

6.1.1 Results of SEM and EDX investigations

The textural and chemical composition of the zeolitic tuff samples were studied by SEM and EDX method. RZT records show agglomerates of different sizes with defined plate shape in the micrometer range (Figure 28 a). The particles have a typical crystalline structure confirmed by XRD (Section 6.1.3). The surface structure of the TZT is presented in Figure 28b, indicating that there is a significant change in the topography of the zeolitic tuff due to partial removal of all associated elements and organic materials during the acidic treatment. EDX data (Table 13) confirmed this result. This finding is in agreement with data reported in the literature (Wang et al., 2010). The TZT has smaller particles with less clear boundaries (Figure 28b).

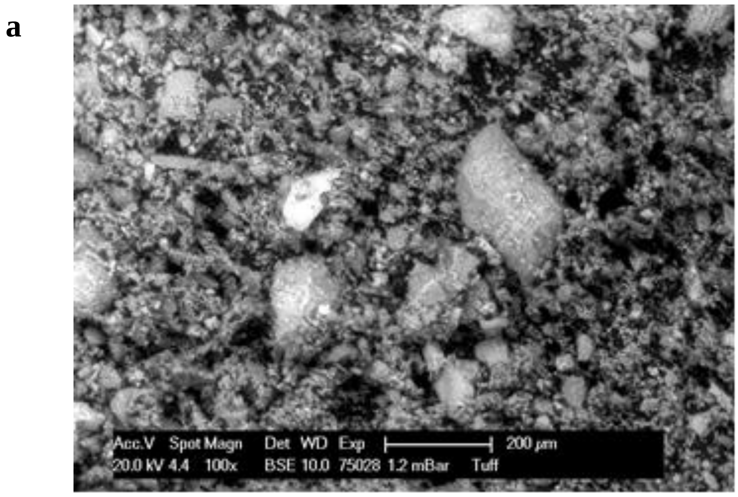

b

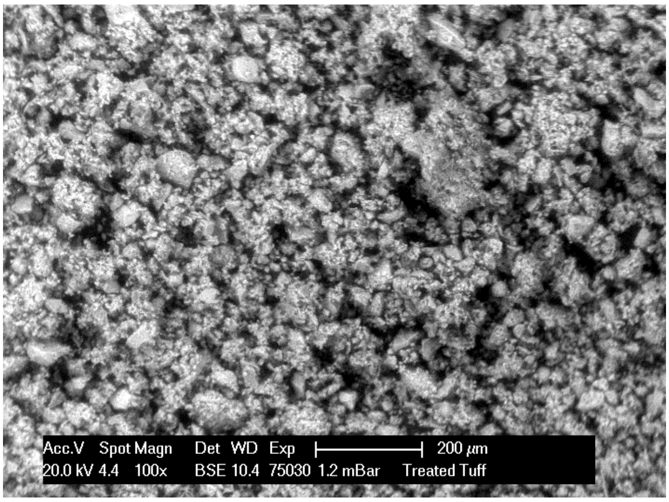

Figure 28: SEM images of raw (a) zeolitic tuff surface and (b) acid-treated (magnifications 300x)

The results of the chemical composition analyses are summarized in Table 13, where: a, b, c indicate the three points of the spot mode measurements. The chemical composition of the examined samples using spot mode analysis shows the relatively homogeneous distribution in the near-surface layer, except for Mn and Fe for RZT (Table 13). Mainly, elements such as K, Na, Ca, Si, Al, O originate from the zeolitic and silicate phases, e.g., the magnesium stems derived from forsterite and diopside, while iron comes from forsterite and hematite and the carbon derived from calcite compounds. The phosphorus, sulfur, chlorine, and manganese are presented as natural impurities in RZT in small quantities (0.3–2.0 wt. %). The phosphorus, sulfur, and manganese were washed out during the acidic treatment from the bulk phase and therefore were not detected in TZT.

EDX data for TZT indicate that the intensity of silicon increased while the intensity of other elements such as K, Na, Ca, Al, Ti, and Mg decreased or disappeared in comparison with RZT. The phases mentioned above were confirmed by XRD analysis. As mentioned earlier, the main aim of acidic treatment is to dealuminate zeolitic tuff. The emphasis was put on following the changes in silicon and aluminium ratios. The elemental composition of the TZT indicates that the silicon to aluminium ratio increased from 2.5 to 15.1 in comparison with RZT, as it can be seen in Table 13 and Figure 29. These considerations related to change in composition were reflected in XRD and FTIR analysis, as well.

Table 13: SEM-EDX results of zeolite-based adsorbents; composition and elemental distribution in the near-surface layer

Element	**RZT spot mode composition (m %)**			**TZT Spot mode composition (m %)**			**Surface mode composition (m %)**	
	a	**b**	**c**	**a**	**b**	**c**	**RZT**	**TZT**
C	-	-	-	2.34	0.51	1.84	16.06	1.84
O	36.02	38.98	39.39	44.87	39.42	41.04	36.12	41.04
Na	2.16	1.87	2.49	0.79	0.61	0.34	1.33	0.34
Mg	4.68	4.87	4.69	1.59	1.74	1.48	4.19	1.48
Al	**8.53**	**7.58**	**8.99**	**2.25**	**2.67**	**2.36**	**5.35**	**2.36**
Si	**20.92**	**19.50**	**20.44**	**35.14**	**37.34**	**35.61**	**13.85**	**35.61**
P	-	0.42	0.64	-	-	-	0.40	-
S	-	0.33	0.44	-	-	-	0.33	-
Cl	0.44	0.55	0.58	6.28	8.16	8.01	0.47	8.01
K	2.11	2.29	1.69	0.52	0.67	0.60	1.28	0.60
Ca	9.53	8.0`8	7.69	2.09	2.90	2.80	6.96	2.80
Ti	2.64	2.43	1.72	1.13	1.65	1.60	2.27	1.60
Mn	-	-	1.95	-	-	-	0.39	-
Fe	-	13.10	9.31	3.01	4.32	4.31	11.00	4.31

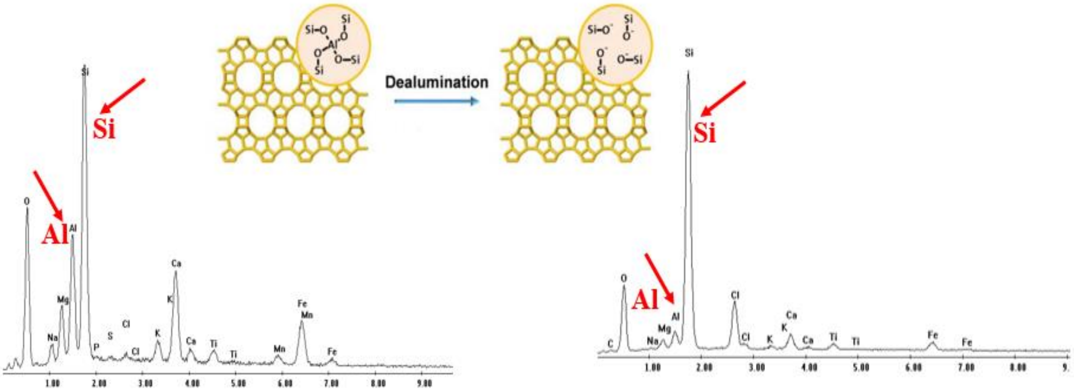

Figure 29: EDX results of RZT and TZT

Coming to µETZT, Figure 30 presents the morphological changes between RZT and µETZT. It is clear that there is a particle growth after microemulsion modification (Figures 28b and d), and it is assumed that the particle size depends on the emulsion composition (Lee and Shantz, 2004). The SEM images are strong evidence that the modification of TZT in the presence of the microemulsion leads to different particle morphologies and sizes than those obtained from acid treatment Figure 28b. Moreover, SEM results indicate that microemulsion is self-aggregated colloidal systems that provide hydrophobic particle growth.

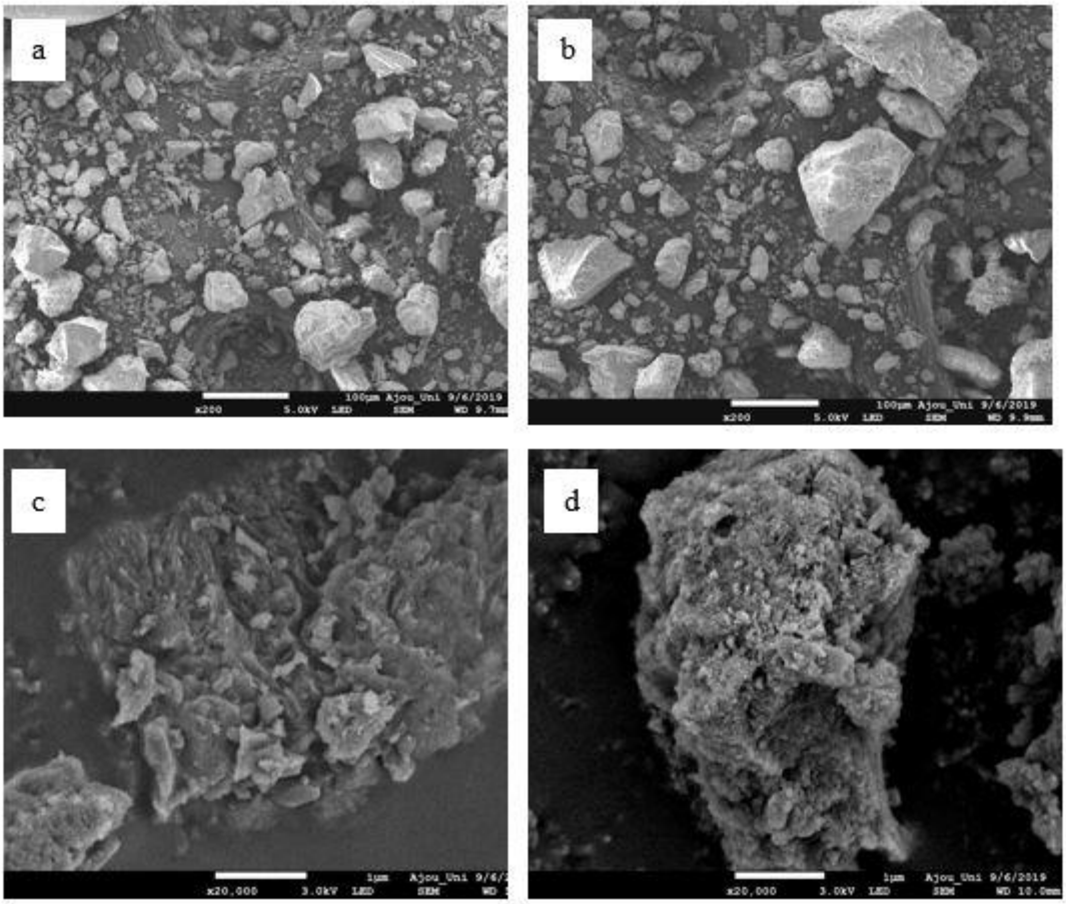

Figure 30: The scanning electron microscopic (SEM) record of the (a) RZT, (b) µTZT at magnification: x 200 and (c) RZT, (d) µETZT at magnification: x 20.000

6.1.2 Results of the morphological measurements

The surface area, pore-volume, average pore size values of the studied samples are summarized in Table 14. The applied acidic treatment resulted in a significant increase in the pore volume and the specific surface area of RZT by about 3.5 times. The acid treatment induced a net decrease of the microporous volume and a significant increase in BET surface area by about 3.5 times while it increased the contribution of the average volume of mesopores amounted to 0.1915 cm^3/g.

Those findings are attributed to the acidic treatment, which resulted in dissolving and washing many elements such as Al, Ca, Na, Fe, Mg, P, S, Mn out from pores. Additionally, the presence of this additional porosity is attributed to the dealumination process, which could be confirmed by the increment of mesopore size. The increment in average pore diameter is due to the collapse of the crystalline structure during the dealumination process, as confirmed by XRD. While the microspores of those of modified zeolites, TZT, and µETZT, are smaller than that of the original TZT. This may be due to the partial destruction of the zeolite framework by dealumination, or to the blocking of zeolite pores by Al atoms that are present out of the framework (Kawai and Tsutsumi, 1992).

Table 14: Characterization with BET for RZT, TZT, µETZT and commercially activated carbon adsorbents

Sample	S_{BET} (m^2/g)	V(cm^3/g)	S_{micro} (m^2/g)	V_{micro} (cm^3/g)	D_{av} (nm)
RZT	74	0.0608	22	0.0100	4.5
TZT	185	0.1915	0	0	4.6
µETZT	156	0.2031	0	0	5.1
Aquacarb 207C	864	0.0476	729	0.3380	2.0
Norit GAC 1240EN	959	0.1442	512	0.2300	2.7

Microemulsion modification of the TZT leads to a decrease in the surface area from 185 to 156 m^2/g as a result of lauric and myristic acid deposition and slightly increased the average pore diameter. The measured surface areas of the commercially activated carbon adsorbents, namely, Aquacarb 207C and Norit GAC 1240EN, are higher in comparison with zeolitic materials. These results are in agreement with the values provided by the manufacturer of the commercial adsorbents. The absence of micro-spores was observed in both TZT and µETZT samples, which in turn, facilitate the adsorbents' regeneration procedure.

To investigate the type of isotherm for the raw and prepared adsorbent, N_2 adsorption isotherm is depicted in Figure 31.The adsorption/desorption isotherms of TZT, RZT, and spent TZT follow **type I** at low p/p°, but **type V** at high p/p° (Kabalan et al., 2016). The main feature of a type I isotherm is the long plateau, which is indicative of a relatively small amount of multilayer adsorption on the open surface. Micropore filling may take place either in pores of molecular dimensions at very low p/p° or in wider micropores over a range of higher p/p°, while **V type** isotherm, which is uncommon; it is related to the type III isotherm in that the adsorbent-adsorbate interaction is weak but is obtained with specific porous adsorbents (Ertan, 2004). As shown in Figure 31, the N_2 isotherm of spent TZT, and TZT exhibited a greater slope than that of RZT, which indicates higher adsorption by dealuminated samples. The amount of adsorption of TZT and spent TZT is higher than that of RZT, which indicated an increase of pore volume of modified zeolite. However, the isotherm of RZT is similar to that of the modified one in its shape.

The relative adsorption capacities of RZT over the entire equilibrium pressure range are related to (i) cationic density and (ii) the limiting volume of the micropore (Hernández-Huesca et al., 1999). For dealuminated sample TZT, the electrostatic field on the surface is decreased (Kawai and Tsutsumi, 1992), and hence the electrostatic field inside the zeolite cages decreases and the surface becomes more hydrophobic. Therefore, the strong polar attraction energies between the surface and molecule are reduced, weaker dispersion forces become dominant, and this can explain the reason behind the type **V type** isotherm of TZT. Adsorption isotherms of water and hexane were not performed in this study, but it is recommended to be performed in future studies as it will give a great indication of the TZT hydrophobicity (Kawai and Tsutsumi, 1992).

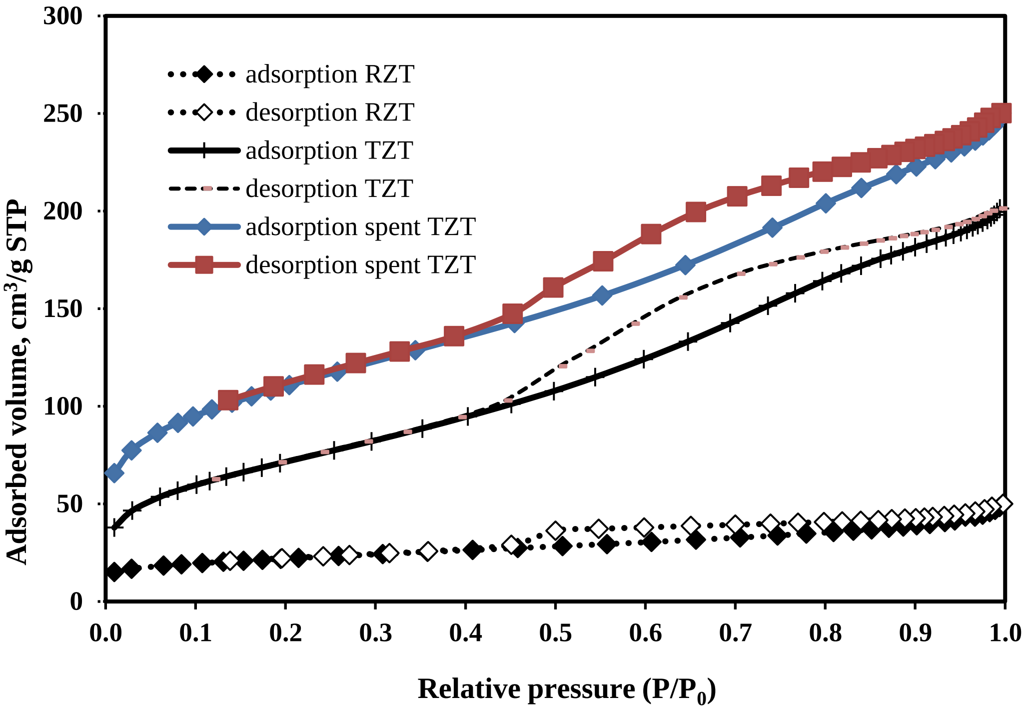

Figure 31: Volume of N_2 adsorption isotherm versus relative pressure for RZT, TZT, and spent TZT

The plot in Figure 32 more specifically indicates that the cumulative pore area in mesopore stems from nitrogen sorptions in pores with a width below 10 nm. The cumulative pore volume is plotted as a function of the pore diameter of fresh and spent adsorbent (Figure 32). Alike the pore volume, the mean pore diameter of the spent adsorbent showed light increment as compared to TZT.

The cumulative pore volume distribution suggests that the aging process and hydrocarbon deposition affect mainly pores with a diameter smaller than 10 nm. Hence, the increment in pore size was generally around 6 %, an indication of sintering.

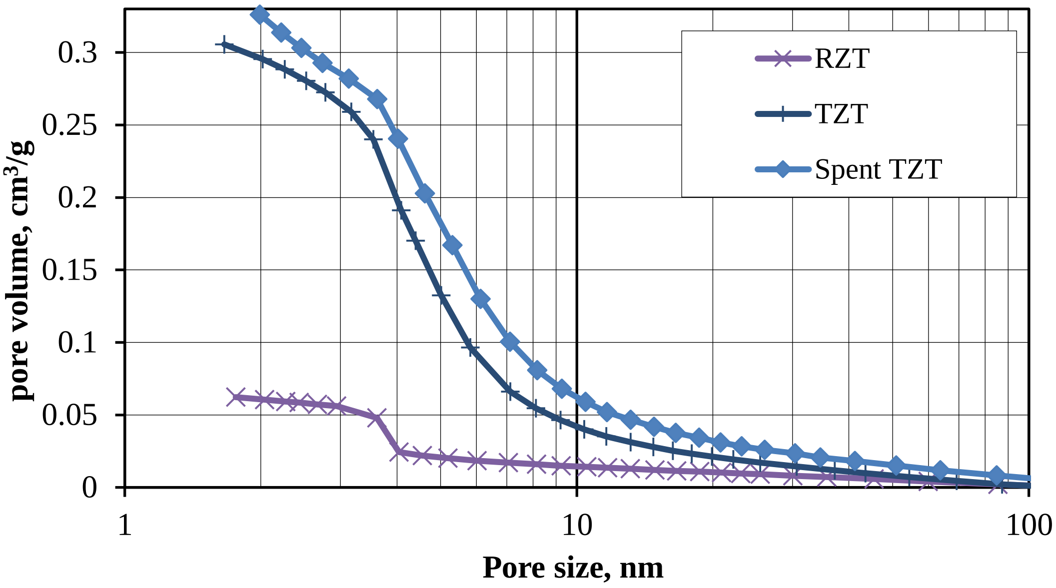

Figure 32: Cumulative pore volume (BJH[5] -calculation method) for RZT, TZT and spent TZT

6.1.3 Results of X-ray diffraction measurements

Figure 33 shows the XRD patterns for the raw and treated zeolitic tuff. The XRD pattern of the RZT shows almost complete crystallinity, and it contains mainly minerals of zeolitic phases: Phillipsite-K [$(K, Na)_2(AlSi)_8O_{16}\cdot 4H_2O$], chabazite-K [$(K, Na)_4Al_4Si_8O_{24}\cdot 8H_2O$], faujasite [$Na_2Al_2 Si_4O_{12}\cdot 8H_2O$]. Other main silicate phases, such as anorthite [$CaAl_2Si_2O_8$], forsterite [$Mg_{1.624}Fe_{0.376}SiO_4$], ferrosilite [$FeSiO_3$], diopside [$CaMg(SiO_3)_2$] and quartz [$SiO_2$]. Hematite [$Fe_2O_3$] and calcite [$CaCO_3$] crystalline phases were also observed in the RZT sample. The crystallinity of the samples was evaluated by comparison of the area of the most intense diffraction peak at 28 at 2 θ to that of the RZT taken as 100% crystalline

---

[5] The BJH method is the appropriate method to measure the mesopore (2 nm-50 nm)

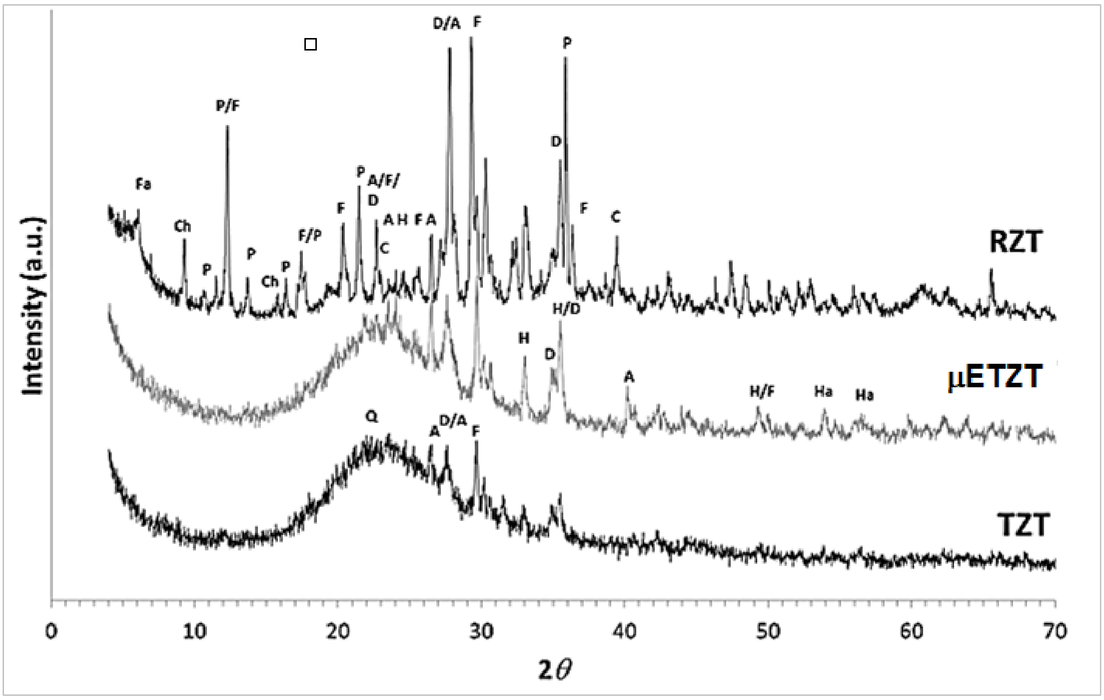

Figure 33: XRD patterns for RZT, TZT, and μETZT where P-phillipsite, Ch-chabazite, F-Faujasite; A-anorthite, F-forsterite; D-diopside; C-calcite; H-hematite; Q-quartz; Ha-halite

According to the literature data, phillipsite, faujasite, chabazite, forsterite, calcite, and anorthite are common mineral components in Jordanian zeolites (Yousef et al., 1999). Upon acidic treatment of RZT, the diffraction profile intensities of modified zeolites (TZT) decreased, which indicates that partial destruction occurred in their structure, showing the collapse of the crystalline structure. The relatively loss of crystallinity is corroborated by the loss of microporous volume (Table 14). Removal of associated elements such as Al, K, Na, Ca, Mg, Fe from the bulk phase were detected. The crystalline phillipsite, faujasite, chabazite, and calcite phases also disappeared in the TZT sample. The broad peak in Figure 33 is assigned to silica content, and the newly created Al-depleted sites (defects). This results in good agreement with the work of Roberge and associates (Roberge et al., 2002). The amorphous phase appeared in TZT sample detected in a range of 20-30° 2θ. In addition to this, the intensity of peaks of the remaining crystalline phases such as anorthite, diopside, forsterite decreased considerably. Phillipsite diffraction peaks of TZT and μETZT shift to a higher angle because of the smaller ionic diameter of Si^{4+} compared to Al^{3+} (Kawai and Tsutsumi, 1992). These significant changes in the peak positions were nevertheless noticed, in agreement with the difference in the chemical composition of the TZT. It is worthy of mentioning not all dealumination process results in loss of crystallinity, and this can be explained by the different starting material used in each study

Hydrochloric acid treatment of the RZT resulted in NaCl formation (dissolution of the charge compensating sodium cations from the zeolite), and halite phase can be observed in the case of TZT. After microemulsion modification, the μETZT exhibited a similar XRD pattern, as obtained in the case of TZT. The data of SEM-EDX analysis (Table 13) could also be explained and confirmed by XRD results indicated in Figure 33.

6.1.4 Results of FT-IR spectroscopy measurements

FTIR spectroscopy was used to investigate the structure of RZT, TZT, and μETZT samples and to monitor the effect of modification occurring in the zeolite framework during the pretreatments. FTIR spectra of all zeolitic tuff samples displayed a broad band at 3700–3100 cm^{-1} (Figure 34a). The shoulder at ~3600 cm^{-1} could be characteristic of H-bonded associated hydroxyl groups of Si(O–H)Al and AlO–H species (Azambre et al., 2015). Nonappearance of bands between ~3738-3749 cm^{-1} indicates the absence of various types of silanol groups (Morin et al., 1997).

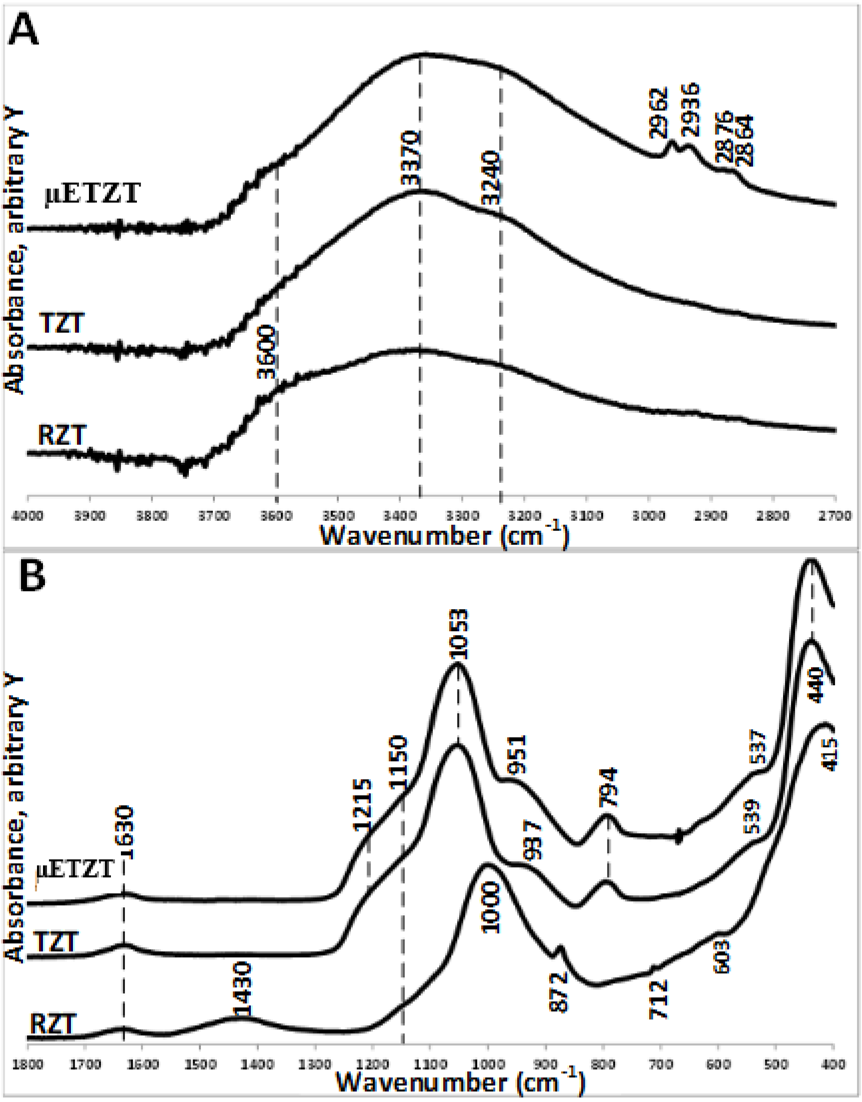

Figure 34: FT-IR spectra of zeolitic tuff samples: A - ν(O–H) and ν(C–H) stretching region (4000-2700 cm^{-1}); B - δ(O-H), ν(Si-O/Al-O) deformation and stretching region (1800–400 cm^{-1})

Stretching bands ν(H-O-H) at ~3370 cm^{-1} and ~3240 cm^{-1}, and bending band δ(H–O–H) at 1630 cm^{-1} indicate the adsorbed water molecules on the surface of the three samples. (Figure 34 A, B) (Mustafa et al., 2010). Also, the μETZT shows new broad bands at 2962, 2936, 2876, and 2864 cm^{-1} in the carbon-hydrogen region, as a result of microemulsion modification. The bands at 2962 and 2936 cm^{-1} are attributed to asymmetric stretching νC–H of the -CH_3 and -CH_2 groups of alkane chain, respectively. The bands at 2876 and 2864 cm^{-1} are attributable to ν symmetric C–H stretch of CH_3 and CH_2 groups of alkane chain, respectively (Azambre et al., 2015).

Observed bands of RZT at 1430, 872, and 712 cm^{-1} disappeared after the acidic treatment (Figure 34 B). Those bands are assigned to the stretching vibration of the CO_3 group of calcite, and the values are attributed to ν_3 asymmetric stretching, ν_2 asymmetric deformation, and ν_4 symmetric deformation modes respectively (Buzgar and Ionut Apopei, 2009). X-ray data also confirmed the presence of crystalline calcite in the raw zeolitic tuff, which reduced after the acid treatment.

Structural data for the studied samples can be obtained from the observed vibrational frequencies of the zeolite framework stretching region of 1300 and 400 cm^{-1}. The strongest vibration band appears in the region of 1200–900 cm^{-1} (Figure 34 B). This band is considered as the characteristic IR band associated with zeolite, as it indicates the internal tetrahedron vibrations, and it is assigned to T–O (T=Si or Al) stretching mode (Pichat et al., 1974). The strong band at 1000 cm^{-1} is due to asymmetric stretching vibrations of bridge bonds, ν_{as} Si–O(Si), and ν_{as} Si–O(Al) in phillipsite (Mozgawa et al., 2011; Salem et al., 2010). This band was shifted after acidic treatment to a higher frequency of 1053 cm^{-1}. Moreover, shoulders appeared around 1215 cm^{-1}, indicating the reduction of aluminium content (Figure 34B).

The new broad band appeared at 794 cm^{-1} for treated samples, and it is assigned to the external symmetric stretching vibration of Si–O–Si bridges bonding two tetrahedral units. The frequency and shape of this band are similar to Si–O–Si band of the reported spectra of HZSM-5 with Si/Al = 15, mesoporous SiO_2, and amorphous SiO_2 (Van Steen et al., 2004). It is given in the literature that with higher Si/Al ratio, the symmetric stretching vibrations bands narrowed, and the band is splitting into several peaks due to the more homogeneous environment of Si–O–Si bonds (Van Steen et al., 2004). It has been shown that the loss of crystallinity (decrease in aluminium content) causes changes in the frequency and the shape of the Si–O–Si band since this band is structure sensitive (Pichat et al., 1974). The Si–O–Si band appears at 794 cm^{-1} after dealumination process in TZT and µETZT at Si/Al ratio of 15.1 confirmed by EDX analysis (Table 13). The reason that band at 794 cm^{-1} was not observed in RZT with Si/Al ratio of 2.6 attributable to the presence of several crystalline zeolite phases in the sample, which causes scattering of bonds length (Mozgawa et al., 2011).

6.1.5 Results of X-ray fluorescence (XRF) measurements

Table 15 shows the chemical compositions of RZT, TZT, and µETZT samples based on the XRF analyses. The treatment of the RZT with concentrated hydrochloric acid has removed 25-30 % wt. of the accompanying volcanic constituents (iron, aluminium, magnesium, calcium, and sodium oxides).

6.1.6 Results of Thermoanalytical investigations

Results obtained from TGA/DTG measurements showed that a continuous weight loss of RZT, TZT, and µETZT samples occurred after heating up to 1000 °C (Figure 35). The detailed mass loss data are summarized in Table 16). The first endothermic mass loss steps can be attributed to dehydration, namely the mass loss steps between 22-128°C and 128-250°C steps belong to the external and loosely bound water losses (Perraki and Orfanoudaki, 2004). The exothermic step between 250-400°C could be attributed to the combustion of organic compounds. In this region, the loss of tightly bound water can also take place (Duvarci et al., 2007; Knowlton, 1981; Yörükoğullar et al., 2010). The two overlapping endothermic steps between 400-613°C belong to the tightly bound water loss from the zeolite tuff structure (Duvarci et al., 2007; Knowlton, 1981; Yörükoğullar et al., 2010). The 3.6 m % endothermic mass loss above 613°C (613-787°C) belongs to calcite decomposition. After acidic treatment, the amount of externally bound water greatly increases, while the endothermic mass loss step above 613°C (calcite impurity in RZT), is completely absent due to its removal by acid treatment. The total mass loss of sample TZT increased significantly as compared to the RZT sample, mostly due to the increased external water content. The µETZT sample shows a decreased amount of externally bound water. The thermal decomposition of adsorbed organic microemulsion compound along with the loss of remaining tightly bound water starts above 218°C in two exothermic processes and finishes around 654 °C. The total mass loss in this temperature range (220-650°C) increases slightly (0.4 m %) compared to the TZT sample. However, in the µETZT, the second mass loss step (411-654°C) has changed from endothermic to exothermic, which indicates that the majority of the water was replaced with organics after microemulsion modification. If the first exothermic mass losses step of µETZT is corrected by the exothermic mass loss of TZT (230-340°C, 2.8 m %), then the amount of microemulsion in µETZT is calculated as 4.2 m % (218-654°C). This excess indicates the amount of adsorbed organics after the microemulsion modification (42 mg in 1000 mg μETZT).

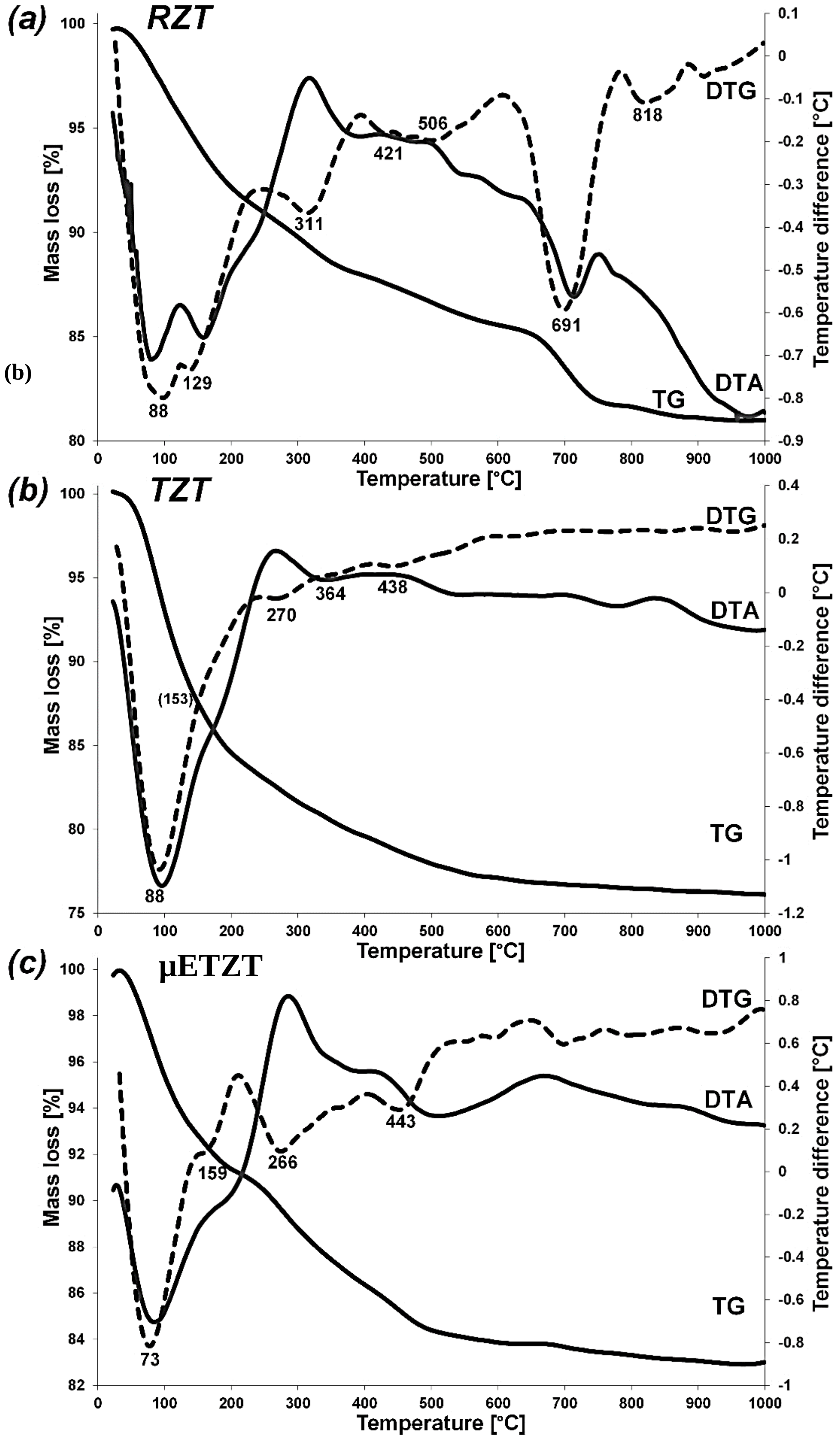

Figure 35: TG, DTG and DTA curves for zeolitic tuff samples: (a) RZT; (b) TZT; (c) µETZT

Table 15: The elemental analysis of RZT, TZT and µETZT samples using XRF technique

Element	Al	Si	P	Cl	K	Ca	Ti	Mn	Fe	S
RZT, ppm	52966	164750	3574	21668	25037	132219	31821	2407	168376	5806
TZT, ppm	17012	301474	1366	106999	8101	41328	26430	593	68731	1700
(↓/↑, %)*	(68 ↓)	(83↑)	(62 ↓)	(394↑)	(68 ↓)	(69 ↓)	(17 ↓)	(75 ↓)	(59 ↓)	(71 ↓)
µETZT, ppm	16782	330752	1627	38211	22913	30869	29519	656	67452	1128
(↓/↑, %)	(68 ↓)	(101↑)	(54 ↓)	(76↑)	(8 ↓)	(77 ↓)	(7 ↓)	(73 ↓)	(60 ↓)	(81 ↓)

* ↓/ ↑, % -decrease or increase elemental concentration, %, in treated samples in comparison with RZT

Table 16: Data from thermo-analytical measurements of zeolitic tuff samples

`	T_{max} (°C)	T_{end} (°C)	Mass loss step (%)	Step attributed to the followings	DTA
Sample: RZT					
22	88	128	4.6	External water loss	Endothermic
128	129	250	4.6	Loosely bound water loss	Endothermic
250	311	400	2.9	Organic matter combustion/Tightly bound water loss	Exothermic
400	412/526	613	2.5	Tightly bound water loss	Endothermic
613	691	787	3.6	Calcite decomposition	Endothermic
787	818	1000	0.8	-	-
Sample mass: 52.2 mg				**Total mass loss: 19.0 m %**	
Sample: TZT					
23	88	170	13.9	External water loss	Endothermic
170	(153)	230	2.4	Loosely bound water loss	Endothermic
230	270	340	2.8	Organic matter combustion/Tightlyboundwaterloss	Exothermic
340	364	415	1.4	Tightly bound water loss	Endothermic
415	438	620	2.4	Tightly bound water loss	Endothermic
620	-	1000	1.0	-	-
Sample mass: 50.3 mg				**Total mass loss: 23.9 m %**	
Sample: µETZT					
24	73	158	7.2	External water loss	Endothermic
158	159	218	1.6	Loosely bound water loss	Endothermic
218	266	411	4.8	Organic matter combustion/Tightly bound water loss	Exothermic
411	443	654	2.2	Organic matter combustion/Tightly bound water loss	Exothermic
654	-	1000	1.0	-	-
Sample mass: 49.8 mg				**Total mass loss: 16.8 m %**	

6.2 ADSORPTION TESTS

6.2.1 Performance evaluation of TZT and µETZT by classical Westinghouse method

The classical Westinghouse method is, perhaps, the simplest approach for correlating adsorption performance for pure hydrocarbons. Table 17 shows the results of kerosene, n-octane, and dodecane sorption using RZT, TZT, and µETZT as adsorbents based on the classical Westinghouse method of absorbability (Muir and Bajda, 2016).

In the case of all analyzed hydrocarbon compounds, it is clear that TZT and µETZT have a much higher affinity in terms of hydrocarbon adsorption as compared to the RZT. These differences can be attributed to the high surface area of TZT, and in the case of µETZT, the differences are due to the chemically attached tail groups of the surfactant, which resulted in the strong hydrophobic character to the adsorbent. One can notice that the average pore diameter, $D_{avg,}$ varied for each sample as the following order; µETZT > TTZ > RZT. This indicates the substantial role that the mesoporous structure can play in adsorption capacities. Each adsorbent does not necessarily show the same adsorption capacities for each hydrocarbon as it depends on the structure and length chain of the adsorbed hydrocarbon. For example, the adsorption capacity of µETZT to dodecane is higher than n-octane as the chain of the former is longer.

For example, µETZT and TZT have high adsorption capacity for pure n-octane than the RZT sample. Similar differences were observed in the case of other hydrocarbons, which support the fact that the sorption properties of the TZT samples are significantly higher than that of the RZT. These results can be explained by that fact that the pre-treated and more hydrophobic zeolites such as TZT and µETZT facilitate the inhibition of pore blockage towards the water, which in turn could result in more pores and potential surface area available for hydrocarbons diffusion and adsorption (De Ridder et al., 2012). Surprisingly, the adsorption capacities of the zeolite-based adsorbent for kerosene are lower than other hydrocarbons, even though kerosene has a longer chain than octane and toluene but it also contains branched-chain paraffin. This can be attributed to preferential molecules being adsorbed on zeolitic tuff -based adsorbent such as long-chain carbons rather than molecules that have branched-chain as kerosene. This result can be explained by the fact that zeolites based adsorbent have the unique property of selectively adsorbing hydrocarbon molecules based on size and shape in addition to polarity (Al-Damkhi et al., 2007). To address this fact, dodecane adsorption was also examined over RZT, TZT, and µETZT, and those adsorption capacities are higher than the values obtained when toluene, n-octane were used as oil model, likely due to the longer hydrocarbon chain.

Table 17: The sorption of kerosene and different hydrocarbon compounds on RZT, TZT and µETZT according to Westinghouse method

Stock	**Sample**	**Sample Weight, M_o (g)**	**Sample Weight + CH (g)**	**Adsorption, MP (g)**	**Sorption (g/g)**
Toluene	µETZT	1.5021	3.5991	2.097	1.39
	TZT	1.5001	3.5561	2.056	1.37
	RZT	1.5003	2.3024	0.8021	0.53
kerosene	µETZT	1.5022	3.2911	1.7889	1.19
	TZT	1.5012	3.1142	1.613	1.07
	RZT	1.5041	2.0127	0.5086	0.34
n-octane	µETZT	1.5008	4.0981	2.5973	1.73
	TZT	1.5002	3.9288	2.4286	1.62
	RZT	1.5019	2.7785	1.2766	0.85
dodecane	µETZT	1.5007	4.7451	3.2534	2.16
	TZT	1.5022	4.001	2.4988	1.66
	RZT	1.5078	3.2544	1.7466	1.16

6.2.2 Performance evaluation of TZT and µETZT by TOC results

In addition to the standard Westinghouse experiments and to determine the maximum C_8 hydrocarbon adsorption over the zeolitic samples, batch experiments were performed in the function of time. Samples were taken at different times, and TOC analyzer measured the C_8 hydrocarbon concentrations. All the experimental parameters, such as n-octane concentration, agitation speed, and sample dosage, were kept constant throughout the experiments. The experimental parameters for this experiment were set at 300-rpm agitation speed, 0.5 g adsorbent dosage, at the initial hydrocarbon concentration of 475 mg C/L (C8-water solution). The experiments were carried out at 27 °C. The dynamic sorptions of the n-octane model compound over the RZT, TZT, µETZT, and AquaCarb sorbents are illustrated in Figure 36. For the sake of comparison, the AquaCarb activated carbon sorbent was used as benchmark adsorbents.

The results indicate that the contact time needed to reach the adsorption equilibrium for C_8 hydrocarbon over RZT, TZT, and µETZT is about 20-30 min. Thus, the chosen contact time of 1.5 h is on the safe margin to reach the equilibrium. It was observed that at the beginning of the experiments, the hydrocarbon adsorbed very rapidly on the TZT, µETZT surfaces due to the availability of large vacancies on the external surface of the TZT and µETZT. As the outside surface of TZT and µETZT becomes covered and saturated with C_8 hydrocarbon droplets, the rate of oil uptake started to decrease and reached equilibrium. The amount of n-octane adsorbed at equilibrium at ambient temperature and pressure and short time indicates TZT and µETZT potentials as oil adsorbents.

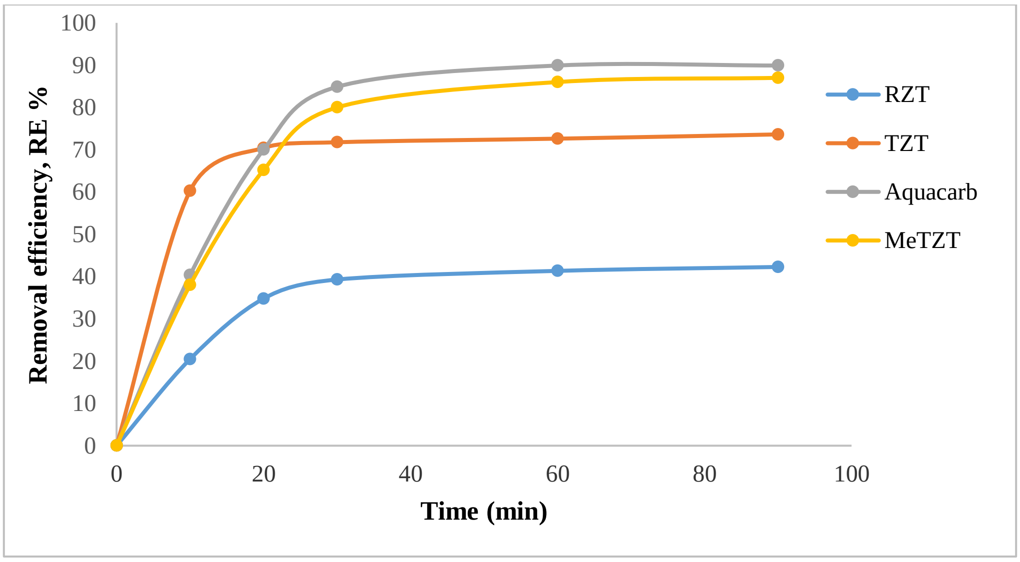

Figure 36: The change in percentage n-octane removal of over RZT, TZT, µETZT, and activated carbon

Regarding the microemulsified adsorbent, µETZT, it can be seen from Figure 36 that it exhibits a high removal efficiency, which is comparable to that of the activated carbon since it reached hydrocarbon removal of 85 % after 60 min on stream. This result can be attributed to the existence of tail groups of the surfactant on the µETZT surface. This means that the hydrophobic character of the zeolite was significantly enhanced. These results are in agreement with the results reported by Ghouti and coworkers (Al-ghouti and Al-degs, 2011). It is to be noted that the time-based results are in accord with the general theory of the oil sorption. As the oil droplets at first have to overcome the boundary layer effect and then diffuse from the boundary layer film onto the adsorbent surface and then finally diffuse into the porous structure of the TZT and µETZT (Nethaji et al., 2013).

Just like µETZT, samples of TZT behaved as a model adsorbent for C_8 with high removal efficiency. This again suggests that the degree of hydrophobicity of zeolitic tuff is directly dependent on the aluminium content of the zeolites. With the decrease of the aluminium content of the zeolite, the ionic charge of zeolite lattice decreased. Decreasing ionic charge zeolite will exhibit less polarity, and it results in lower hydrophilicity and higher hydrophobicity feature. It can be concluded that the chemical compositions of the treated zeolitic material influence the interaction between water molecules and the zeolite since the water molecules can interact with Al sites of zeolite framework and by dealumination this interaction significantly decreases (Bolis et al., 2006). The elemental composition of the TZT and µETZT as compared to RZT indicates that the silicon to aluminium ratio increased from 3.1 to 17.7 and 19.7 for TZT and µETZT, respectively (Table 13). The increase of Si content in TZT and µETZT influences its hydrophobic properties. The obtained results are in accord with the results published by others (Grieco and Ramarao, 2013; Yonli et al., 2012).

The obtained results show that the TZT and µETZT have improved adsorption capacity for hydrocarbon removal from the hydrocarbon-water mixture, as evidenced by the experiments carried out with n-paraffin as a model hydrocarbon. The hydrocarbon removal efficiency was significantly higher over the TZT surface as compared to the RZT by the Westinghouse method. In the case of kerosene, a higher sorption capacity (1.07 g/g) was obtained, while the RZT resulted in only 3.4 g/g adsorption capacity. Similar tendencies were observed with n-octane and dodecane over TZT and RZT samples. The µETZT exhibited even higher hydrophobicity than the TZT. The results show that the acidic treatment is very effective in removing framework aluminium as the Si/Al ratio increases from 2.58 to 15.06. The results in this study validated that the framework Si/Al ratio of zeolites is an important parameter that exerts a strong influence on hydrophobicity.

The reusability of the zeolitic tuff (TZT) was studied, as well. Additional tests were performed to study the changes in sorption capacity and the structural properties of TZT after the first test of adsorption. For this purpose, 0.5 g of spent adsorbent was reused for 100 ml n-octane/water samples under the same conditions as above to check the stability of the hydrocarbon removal efficiency of the TZT. The spent adsorbent was regenerated by washing with ethanol and dried at 105°C. The spent adsorbents were reused under the same conditions. The removal efficiencies measured were approximately 50-55 % for three cycles at 30 min contact time. It can be concluded that the removal efficiency remained as high as in the case of the fresh TZT sample.

6.2.3 Performance evaluation of TZT and µETZT by GC results

Kerosene was used as model petroleum cut in the hydrocarbon-water mixture to study the hydrocarbon removal efficiency of the raw, treated and microemulsified zeolitic tuff and activated carbons. Usually, for the determination of hydrocarbon composition GC method is used (Sivagami et al., 2019).

Kerosene standard has GC peaks appearing in the C_{10}–C_{16} range. GC peaks of n-C_{10}–C_{16} were identified with external standards of normal alkanes. All the experiments were performed in duplicate, and the average values are reported in Table 18. Kerosene removal from water by adsorption method was around 10.6 % in the presence of RZT in the investigated range. By using µETZT, this value increased up to 34.1%, and the highest value of 42.7% was achieved over TZT. Hence, microemulsion and surfactant modification can alter the surface functionality by the attached hydrophobic groups and thus enhancing adsorption capacity for various organics.

The best hydrocarbon removal efficiencies were achieved during the treatment of the hydrocarbon-polluted water samples with Aquacarb 207 C, and Norit GAC 1240EN activated carbon adsorbents, as they were able to remove 72% and 82% of hydrocarbons respectively. This result is in harmony with the results published by Wang and coworkers (Wang and Peng, 2010) as they demonstrated that the natural zeolite displays slight adsorption of organics in aqueous solution as a result of its hydrophilic properties.

Table 18: GC analysis data for kerosene adsorption from water over raw, treated and microemulsified zeolitic tuff and activated carbons

Sample	**Peak area of n-C_{10}–C_{16} (pA*s)**	**Conc. (C mg/L)**	**RE (%)**	**q_e (g/g)**
Blank	60948	560.0	0.0	-
RZT	54488	500.6	10.6 ± 5	0.15
TZT	34908	320.7	42.7 ± 5	0.6
µETZT	40175	369.1	34.1 ± 5	0.5
Aquacarb 207C	16822	154.6	72.4 ± 5	1.0
Norit GAC 1240EN	11092	101.9	81.8 ± 5	1.2

Table 19 shows the examined adsorption capacities for different kinds of zeolites. It is worthy of mentioning that the variation in adsorption capacities for zeolites is attributed to the diverse range of structure, pores structure, and surface area for each type of zeolite.

Table 19: Adsorption capacities of hydrocarbons over zeolites adsorbents

Zeolite Type	q_e (g/g)	Ref.
Na-X	0.75–0.79	(Bandura et al., 2015a)
Zeolites X	0.37-1.33	(Sakthivel et al., 2013)
Na-P1	1.24-1.40	(Bandura et al., 2015b)

6.2.4 Adsorption kinetic experiments over TZT

Kinetic study over TZT in water/dodecane mixture and water/octane mixture was also carried out. The kinetics of the oil adsorption process over the dealuminated zeolitic tuff TZT can be described as pseudo-second-order adsorption. Table 20, in conjunction with Figure 37 and Figure 38, summarize the pseudo-second-order parameters for the adsorption of the two hydrocarbons.

Table 20: Kinetic parameters of pseudo 2nd models for n-octane and dodecane adsorption over TZT

Hydrocarbon	**Parameter**		
	Pseudo-second order model		
Octane	k_2 (min^{-1})	$q_{e,\ cal}$ (g/g)	$q_{e\ ,\ exp}$ (g/g)
	0.70183	0.91274	0.9239
Dodecane	k_2 (min^{-1})	$q_{e,\ cal}$ (g/g)	$q_{e\ ,\ exp}$ (g/g)
	31.3986	0.9265	0.9269

It can be observed from Table 20 that the values of the residual standard error (R^2) for the pseudo-second-order kinetic model are higher than 0.999 for both hydrocarbons, and the values of $q_{e,\ cal}$ are very close to that of $q_{e,exp}$, which indicates that the pseudo-second-order kinetic model fits the adsorption of n-octane and dodecane over TZT. These results demonstrate that the main oil adsorption mechanism is possibly a chemisorption reaction.

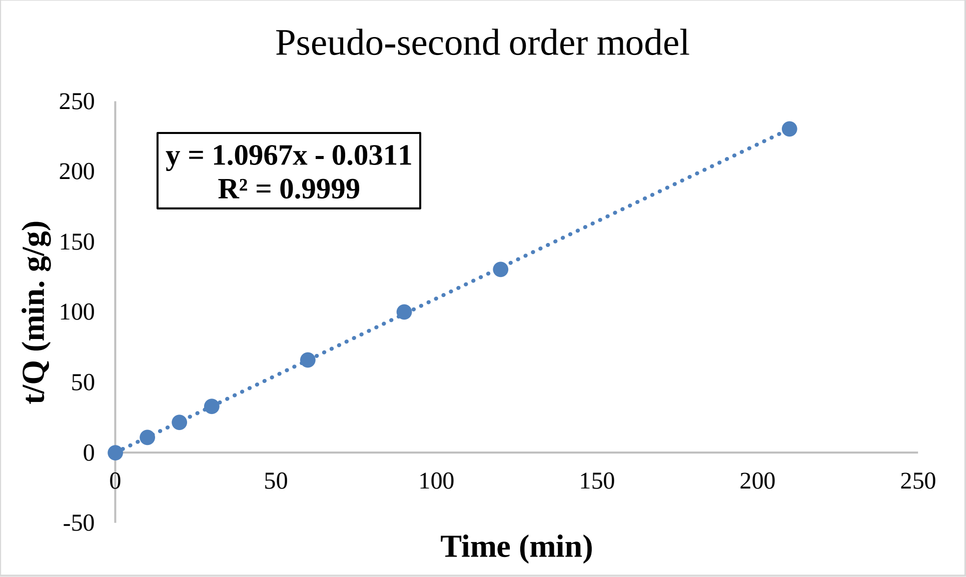

Figure 37: Effect of adsorption time on the adsorption capacity of TZT using n-octane as a model hydrocarbon. (Dosage of material= 0.5 g, C_i n-octane = 470 mg C/L, temperature= 25 °C)

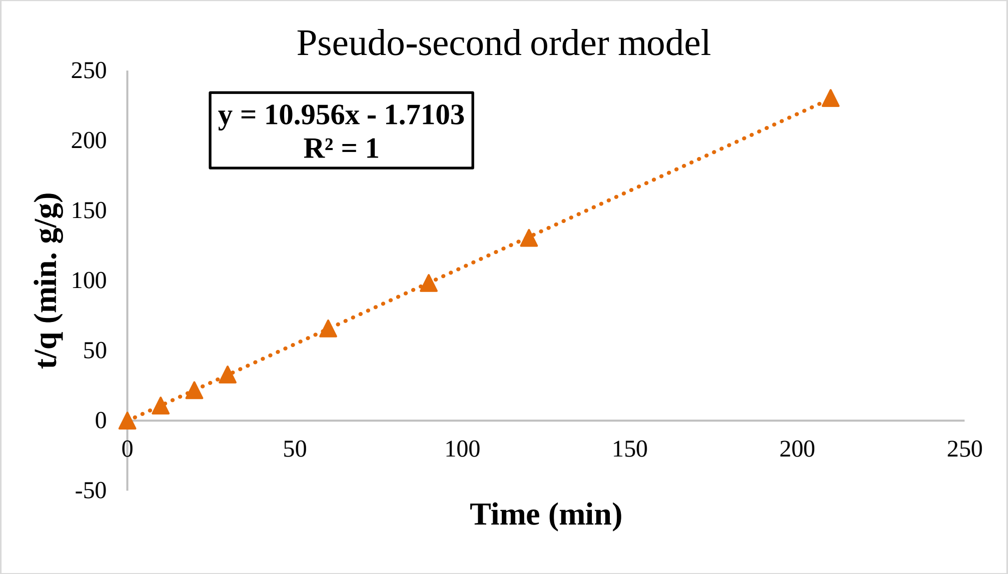

Figure 38: Effect of adsorption time on the adsorption capacity of TZT using un-decane as a model hydrocarbon. (Dosage of material= 0.5 g, C_i n- dodecane = 470 mg C /L, temperature= 25 ^{o}C)

Chapter 7: Discussion of zeolite-based adsorbents results

To improve the oil adsorptive potential of zeolitic tuff as a hydrocarbon adsorbent, modification of the material properties of the zeolitic tuff was performed by two methods: first, dealumination of the zeolitic tuff to obtain higher Si/Al ratio and followed by functionalization of the particle surfaces to impart hydrophobicity.

- Dealumination via acid leaching

Dealumination via acidic treatment was judiciously performed, as it deserves greater attention among the methods used to increase the Si/Al ratio. The acidic treatment resulted in a reduction of 25% to 30% in the volcanic constituents (iron, aluminium, magnesium, calcium, and sodium oxides), as evidenced by EDX results, which showed a significant decrease of the aluminium content (Figure 39a). The materials thus obtained are thermally stable, and their composition may be tuned by varying the acid concentration.

- Microemuslification of TZT

The treatment aimed to increase the hydrophobic properties of the external surface of the dealuminated zeolitic tuff, TZT, by decorating the external surface with a chain of hydrocarbon (to enhance their hydrophobic properties in order to increase the oil uptake capacity from the water (Figure 39b).

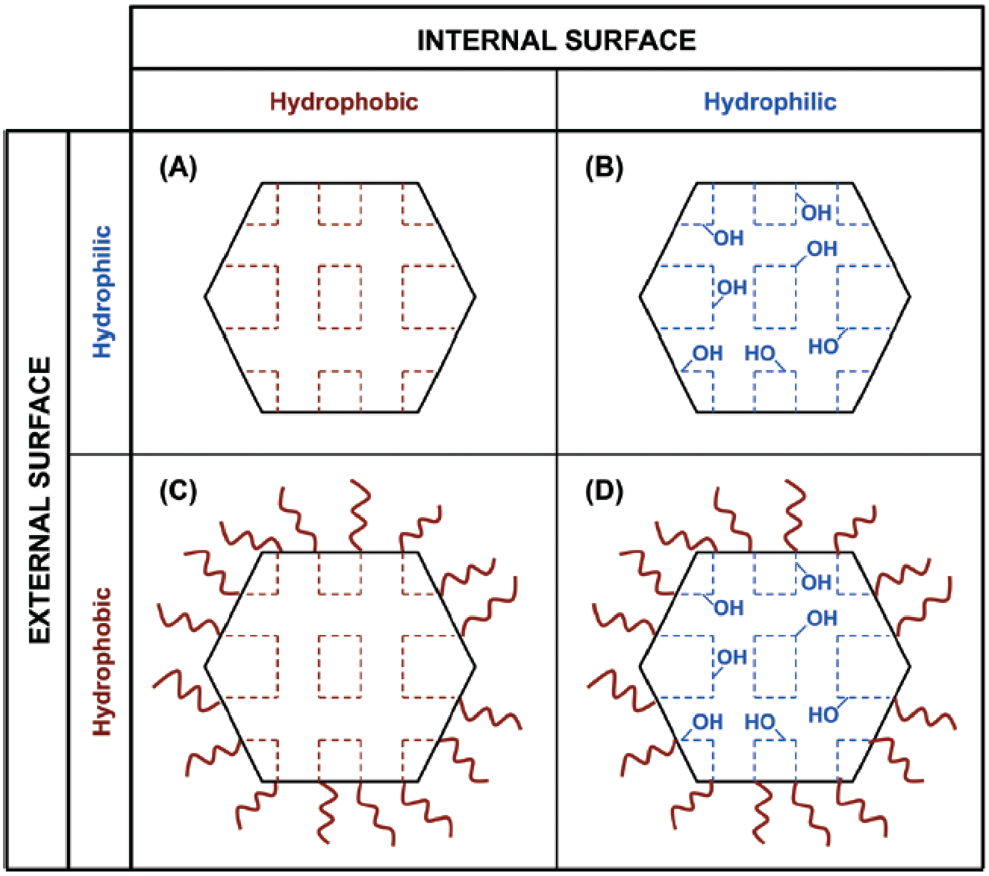

Figure 39: Schematic depiction of zeolite crystals with hydrophobic (red) or hydrophilic (blue) domains located at external crystal surfaces (solid lines) or internal pore surfaces (dashed lines)

Dealumination via acid leaching

Attention was given to the fundamental studies that have been made, especially by Chen and co-workers (Chen, 1976; Müller et al., 2000) and their associates, concerning zeolite dealumination. Their findings have usefully guided the interpretation of enhanced hydrophobicity and its relation with aluminium content. Since the Si/Al ratio plays a vital role in the hydrophobic properties of zeolites, the impact of the change in the Si/Al ratio was studied (Wang and Peng, 2010). The hydrophobicity of high silica zeolite is attributed to the existence of =Si-O-Si=, which is truly hydrophobic (Chen, 1976). It is also stated that if the aluminium is sequentially eliminated from the zeolite, then, the water molecules will no longer fill the pores of the dealuminated samples. On the other hand, the hydrocarbon molecules remain to fill the pores at low relative pressures. Consequently, these highly siliceous zeolites are truly hydrophobic.

The acidic treatment of the zeolitic tuff was implemented to enhance the Si/Al ratio. Acidic treatment resulted in the upgrading of the Si/Al ratio from 2.5 to 15.1 due to the leaching of the aluminium from the lattice framework. As every Al in the framework introduces a negative charge into the whole structure, therefore hydrophilic zeolites have a Si/Al ratio of slightly over one, while hydrophobic zeolites have less amount of aluminium, and their Si/Al ratio is above 3, in many cases up to 3000.

Usually, the acidic activation involves three steps: removal of exchangeable cations (de-cationating), dealumination of the framework, and formation of amorphous silicon-oxygen phase (Belchinskaya et al., 2013). Figure 40 shows how the dealumination process takes place during the acidic treatment of RZT similarly to the dealumination of the clinoptilolite framework $(Na, K, Ca)_{2-3}Al_3(Al, Si)_2Si_{13}O_{36} \cdot 12H_2O$ (Belchinskaya et al., 2013).

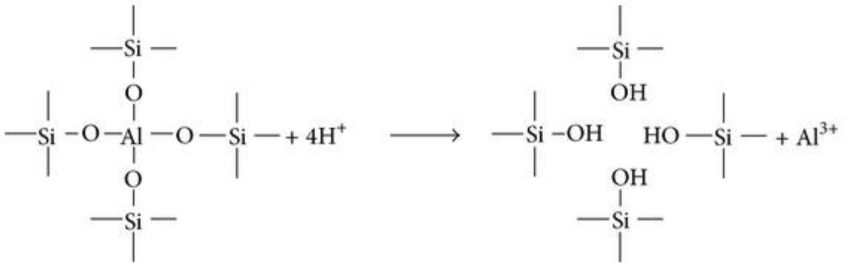

Figure 40: Dealumination process of zeolites (Belchinskaya et al., 2013)

According to the XRD and FTIR investigations, it can be concluded that the dealumination process changed the structure and linkages in the framework in a significant manner. The crystalline structure of the RZT is lost, and the amorphous structure formed.

The dealumination process changes morphology, elemental composition, crystallinity, and, therefore, physical-chemical properties of the zeolitic tuff. As mentioned earlier, one of the limiting properties of natural zeolite is its relatively small surface area compared to activated carbon and nanomaterials. It was reported that the BET specific surface area of zeolitic tuff ranges between 7.8 and 12.3 m^2/g (Ghrair et al., 2009). Mechanical milling of zeolitic material increases the surface area up to 80 m^2/g (Ghrair et al., 2009). The BET specific surface area of the TZT in the present study increased from 74 m^2/g to 185 m^2/g for TZT as a result of the dealumination and removing all associated materials. µETZT exhibits a decrease in surface area due to the lauric and myristic acid deposition.

The degree of hydrophobicity of zeolites is directly dependent on their aluminium content. If the aluminium content decreased in the zeolite, the ionic charge of zeolite lattice would decrease. Less ionic charge means less polarity and so less hydrophilicity/more hydrophobicity features. The hydrocarbon removal experiments from the kerosene-water mixture support this concept since the removal efficiency of RZT is 10.6%, and it increased to 42.7% over TZT.

It should be noted that the type of hydrocarbon and its configuration plays a dominant role in the behavior of the adsorption system. Within the series of the prepared zeolitic-based adsorbents, the highest sorption capacity towards oils was observed when dodecane -water emulsion was used as a hydrocarbon model compound. This probably can be endorsed to the longest chain structure of dodecane in comparison with the other tested hydrocarbons (Table 17).

One possible explanation is that the treatment changed the micropores' environment, and thus, kerosene molecules could not reach the adsorption sites. Therefore, it was proved that the zeolite's adsorption capacities for a straight-chain hydrocarbon like octane are higher than a branching-chain hydrocarbon like isooctane (Salih, 2018). For other model hydrocarbons, the sorption capacities of µETZT confirmed the hydrophobic character of µETZT. Figure 41 depicted a schematic for the interaction of the surfactant on the surface of the µETZT. The surface modification of the TZT by organic functional groups slightly contributed to a further increase in zeolite's hydrophobicity.

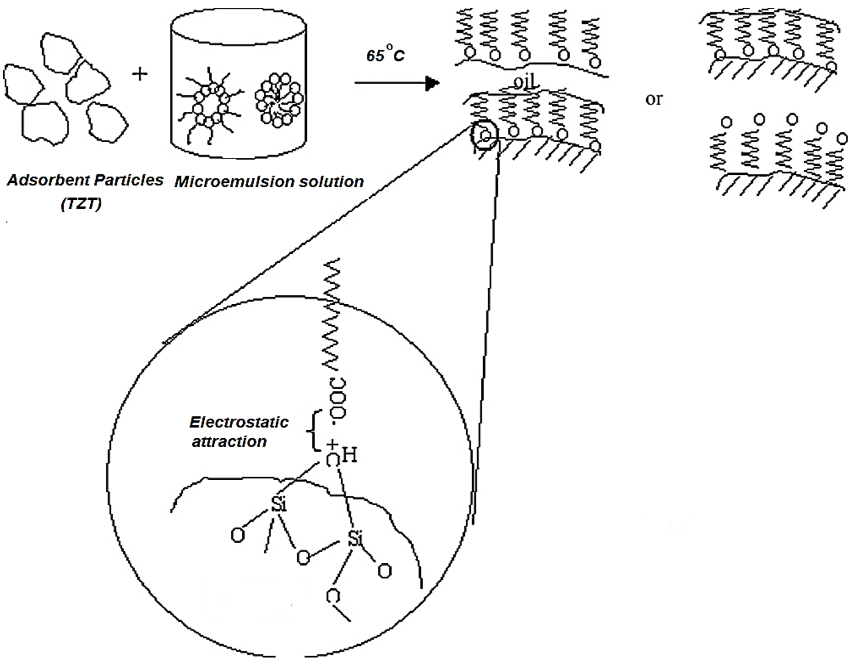

Figure 41: Schematic showing the interaction of the surfactant on the surface of the μETZT

The adsorption capacity of zeolitic material was compared with commercially available activated carbon adsorbents, namely, Norit GAC 1240EN and Aquacarb 207C. The results revealed that the adsorption efficiency of activated carbon is about two times higher than that of the TZT. This result is attributed to the fact that activated carbon has a higher surface area (about five times higher) and exhibits a lower density than that of the TZT sample. Thus, better interaction between adsorbent and hydrocarbon spreading over the water surface can take place. For further studies, it is recommended to increase the concentration of acid during delaumination process and to change the type of surfactants used for microemulsion preparation as long chains surfactant such as dodecyl-dimethyl-ammonium bromide (DDDMA) will provide more sites for interaction with the hydrocarbon molecules (Carmody et al., 2007).

Chapter 8: Conclusions

This work has shown the feasibility of preparing valuable oil adsorbents from non-costly material such as zeolitic tuff and straightforward functionalization techniques such as microemulsion.

The adsorption behaviour of modified zeolitic tuff TZT and functionalized MWCNTs reinforce the need to appreciate the structural and hydrophobic properties brought about by the reduction of the aluminium content and by functionalization via micro-emulsion, and the effects that this kind of modification may have on oil adsorption capacity. Recognition of these effects might go far towards resolving several environmental problems.

The innovation of the microemulsion solved one main issue regarding MWCNTs functionalization as it proved to be beneficial for producing hydrophobic adsorbent with keeping the high crystallinity and uniformity of MWCNTs surface and without the need of additional functionalization and substitution steps to install the hydrocarbon side chains. Another major advantage of microemulsification in comparison to other functionalization methods is stemming from its ability to functionalize MWCNTs without altering their structures. However, up to date, there are no investigations reported on the adsorption of organic pollutants onto µEMWCNTs.

Bench-scale tests were performed using synthesized adsorbents and commercial activated carbons to evaluate their hydrocarbon removal efficiency from contaminated water under similar experimental conditions. The classical adsorption test, which originally proposed by Muir and Bajda (Muir and Bajda, 2016), fully harmonize with other results obtained via other analytical techniques such as GC, TOC, and UV-Vis. Of this group, UV-vis is perhaps the most common method, and it showed pronounced promise for fast analysis, since it allows performing analyses, fast and precisely, with a lower volume of solvent compared to that used in the analyses by conventional methods. The following highlights can be concluded:

- Microemulsification treatment proved to be a novel method for MWCNTs modification that combined simplicity, rapidity, low consumption of chemicals and resulted in high adsorption performance. The results revealed that the adsorption capacity of µEMWCNTs outperforms that of activated carbon. In the case of kerosene adsorption (GC analysis) the removal efficiency was in the following order µEMWCNTs (96%) > Chemiviron carbon (53%) > MWCNTs (35 %) > Norit GAC 1240EN (27%). In the case of Undecane, the adsorption capacity of µEMWCNTs was enhanced by 40% in comparison with MWCNTs.

- The adsorption capacities of µEMWCNTs are higher than MWCNTs for all model hydrocarbon (adsorption capacity of µEMWCNTs are in the range of 6.07 to 5.68; while adsorption capacity of MWCNTs is in the range of 2.48 to 4.64). Moreover, µEMWCNTs have zero affinity to adsorb water. This result can be attributed to the fact that the adsorption capacity of modified adsorbent is more dependent on total pore volume (D_{avg}), not on the micropore volume (V_{micro}). After modification, a significant increase in total pore volume was detected as it increased from 12.5 nm to 18.3 nm, further reduction in surface area and diminishing in micropore volume for µEMWCNTs were detected. In this regard, much attention has been given in this work to understand how the composition and structure of the modified adsorbent affect its ability as an oil adsorbent.
- Adding surfactant such as SLES and SAS to the oil-contaminated water (hydrocarbon model/water solution) helped to increase the removal efficiency. For example, the removal efficiency of µEMWCNTs using SLES with undecane/water as model hydrocarbon enhanced to reach up to 79 ± 5 % while when SAS was used as a surfactant, the removal efficiency over the same adsorbent reached up to 83± 5 % (supported by TOC analysis). Though, adding surfactants does not seem to influence the oil adsorption.
- Based on the classical Westinghouse method, the hydrocarbon chain length of molecules is found to have a significant effect on the adsorption capacity of µEMWCNTs as well as hydrophobic interaction mechanisms as the effectiveness of hydrophobic interactions increases with increasing carbon chain length. The adsorption capacities of µEMWCNTs as per the carbon chain length follow this order: Dodecane (n-$C_{12}H_{26}$); 5.93 g/g > undecane (n-$C_{11}H_{24}$); 5.83 g/g

>> toluene; C_7H_8 5.68 g/g. this result is attributed to the fact that the modification occurred on the surface of MWCNTs. Thus the reason behind selective adsorption is related to hydrocarbon chain length as a larger hydrocarbon chain or ring creates a nonpolar (more hydrophobic) region. This finding is in agreement with the published work (Ersoy and Çelik, 2003). The adsorption capacity of µEMWCNTs is much higher than that of conventional activated carbon (AC), which reached up only to 0.109 g/g (Huang et al., 2018).

- The kinetic studies illustrated that the pseudo-second-order model is the best-correlating model for toluene removal over µEMWCNTs with equilibrium removal capacity reaching up to 4.9 g/g with a rate constant of k_2 0.00753 min^{-1}. This result based on the assumption that the rate-limiting step is the chemisorption involving valency forces through sharing or exchange of electrons between sorbent and sorbate, thus this model provided the best correlation of the data.
- Based on the kinetic studies over µEMWCNTs, it was observed that the adsorption capacity increased with an increase in temperature from 25 to 60 ⁰C. The calculated 40 min adsorption capacity at 25 and 60 ⁰C were 4.81and 4.97 g/g, respectively. The effect of changing the temperature on the equilibrium capacity of the µEMWCNTs is attributed to the reduction of solution viscosity at a higher temperature, which in turn, will increase the rate of diffusion of toluene across the external boundary layer and into the internal pores of the µEMWCNTs.
- Toluene was chosen as a model hydrocarbon to propose an adsorption mechanism. It was found that the adsorption affinity over toluene by µMWCNTs increases by -C=O and aromatic π- π bonds and/or by aromatic –Ok substitution. This conclusion is affected by the adsorbent's structure and the adsorbed entities.

Regarding zeolite-based adsorbents, the ease the production of adsorbent of Jordanian zeolitic tuff demonstrates its suitability for hydrocarbon removal from the water surface. Although the impurities present in zeolitic tuff such as phosphorus, sulphur, chlorine, and manganese causes the dealumination route to be slightly more arduous than that of most available natural zeolites.

Jordanian zeolitic tuff has been dealuminated by reaction with hydrochloric acid. Si/Al ratio greater than 15 was obtained in a single step, without significant loss of crystallinity, porous volume, and thermal stability. The RZT contains mesopores and microporous pore. The latter is readily vanished by acid treatment. In general, the results showed that the dealuminated zeolite is comparable to the other outstanding oil adsorbents such as those functionalized with side chains or synthesized in isoreticular series with varied pore sizes, e.g., the obtained adsorption capacity of TZT is 0.6 g/g, while the adsorption capacity of zeolites X reached 0.37 g/g

The characterization revealed essential properties of the RZT and the corresponding derived adsorbents. The features can be summarized as followed:

- The most important effect of dealumination with concentrated acid is to remove framework aluminum selectively from positions close to defect's sites and on the external surface area. Moreover, acid treatment passivates any impurities that could be present in tuffs deposits. It is expected by using the experimental conditions presented in this work, that the final composition of the zeolite can be tuned by varying the concentration of the acid; thus, Si/Al can be changed between 15 and 100.
- Markedly, the acid treatments increased the surface area so that the intrinsic properties of the modified RZT microporous structure come into effect. The specific surface area of TZT is 3.5 times higher than that of RZT. The changes in the morphology and composition were correlated with the hydrocarbon adsorption capacity of the zeolitic tuff. Nevertheless, new optima may readily be achieved by the outlined dealumination procedure defined in this thesis since the degree of delamination correlates with the degree of zeolite hydrophobicity.
- XRD showed a loss of crystallinity after dealumination, and this aspect is also corroborated by the morphology and XRF studies. The crystallinity of the samples was evaluated by comparison of the area of the most intense diffraction peak at 28 at 2θ to that of the RZT taken as 100% crystalline, while the reduction in peak intensity was detected for TZT. According to literature, not all dealumination processes resulted in this loss, and this can be explained by different zeolites' origin used in each study.

- Average pore diameter, D_{avg}, varied for each sample as the following order; μETZT (5.1 nm) > TTZ (4.6 nm) > RZT (4.5 nm). This indicates the substantial role that the mesoporous[6] structure can play in adsorption capacities. This observation may ennoble conclusions on the sizes of adsorption sites deduced by altering the composition of dealuminated and microemulsified zeolitic tuff.
- Thermoanalytical investigation showed that the amount of adsorbed organics after the microemulsion modification was 42 mg in 1000 mg μETZT.
- Dealuminated zeolitic tuff exhibits a strong hydrophobic/organophilic character since the adsorption capacity is directly dependent on their aluminium content and hydrophobicity increases with an increase in the Si/Al ratio (with Si/Al =2.5, the adsorption capacity of RZT for kerosene is 0.15 g/g while in of the case TZT which having Si/Al ratio of 15 the TZT adsorption capacity for kerosene reached 0.6 g/g). This result proved that the Si/Al ratio plays a vital role in the hydrophobic properties of zeolites.

The following concluding remarks summarize the findings of using TZT and μETZTas hydrocarbon adsorbents:

- The prepared zeolites based adsorbents have a higher affinity to adsorb straight-chain hydrocarbon than kerosene. As zeolites, in general, have the unique property of selectively adsorbing hydrocarbon molecules based on size and shape in addition to the polarity of the hydrocarbon. This result was proved by the classical Westinghouse method. For example, in case of μETZT the adsorption capacity increased as per the following order, kerosene (1.19 g/g) < toluene (1.39 g/g) < n-octane (1.73 g/g) < dodecane (2.16 g/g).
- The kerosene removal efficiency enhanced by 32% using dealuminated ZT instead of RZT; however, this result is still moderate in comparison with that

---

[6] Division to micropores (up to 2 nm, diameter, or width in slit type pores), mesopores (2-50 nm) and macropores (>50 nm) gives a good classification

achieved by commercial activated carbon, which reached removal efficiency of 72-82%.

- The achieved adsorption capacity of the TZT in this work in acceptance with the adsorption capacity of natural mineral, which generally in the range 0.20–0.50 g/g. The adsorption capacities of kerosene were enhanced by 76% and 70% for TZT and µETZT, respectively. It can be concluded that the presence of a hydrocarbon chain on the surface of the µETZT increased the hydrophobic and oleophilic properties.
- The hydrophobic functionalization of external zeolite crystallite surfaces can prevent liquid water from penetrating into internal void spaces; hence, µETZT exhibited a high removal efficiency for n-octane, which is comparable to that of the activated carbon since the hydrocarbon removal reached up to 85 % after 60 min. This result can be attributed to the existence of tail groups of the surfactant on the µETZT surface.
- The synthesized adsorbents derived from RZT showed its ability to be regenerated, e.g., the removal efficiency of n-octane was approximately 50-55 % for three cycles at 30 min contact time. It can be concluded that the removal efficiency remained as high as in the case of the fresh TZT sample.
- The experimental data of n-octane and dodecane adsorption over TZT fitted well to the second-order kinetic model as the calculated values of kinetic parameters of pseudo-second-order models are very close to the experimental one. The calculated value of equilibrium adsorption capacity ($qe_{, cal}$) reached up to 0.91274 (g/g) while the experimental value reached up to $q_{e, exp}$ 0.9239 (g/g). The relatively good agreement between these two values indicates that the adsorption fitted well with the second-order kinetic model.

The obtained adsorbents showed strong hydrophobicity and excellent mechanical properties. Therefore, as concluding remark, a more extensive studies on microemulsion and dealumination will be able to guide efforts to fine-tune the functionalization of the external and internal surfaces of porous solids and CNTs and to induce the desired changes in the adsorptive properties, which in turn, will further improve the performance of these materials in oil spills remediation and open new areas for their application.

Chapter 9: New scientific findings / theses

The new scientific results obtained during my Ph.D. research work were formulated in several theses as follow:

9.1 CARBON NANOTUBE-BASED ADSORBENT

I developed a new approach for MWCNTs functionalization via microemulsion technique. However, up to date, and to the best of my knowledge, there are no investigations reported on the adsorption of organic pollutants onto µEMWCNTs.

- I have demonstrated another significant advantage of microemulsification in comparison to other functionalization methods, which stem from its ability to functionalize MWCNTs without altering their structures. This fact evidenced by the results obtained by XRD as the most intensive peak for MWCNTs and µEMWCNTs appeared at $2\theta = 25.3°$ without loss of its intensity.
- I have confirmed that the adsorption capacities of µEMWCNTs are higher than MWCNTs for all model hydrocarbon (q of µEMWCNTs are in the range of 6.07 to 5.68; while q of MWCNTs are in the range of 2.48 to 4.64). Moreover, µEMWCNTs have zero affinity to adsorb water. This result can be attributed to the fact that the adsorption capacity of modified adsorbent is more dependent on total pore volume (D_{avg}), not on the micropore volume (V_{micro}). After modification, a significant increase in total pore volume was detected as it increased from 12.5 nm to 18.3 nm; further reduction in surface area and diminishing in micropore volume for µEMWCNTs were detected.
- I confirmed that the pseudo-second-order model is the best-correlated model for toluene removal over µEMWCNTs with equilibrium removal capacity reaching up to 4.9 g/g with rate constant k_2 0.00753 min^{-1}. The adsorption capacity of µEMWCNTs is much higher than that of conventional activated carbon (AC), which reached up only to 0.109 g/g.

- Based on the kinetic studies over µEMWCNTs, I have observed that the adsorption capacity increased with an increase in temperature from 25 to 60 ºC. The calculated 40 min adsorption capacity at 25 and 60 ºC were 4.811 and 4.97 g/g, respectively. The effect of changing the temperature on the equilibrium capacity of the µEMWCNTs is attributed to the reduction of solution viscosity at a higher temperature, which in turn, will increase the rate of diffusion of toluene across the external boundary layer and in the internal pores of the µEMWCNTs.
- Regarding mechanism investigation, I have chosen toluene as a model hydrocarbon to propose an adsorption mechanism. I found that the adsorption affinity of toluene by µMWCNTs increases by -C=O and aromatic π- π bonds and/or by aromatic–ONa^+ substitution.

9.2 ZEOLITE-BASED ADSORBENT

This work has shown the feasibility of preparing valuable zeolites from non-costly Jordanian zeolitic tuff raw material. I found that the ease the production of adsorbent of Jordanian zeolitic tuff demonstrates its suitability for hydrocarbon removal from the water surface. Although the impurities presented in RZT, such as phosphorus, sulfur, chlorine, and manganese, cause the dealumination route to be slightly more arduous than that of most available natural zeolites. The following points summarize the main obtained findings /theses:

- Dealumination of RZT via acid treatment. Markedly, the acid treatments increased the surface area from 74 to 185 m^2/g. Moreover, the RZT microporous were vanished by acid treatment (Vmicro of RZT = 0.0100 cm^3/g and V_{micro} of TZT = 0.000 cm^3/g). Average pore diameter, D_{avg}, varied for each sample as the following order; µETZT (5.1 nm) > TTZ (4.6 nm) > RZT (4.5 nm). This indicates the substantial role that the mesoporous structure plays in adsorption capacities. This observation may ennoble conclusions on the sizes of adsorption sites deduced by altering the composition of dealuminated and microemulsified zeolitic tuff.
- I proved that the Si/Al ratio plays a vital role in the hydrophobic properties of zeolites. Since dealuminated zeolitic tuff exhibits a strong hydrophobic/organophilic character since the adsorption capacity is directly dependent on their

aluminium content and hydrophobicity increase with an increase in the Si/Al ratio. I found that the kerosene removal efficiency enhanced by 32% using dealuminated ZT instead of RZT; however, this result is still moderate in comparison with that achieved by commercial activated carbon, which reached removal efficiency of 72-82%. The result showed that the adsorption capacity of RZT (Si/Al =2.5), of kerosene, is 0.15 g/g while for with TZT, which has 15 Si/Al attained adsorption capacity of kerosene enhanced to reach 0.6 g/g.

- I proved that the prepared zeolites-based adsorbents have a higher affinity to adsorb straight-chain hydrocarbons than kerosene. This result was proved by classical Westinghouse method, for example, in the case of μETZT the removal adsorption capacity increased as per the following order, kerosene (1.19 g/g) < toluene (1.39 g/g) < n-octane (1.73 g/g) < dodecane (2.16 g/g). Thus, the presence of a hydrocarbon chain on the surface of the μETZT increased the hydrophobic and oleophilic properties. I also evidenced that the hydrophobic functionalization of external zeolite crystallite surfaces can prevent liquid water from penetrating within internal void spaces; hence, μETZT exhibited a high removal efficiency for n-octane, which is comparable to that of the activated carbon since the hydrocarbon removal reached up to 85 % after 60 min over μETZT. This result can be attributed to the existence of tail groups of the surfactant on the μETZT surface.
- I concluded that the achieved adsorption capacity of the TZT in this work (specifically 0.6 g/g) in acceptance with the adsorption capacity of natural mineral, which generally in the range 0.20–0.50 g/g. The adsorption capacities of kerosene were enhanced by 76% and 70% for TZT and μETZT, respectively. The synthesized adsorbents derived from RZT showed its ability to be regenerated. The removal efficiency of n-octane was approximately 50-55 % for three cycles at 30 min contact time. I concluded that the removal efficiency remained as high as in the case of the fresh TZT sample.
- I studied different kinetics models to describe the adsorption behaviour of n-octane and undecane over TZT. I found that the experimental data fitted well to the second-order kinetic model. As the calculated values of kinetic parameters of pseudo, second models are very close to experimental one; e.g., in the case of n-octane, calculated adsorption capacity (qe, cal) reached up to 0.91274

g/g while the experimental value reached up to (qe, exp) 0.9239 g/g. These two numbers are in good agreement.

Bibliography

Abdelwahab, O., Nasr, S.M., Thabet, W.M., 2017. Palm fibers and modified palm fibers adsorbents for different oils. Alexandria Eng. J. 56, 749–755. https://doi.org/10.1016/j.aej.2016.11.020

Abdul Khalil, H.P.S., Jawaid, M., Firoozian, P., Rashid, U., Islam, A., Akil, H.M., 2013. Activated carbon from various agricultural wastes by chemical activation with KOH: Preparation and characterization. J. Biobased Mater. Bioenergy 7, 708–714. https://doi.org/10.1166/jbmb.2013.1379

Adebajo, M.O., Frost, R.L., Kloprogge, J.T., Carmody, O., 2003. Porous materials for oil spill cleanup: A review of synthesis and absorbing properties. J. Porous Mater. · 10, 159–170. https://doi.org/10.1023/A

Aguilera, F., Méndez, J., Pásaroa, E., Laffona, B., 2010. Review on the effects of exposure to spilled oils on human health. J. Appl. Toxicol. 30, 291–301. https://doi.org/10.1002/jat.1521

Ahmaruzzaman, M., 2011. Industrial wastes as low-cost potential adsorbents for the treatment of wastewater laden with heavy metals. Adv. Colloid Interface Sci. 166, 36–59. https://doi.org/10.1016/j.cis.2011.04.005

Al-Damkhi, A.M., Al-Ameeri, R.S., Jeffreys, G. V., Mumford, C.J., 2007. Optimal separation of n-paraffins from Kuwait kerosene using a molecular sieve adsorbent. J. Chem. Technol. Biotechnol. 37, 215–228. https://doi.org/10.1002/jctb.280370402

Al-ghouti, M.A., Al-degs, Y.S., 2011. New adsorbents based on microemulsion modified diatomite and activated carbon for removing organic and inorganic pollutants from waste lubricants. Chem. Eng. J. 173, 115–128. https://doi.org/10.1016/j.cej.2011.07.047

Al-Jammal, N., Juzsakova, T., 2017. Review on the effectiveness of adsorbent materials in oil spills clean up. 7th Int. Conf. ICEEE 131–138.

Al-Jammal, N., Juzsakova, T., Zsirka, B., Sebestyén, V., Németh, J., Cretescu, I., Halmágyi, T., Domokos, E., Rédey, Á., 2019. Modified Jordanian zeolitic tuff in hydrocarbon removal from surface water. J. Environ. Manage. 239, 333–341. https://doi.org/10.1016/j.jenvman.2019.03.079

Alaa El-Din, G., Amer, A.A., Malsh, G., Hussein, M., 2017. Study on the use of banana peels for oil spill removal. Alexandria Eng. J. 57, 2061–2068. https://doi.org/10.1016/j.aej.2017.05.020

Allen, T.W., Kuyucak, S., Chung Prot, S.H., 1999. The effect of hydrophobic and hydrophilic channel walls on the structure and diffusion of water and ions. J. Chem. Phys. 111, 7985–7999. https://doi.org/10.1063/1.480132

Annunciado, T.R., Sydenstricker, T.H.D., Amico, S.C., 2005. Experimental investigation of various vegetable fibers as sorbent materials for oil spills. Mar. Pollut. Bull. 50, 1340–1346. https://doi.org/10.1016/j.marpolbul.2005.04.043

ASTM International, 1995. Standard test method for determination of the saponification value of fats and oils. West Conshohocken, PA. https://doi.org/10.1520/D5558-95

Auerbach, M., 2003. Handbook of zeolite science and technology. CRC press.

Azambre, B., Westermann, A., Finqueneisel, G., Can, F., Comparot, J.D., 2015. Adsorption and desorption of a model hydrocarbon mixture over HY zeolite under dry and wet conditions. J. Phys. Chem. C 119, 315–331. https://doi.org/10.1021/jp509046n

Bandura, L., Franus, M., Józefaciuk, G., Franus, W., 2015a. Synthetic zeolites from fly ash as effective mineral sorbents for land-based petroleum spills cleanup. Fuel 147, 100–107. https://doi.org/10.1016/j.fuel.2015.01.067

Bandura, L., Franus, M., Panek, R., Woszuk, A., Franus, W., 2015b. Characterization of zeolites and their use as adsorbents of petroleum substances. Przem. Chem. 94, 323–327. https://doi.org/10.15199/62.2015.3.11

Bandura, L., Woszuk, A., Kołodyńska, D., Franus, W., 2017. Application of mineral sorbents for removal of petroleum substances: a review. Minerals 7, 37. https://doi.org/10.3390/min7030037

Bansal, R.C., Goyal, M., 2005. Activated carbon adsorption, CRC press. https://doi.org/10.1007/BF02276400

Barrer, R.M., Makki, M.B., 1964. Molecular sieve sorbents from clinoptilolite. Can. J. Chem. 42, 1481–1487. https://doi.org/10.1139/v64-223

Bayat, A., Aghamiri, S., Moheb, A., 2008. Oil sorption by synthesized exfoliated graphite (EG). Iran. J. Chem. Eng. 5, 51–64.

Behnood, R., Anvaripour, B., Jaafarzade, N., Fard, H., 2013. Application of natural sorbents in crude oil adsorption. Iran. J. Oil Gas Sci. Technol. 2, 1–11. https://doi.org/10.22050/IJOGST.2013.4792

Belchinskaya, L., Novikova, L., Khokhlov, V., Ly Tkhi, J., 2013. Contribution of ion-exchange and non-ion-exchange reactions to sorption of ammonium ions by natural and activated aluminosilicate sorbent. J. Appl. Chem. 2013, 1–9. https://doi.org/10.1155/2013/789410

Beyer, H.K., 2002. Dealumination techniques for zeolites, in: Post-Synthesis Modification I. Springer, Berlin, Heidelberg, pp. 203–255. https://doi.org/10.1007/3-540-69750-0

Birch, M.E., Ruda-Eberenz, T.A., Chai, M., Andrews, R., Hatfield, R.L., 2013. Properties that influence the specific surface areas of carbon nanotubes and nanofibers. Ann. Occup. Hyg. 57, 1148–1166. https://doi.org/10.1093/annhyg/met042

Bokhoven, J.A. van, Koningsberger, D.C., Kunkeler, P., Van Bekkum, H., Kentgens, A.P.M., 2000. Stepwise dealumination of zeolite Beta at specific T-sites observed with ^{27}Al MAS and ^{27}Al MQ MAS NMR. J. Am. Chem. Soc. 122, 12842–12847. https://doi.org/10.1021/ja002689d

Bolis, V., Busco, C., Ugliengo, P., 2006. Thermodynamic study of water adsorption in high-silica zeolites. J. Phys. Chem. B 110, 14849–14859. https://doi.org/10.1021/jp061078q

Boveri, M., Márquez-Álvarez, C., Laborde, M.Á., Sastre, E., 2006. Steam and acid dealumination of mordenite. Characterization and influence on the catalytic performance in linear alkylbenzene synthesis. Catal. Today 114, 217–225. https://doi.org/10.1016/j.cattod.2006.01.012

Buzgar, N., Ionut Apopei, A., 2009. The Raman study of carbonates. Geologie 55, 97–112.

Campbell, S.M., Bibby, D.M., Coddington, J.M., Howe, R.F., Meinhold, R.H., 1996. Dealumination of HZSM-5 zeolites I. Calcination and hydrothermal treatment. J. Catal. 161, 338–349. https://doi.org/10.1006/jcat.1996.0191

Carmody, O., Frost, R., Xi, Y. and, Kokot, S., 2007. The use of organo-clays sorbents for cleaning up oil spills. J. Colloid Interface Sci. 305, 17–24. https://doi.org/https://doi.org/10.1016/j.jcis.2006.09.032

Ceylan, D., Dogu, S., Karacik, B., Yakan, S.D., Okay, O.S., Okay, O., 2009. Evaluation of butyl rubber as sorbent material for the removal of oil and polycyclic aromatic hydrocarbons from seawater. Environ. Sci. Technol. 43, 3846–3852. https://doi.org/10.1021/es900166v

Chang, S.E., Stone, J., Demes, K., Piscitelli, M., 2014. Synthesis, part of a special feature on vulnerability and adaptation to oil spills consequences of oil spills: a review and framework for informing planning. Ecol. Soc. 19, 26. https://doi.org/10.5751/ES-06406-190226

Chemvioncarbon, 2018. AQUACARBTM 207C 12X30 coconut based granular activated carbon.

Chen, D., Wang, L., Ma, Y., Yang, W., 2016. Super-adsorbent material based on functional polymer particles with a multilevel porous structure. NPG Asia Mater. 8, 301. https://doi.org/10.1038/am.2016.117

Chen, N.Y., 1976. Hydrophobic properties of zeolites. J. Phys. Chem. 80, 60–64. https://doi.org/10.1021/j100542a013

Ci, B.L., Manikoth, S.M., Li, X., Vajtai, R., Ajayan, P.M., 2007. Ultrathick freestanding aligned carbon nanotube films. Adv. Mater. 19, 3300–3303. https://doi.org/10.1002/adma.200602974

Cretescu, I., Soreanu, G., Harja, M., 2015. A low-cost sorbent for removal of copper ions from wastewaters based on sawdust/fly ash mixture. Int. J. Environ. Sci. Technol. 12, 1799–1810. https://doi.org/10.1007/s13762-014-0596-x

Csicsery, S.M., 1986. Catalysis by shape selective zeolites - science and technology. Pure Appl. Chem. 58, 841–856. https://doi.org/10.1351/pac198658060841

Das, R., Tuhi, S. Das, Mohammed, S., Zaidi, J., 2018. Adsorption, in: Carbon Nanotubes for Clean Water. Springer International Publishing, pp. 90–91. https://doi.org/10.1007/978-3-319-95603-9

Davis, R.J., 2003. New perspectives on basic zeolites as catalysts and catalyst supports. J. Catal. 216, 396–405. https://doi.org/10.1016/S0021-9517(02)00034-9

De Castro Dantas, T.N., Neto, A.A.D., De A. Moura, M.C.P., 2001. Removal of chromium from aqueous solutions by diatomite treated with microemulsion. Water Res. 35, 2219–2224. https://doi.org/10.1016/S0043-1354(00)00507-8

De Gisi, S., Lofrano, G., Grassi, M., Notarnicola, M., 2016. Characteristics and adsorption capacities of low-cost sorbents for wastewater treatment: A review. Sustain. Mater. Technol. 9, 10–40. https://doi.org/10.1016/j.susmat.2016.06.002

De Lucas, A., Canizares, P., Durán, A., Carrero, A., 1997. Dealumination of HZSM-5 zeolites: Effect of steaming on acidity and aromatization activity. Appl. Catal. A Gen. 154, 221–240. https://doi.org/10.1016/S0926-860X(96)00367-5

De Ridder, D.J., Verberk, J.Q.J.C., Heijman, S.G.J., Amy, G.L., Van Dijk, J.C., 2012. Zeolites for nitrosamine and pharmaceutical removal from demineralised and surface water: Mechanisms and efficacy. Sep. Purif. Technol. 89, 71–77. https://doi.org/10.1016/j.seppur.2012.01.025

Deschamps, G., Caruel, H., Borredon, M.E., Bonnin, C., Vignoles, C., 2003. Oil removal from water by selective sorption on hydrophobic cotton fibers. 1. Study of sorption properties and comparison with other cotton fiber-based sorbents. Environ. Sci. Technol. 37, 1013–1015. https://doi.org/10.1021/es020061s

Dettmer, K., Knobloch, T., Engewald, W., 2000. Stability of reactive low boiling hydrocarbons on carbon based adsorbents typically used for adsorptive enrichment and thermal desorption. Fresenius. J. Anal. Chem. 366, 70–78. https://doi.org/10.1007/s002160050014

Dileo, R.A., Landi, B.J., Raffaelle, R.P., Dileo, R.A., 2007. Purity assessment of multiwalled carbon nanotubes by Raman spectroscopy. J. Appl. Phys. 101, 064307. https://doi.org/10.1063/1.2712152

Doyle, D.H., Brown, A.B., 1997. Field test of produced water treatment with polymer modified bentonite, Society of Petroleum Engineers. Casper, Wyoming, 18-21 May.

Dresselhaus, M.S., Dresselhaus, G., Saito, R., Jorio, A., 2005. Raman spectroscopy of carbon nanotubes. Phys. Rep. 409, 47–99. https://doi.org/10.1016/j.physrep.2004.10.006

Duong, H.T.T., Burford, R.P., 2006. Effect of foam density, oil viscosity, and temperature on oil sorption behavior of polyurethane. J. Appl. Polym. Sci. 99, 306–367. https://doi.org/10.1002/app.22426

Duvarci, Ö.Ç., Akdeniz, Y., Özmihçi, F., Ülkü, S., Balköse, D., Çiftçioğlu, M., 2007. Thermal behaviour of a zeolitic tuff. Ceram. Int. 33, 795–801. https://doi.org/10.1016/j.ceramint.2006.01.003

Eatemadi, A., Daraee, H., Karimkhanloo, H., Kouhi, M., Zarghami, N., Akbarzadeh, A., Abasi, M., Hanifehpour, Y., Joo, S., 2014. Carbon nanotubes: Properties, synthesis, purification, and medical applications. Nanoscale Res. Lett. 9, 393. https://doi.org/10.1186/1556-276X-9-393

EPA, 2018. 2018 Edition of the drinking water standards and health advisories tables, EPA 822-F-18-001 Office of water. Washington, DC.

EPA, 2015. Case study: analysis of the impacts of water acquisition for hydraulic fracturing on local water availability, Environmental Protection Agency Office of Research and Development. Washington, D.C.

Erdem, E., Karapinar, N., Donat, R., 2004. The removal of heavy metal cations by natural zeolites. J. Colloid Interface Sci. 280, 309–314. https://doi.org/10.1016/j.jcis.2004.08.028

Ersoy, B., Çelik, M.S., 2003. Effect of hydrocarbon chain length on adsorption of cationic surfactants onto clinoptilolite. Clays Clay Miner. 51, 172–180. https://doi.org/10.1346/CCMN.2003.0510207

Ertan, A., 2004. CO_2, N_2 and Ar adsorption on zeolites. Master's thesis, Izmir Institute of Technology.

F. Elkady, M., 2017. Equilibrium and kinetics behavior of oil spill process onto synthesized nano-activated carbon. Am. J. Appl. Chem. 3, 22. https://doi.org/10.11648/j.ajac.s.2015030301.14

Ferey, G., 2002. The new microporous compounds and their design. Comptes Rendus l'Académie des Sci. - Ser. IIC - Chem. 1, 1–13. https://doi.org/10.1016/s1251-8069(97)86253-7

Fingas, M., 2016. Oil spill science and technology prevention, response, and cleanup. Gulf professional publishing, The Boulevard, Langford Lane, Kidlington, Oxford.

Flanigen, E.M., 1980. Molecular sieve zeolite technology - the first twenty-five years. Pure Appl. Chem. 52, 2191–2211. https://doi.org/10.1351/pac198052092191

Fritt-Rasmussen, J., Brandvik, P.J., 2011. Measuring ignitability for in situ burning of oil spills weathered under Arctic conditions: From laboratory studies to large-scale field experiments. Mar. Pollut. Bull. 62, 1780–1785. https://doi.org/10.1016/j.marpolbul.2011.05.020

Fu, Y., Cao, H.J., 2011. A new coagulant for spilled oil removal with bentonite and calcium chlorine and sawdust. Adv. Mater. Res. 284–286, 2513–2516. https://doi.org/10.4028/www.scientific.net/AMR.284-286.2513

Fuoco, D., 2012. A new method for characterization of natural zeolites and organic nanostructure using atomic force microscopy. Nanomaterials 2, 79–91. https://doi.org/10.3390/nano2010079

Gapingsi, G.E., Korbas, R., Santos, M., 2017. Modelling and control of a flexible floating boom: First approach. IFAC-PapersOnLine 50, 13108–13113. https://doi.org/10.1016/j.ifacol.2017.08.2163

Ge, B., Zhang, Z., Zhu, X., Ren, G., Men, X., Zhou, X., 2013. A magnetically superhydrophobic bulk material for oil removal. Colloids Surfaces A Physicochem. Eng. Asp. 429, 129–133. https://doi.org/10.1016/j.colsurfa.2013.04.004

Gedik, K., Imamoglu, I., 2008. Removal of cadmium from aqueous solutions using clinoptilolite: Influence of pretreatment and regeneration. J. Hazard. Mater. 155, 385–392. https://doi.org/10.1016/j.jhazmat.2007.12.101

Gheorghiu, C.C., Machado, B.F., Gouygou, M., Serp, P., 2014. Chiral rhodium complexes covalently anchored on carbon nanotubes for enantioselective. Dalt. Trans. 43, 7455–7463. https://doi.org/10.1039/c3dt53301h

Ghrair, A.M., Ingwersen, J., Streck, T., 2009. Nanoparticulate zeolitic tuff for immobilizing heavy metals in soil: Preparation and characterization. Water. Air. Soil Pollut. 203, 155–168. https://doi.org/10.1007/s11270-009-9999-6

Golnabi, H., 2012. Carbon nanotube research developments in terms of published papers and patents, synthesis and production. Sci. Iran. 19, 2012–2022. https://doi.org/10.1016/j.scient.2012.10.036

Gounder, R., 2014. Hydrophobic microporous and mesoporous oxides as Brønsted and Lewis acid catalysts for biomass conversion in liquid water. Catal. Sci. Technol. 4, 2877–2886. https://doi.org/10.1039/c4cy00712c

Grieco, S.A., Ramarao, B. V., 2013. Removal of TCEP from aqueous solutions by adsorption with zeolites. Colloids Surfaces A Physicochem. Eng. Asp. 434, 329–338. https://doi.org/10.1016/j.colsurfa.2013.04.042

Gryta, M., Karakulski, K., Morawski, A.W., 2001. Purification of oily wastewater by hybrid ultrafiltration. Water Res. 35, 3665–3669. https://doi.org/10.1016/S0043-1354(01)00083-5

Gu, J., Xiao, P., Chen, J., Zhang, J., Huang, Y., Chen, T., 2014. Janus polymer/carbon nanotube hybrid membranes for oil/water separation. Appl. Mater. Interfaces 6, 16204–16209. https://doi.org/dx.doi.org/10.1021/am504326m

Gui, B.X., Wei, J., Wang, K., Cao, A., Zhu, H., Jia, Y., Shu, Q., Wu, D., 2010. Carbon nanotube sponges. Adv. Mater. 22, 617–621. https://doi.org/10.1002/adma.200902986

Gui, X., Li, H., Wang, K., Wei, J., Jia, Y., Li, Z., Fan, L., Cao, A., Zhu, H., Wu, D., 2011. Recyclable carbon nanotube sponges for oil absorption. Acta Mater. 59, 4798–4804. https://doi.org/10.1016/j.actamat.2011.04.022

Gui, X., Zeng, Z., Lin, Z., Gan, Q., Xiang, R., Zhu, Y., Cao, A., Tang, Z., 2013. Magnetic and highly recyclable macroporous carbon nanotubes for spilled oil sorption and separation. ACS Appl. Mater. Interfaces 5, 5845–5850. https://doi.org/10.1021/am4015007

Guodong, Q., Yupeng, Z., Xuhe, R., Jie, C., 2015. Research on development and effectiveness, evaluation technology of new environment-friendly oil spill dispersant. Aquat. Procedia 3, 245–253. https://doi.org/10.1016/j.aqpro.2015.02.218

Gupta, S., Tai, N., 2016. Carbon materials as oil sorbents: A review on the synthesis and performance. J. Mater. Chem. A Mater. energy Sustain. 4, 1550–1565. https://doi.org/10.1039/c5ta08321d

Hernández-Huesca, R., Díaz, L., Aguilar-Armenta, G., 1999. Adsorption equilibria and kinetics of CO_2, CH_4 and N_2 in natural zeolites. Sep. Purif. Technol. 15, 163–173. https://doi.org/10.1016/S1383-5866(98)00094-X

Hirsch, A., 2002. Functionalization of single-walled carbon nanotubes. Minireview 41, 1853–1859.

Ho, Y.S., Mckay, G., 1999. Pseudo-second order model for sorption. Process Biochem. 34, 451–465.

Hosseini Hashemi, M.S., Eslami, F., Karimzadeh, R., 2019. Organic contaminants removal from industrial wastewater by CTAB treated synthetic zeolite Y. J. Environ. Manage. 233, 785–792. https://doi.org/10.1016/j.jenvman.2018.10.003

Huang, X., Yu, F., Peng, Q., Huang, Y., 2018. Superb adsorption capacity of biochar derived from leather shavings for Congo red. RSC Adv. 8, 29781–29788. https://doi.org/10.1039/c8ra06370b

Husseien, M., Amer, A.A., El-maghraby, A., Hamedallah, N., 2009. Characterization of corn stalk and study of carbonized corn stalk in dye and gas oil sorption. J. Anal. Appl. Pyrolysis 86, 360–363. https://doi.org/10.1016/j.jaap.2009.08.003

Hyung-Mln, C., Cloud, R.M., 1992. Natural sorbents in oil spill cleanup. Environ. Sci. Technol. 26, 772–776. https://doi.org/10.1021/es00028a016

Ihsanullah, Al-khaldi, F.A., Abu-sharkh, B., Mahmoud, A., Imran, M., Laoui, T., Ali, M., 2015. Effect of acid modification on adsorption of hexavalent chromium (Cr(VI)) from aqueous solution by activated carbon and carbon nanotubes. Desalin. Water Treat. 57, 7232–7244. https://doi.org/10.1080/19443994.2015.1021847

ITOPF Limited, 2019. Oil tanker spill statistics 2018. London.

Ivshina, I.B., Kuyukina, M.S., Krivoruchko, A. V., Elkin, A.A., Makarov, S.O., Cunningham, C.J., Peshkur, T.A., Atlas, R.M., Philp, J.C., 2015. Oil spill problems and sustainable response strategies through new technologies. Environ. Sci. Process. Impacts 17, 1201–1219. https://doi.org/10.1039/c5em00070j

Jameel, A.T., Alam, A.M.Z., Abass O, A., Muyubi, S.A., Abdul Karim, M.I., 2011. Removal of oil and grease as emerging pollutants of concern (EPC) in wastewater stream. IIUM Eng. J. 12, 4. https://doi.org/10.31436/iiumej.v12i4.218

Jeon, I., Chang, D.W., 2011. Functionalization of carbon nanotubes, in: Carbon Nanotubes – Polymer Nanocomposites. INTECH Open Access Publisher, pp. 91–110.

Jian, W., Kitanaka, A., Nishijima, W., Baes, A.U., Okada, M., 1999. Removal of oil pollutants in seawater as pretreatment of reverse osmosis desalination process. Water Res. 33, 1857–1863. https://doi.org/10.1016/S0043-1354(98)00404-7

Jiang, N., Shang, R., Heijman, S.G.J., Rietveld, L.C., 2018. High-silica zeolites for adsorption of organic micro-pollutants in water treatment: A review. Water Res. 144, 145–161. https://doi.org/10.1016/j.watres.2018.07.017

Jones, C.W., Hwang, S.J., Okubo, T., Davis, M.E., 2001. Synthesis of hydrophobic molecular sieves by hydrothermal treatment with acetic acid. Chem. Mater. 13, 1041–1050. https://doi.org/10.1021/cm0007961

Kabalan, I., Lebeau, B., Fadlallah, M.-B., Toufaily, J., Hamieh, T., Bellat, J.P., Daou, T.J., 2016. Hierarchical faujasite-type zeolite for molecular decontamination. J. Nanosci. Nanotechnol. 16, 9318–9322. https://doi.org/10.1166/jnn.2016.12884

Kar, T., Bettinger, H.F., Scheiner, S., Roy, A.K., 2008. Noncovalent π - π stacking and CH- π interactions of aromatics on the surface of single-wall carbon nanotubes : An MP2 study. J. Phys. Chem. C 27, 20070–20075.

Karousis, N., Tagmatarchis, N., 2010. Current progress on the chemical modification of carbon nanotubes. Chem. Rev. 110, 5366–5397. https://doi.org/10.1021/cr100018g

Kaushik, B.K., Majumder, M.K., 2015. Carbon nanotube: properties and applications, in: Carbon Nanotube Based VLSI Interconnects. Analysis and Design. SpringerBriefs in Applied Sciences and Technology, pp. 17–37. https://doi.org/10.1007/978-81-322-2047-3

Kawai, T., Tsutsumi, K., 1992. Evaluation of hydrophilic-hydrophobic character of zeolites by measurements of their immersional heats in water. Colloid Polym. Sci. 270, 711–715. https://doi.org/10.1007/BF00654048

Kerr, G.T., 1968. Chemistry of crystalline aluminosilicates. V. preparation of aluminum-deficient faujasites. J. Phys. Chem. 72, 2594–2596. https://doi.org/10.1021/j100853a058

Kesraoui-Ouki, S., Cheeseman, C.R., Perry, R., 1994. Natural zeolite utilization in pollution control: A review of applications to metals′ effluents. J. Chem. Tech. Biorechnol. 59, 121–126. https://doi.org/10.1002/chin.199432295

Khosravi, M., Azizian, S., 2015. Synthesis of a novel highly oleophilic and highly hydrophobic sponge for rapid oil spill clean up. Appl. Mater. Interfaces 7, 25326–25333. https://doi.org/10.1021/acsami.5b07504

Kim, J.-W., Kotagiri, N., 2014. Stealth nanotubes: strategies of shielding carbon nanotubes to evade opsonization and improve biodistribution. Int. J. Nanomedicine 85. https://doi.org/10.2147/ijn.s51854

Knowlton, G.D., 1981. Thermal study of types of water associated with clinoptilolite. Clays Clay Miner. 29, 403–411. https://doi.org/10.1346/ccmn.1981.0290510

Kong, L., Chen, X., Yu, L., Wu, Z., Zhang, P., 2015. Superhydrophobic cuprous oxide nanostructures on phosphor- copper meshes and their oil–water separation and oil spill cleanup. ACS Appl. Mater. Interfaces 7, 2616–2625. https://doi.org/10.1021/am507620s

Küntzel, J., Ham, R., Melin, T., 1999. Regeneration hydrophober Zeolithe mittels Wasserdampf. Chemie-Ingenieur-Technik 71, 508–511.

https://doi.org/10.1002/cite.330710520

Lami, E.B., Fajula, F., Anglerot, D., Des Courieres, T., 1993. Single step dealumination of zeolite beta precursors for the preparation of hydrophobic adsorbents. Microporous Mater. 1, 237–245. https://doi.org/10.1016/0927-6513(93)80067-5

Lau, K.K.S., Teo, K.B.K., Chhowalla, M., Amaratunga, G.A.J., Milne, W.I., Mckinley, G.H., Gleason, K.K., 2003. Superhydrophobic carbon nanotube forests. Nano Lett. 3, 1701–1705. https://doi.org/doi.org/10.1021/nl034704t

Le, V.T., Ngo, C.L., Le, Q.T., Ngo, T.T., Nguyen, D.N., Vu, M.T., 2013. Surface modification and functionalization of carbon nanotube with some organic compounds. Adv. Nat. Sci. Nanosci. Nanotechnol. 4, 035017. https://doi.org/10.1088/2043-6262/4/3/035017

Lee, C., Johnson, N., Drelich, J., Yap, Y.K., 2010. The performance of superhydrophobic and superoleophilic carbon nanotube meshes in water – oil filtration. Carbon N. Y. 49, 669–676. https://doi.org/10.1016/j.carbon.2010.10.016

Lee, S., Shantz, D.F., 2004. Modifying zeolite particle morphology and size using water/ oil/surfactant mixtures as confined domains for zeolite growth. Chem. Commun 3492, 680–681. https://doi.org/10.1039/B315646J

Lehman, J.H., Terrones, M., Meunier, V., Mansfield, E., Hurst, K.E., 2011. Evaluating the characteristics of multiwall carbon nanotubes. Carbon N. Y. 49, 2581–2602. https://doi.org/10.1016/j.carbon.2011.03.028

Lercher, J.A., Jentys, A., Brait, A., 2008. Catalytic test reactions for probing the acidity and basicity of zeolites. Mol. Sieves - Sci. Technol. 6, 153–212. https://doi.org/10.1007/3829_2007_017

Li, F., Wang, Y., Wang, D., Wei, F., 2004. Characterization of single-wall carbon nanotubes by N_2 adsorption. Carbon N. Y. 42, 2375–2383. https://doi.org/10.1016/j.carbon.2004.02.025

Li, Y., Li, L., Yu, J., 2017. Applications of Zeolites in Sustainable Chemistry. Chem 3, 928–949. https://doi.org/10.1016/j.chempr.2017.10.009

Liu, T., Chen, S., Liu, H., 2015. Oil adsorption and reuse performance of multi-walled carbon nanotubes oil adsorption and reuse performance of multi-walled carbon nanotubes. Procedia Eng. 102, 1896–1902. https://doi.org/10.1016/j.proeng.2015.01.329

Liu, Y., Kujawinski, E.B., 2015. Chemical composition and potential environmental impacts of water-soluble polar crude oil components inferred from ESI FT-ICR MS. PLoS One 10, 1–18. https://doi.org/10.1371/journal.pone.0136376

Lutz, W., 2014. Zeolite Y: Synthesis, modification, and properties - A case revisited. Adv. Mater. Sci. Eng. 2014. https://doi.org/10.1155/2014/724248

Lv, N., Wang, X., Peng, S., Zhang, H., Luo, L., 2018. Study of the kinetics and equilibrium of the adsorption of oils onto hydrophobic jute fiber modified via the sol-gel method. Int. J. Environ. Res. Public Health 15, 969. https://doi.org/10.3390/ijerph15050969

Maesen, T., Marcus, B., 2001. The zeolite scene- an overview, in: Studies in Surface Science and Catalysis. Elsevier Science B.V., pp. 1–9. https://doi.org/10.1016/S0167-2991(01)80242-1

Malik, M.A., Wani, M.Y., Hashim, M.A., 2012. Microemulsion method: A novel route to synthesize organic and inorganic nanomaterials. 1st Nano Update. Arab. J. Chem. 5, 397–417. https://doi.org/10.1016/j.arabjc.2010.09.027

Margeta, K., Zabukovec, N., Siljeg, M., Farkas, A., 2013. Natural zeolites in water treatment – How effective is their use, in: Water Treatment. pp. 81–112. https://doi.org/10.5772/50738

Mastinu, A., Kumar, A., Maccarinelli, G., Bonini, S.A., Kumar, A., Maccarinelli, G., Bonini, S.A., Premoli, M., Aria, F., Gianoncelli, A., Memo, M., 2019. Zeolite clinoptilolite: Therapeutic virtues of an ancient mineral. Molecules 24, 1517. https://doi.org/doi:10.3390/molecules24081517

Masuelli, M., Marchese, J., Ochoa, N.A., 2009. SPC/PVDF membranes for emulsified oily wastewater treatment. J. ofMembrane Sci. 326, 688–693. https://doi.org/10.1016/j.memsci.2008.11.011

Maulion, R. V, Abacan, S.A., Allorde, G.G., Cherrielyne, M., Umali, S., 2015. Oil spill adsorption capacity of activated carbon tablets from corncobs in simulated oil-water mixture. Asia Pacific J. Multidiscip. Res. 3, 146–151.

McCallum, C.L., Bandosz, T.J., McGrother, S.C., Muller, E.A., Gubbins, K.E., 1999. Molecular model for adsorption of water on activated carbon: Comparison of simulation and experiment. Langmuir 15, 533–544. https://doi.org/10.1021/la9805950

Meng, L., Fu, C., Lu, Q., 2009. Advanced technology for functionalization of carbon nanotubes. Prog. Nat. Sci. 19, 801–810. https://doi.org/10.1016/j.pnsc.2008.08.011

Morin, S., Berreghis, A., Ayrault, P., Gnep, N.S., Guisnet, M., 1997. Dealumination of zeolites part VIII acidity and catalytic properties of HEMT zeolites dealuminated by steaming. J. Chem. Soc. Faraday Trans. 93, 3269–3275. https://doi.org/10.1039/a702538f

Moss, L., 2010. The 13 largest oil spills in history. Mother Nat. Netw. 16.

Moura, C.C., Lago, R.M., 2009. Environmental catalytic growth of carbon nanotubes and nanofibers on vermiculite to produce floatable hydrophobic “nanosponges” for oil spill remediation. Appl. Catal. B Environ. 90, 436–440. https://doi.org/10.1016/j.apcatb.2009.04.003

Mozgawa, W., Król, M., Barczyk, K., 2011. FT-IR studies of zeolites from different structural groups. Chemik 671–674.

MSZ, 2009. Water quality. Part 7: Determination of extractable petroleum hydrocarbon content in a boiling point range from 160°C to 520°C by gas chromatographic method. Hungarian Natl. Stand. MSZ.

Muir, B., Bajda, T., 2016. Organically modified zeolites in petroleum compounds spill cleanup - Production, efficiency, utilization. Fuel Process. Technol. J. 149, 153–162. https://doi.org/10.1016/j.fuproc.2016.04.010

Müller, M., Harvey, G., Prins, R., 2000. Comparison of the dealumination of zeolites beta, mordenite, ZSM-5 and ferrierite by thermal treatment, leaching with oxalic acid and treatment with $SiCl_4$ by ^1H, ^{29}Si and ^{27}Al MAS NMR. Microporous Mesoporous Mater. 34, 135–147. https://doi.org/10.1016/S1387-1811(99)00167-5

Munthali, M., Johan, E., Matsue, N., 2015. Proton adsorption selectivity of zeolites in aqueous media: Effect of exchangeable cation species of zeolites, in: Environments. pp. 91–104. https://doi.org/10.3390/environments2010091

Mustafa, F., Al-Ghouti, M.A., Khalili, F.I., Al-Degs, Y.S., 2010. Characteristics of organosulphur compounds adsorption onto Jordanian zeolitic tuff from diesel fuel. J. Hazard. Mater. 182, 97–107. https://doi.org/10.1016/j.jhazmat.2010.06.003

Naseer, A., Jamshaid, A., Hamid, A., Muhammad, N., Ghauri, M., Iqbal, J., Rafiq, S., Khuram, S., Shah, N.S., 2019. Lignin and lignin based materials for the removal of heavy metals from waste water - An overview. Zeitschrift fur Phys. Chemie 233, 315–345. https://doi.org/10.1515/zpch-2018-1209

Nethaji, S., Sivasamy, A., Mandal, A.B., 2013. Adsorption isotherms, kinetics and mechanism for the adsorption of cationic and anionic dyes onto carbonaceous particles prepared from Juglans regia shell biomass. Int. J. Environ. Sci. Technol. 10, 231–242. https://doi.org/10.1007/s13762-012-0112-0

Nguyen, D.D., Tai, N.-H., Leea, S.-B., Kuob, W.-S., 2012. Environmental science fabricated using a facile dip coating method. Energy Environ. Sci. 7908–7912. https://doi.org/10.1039/c2ee21848h

Noor-Ul-Amin, 2014. A multi-directional utilization of different ashes. RSC Adv. 4, 62769–62788. https://doi.org/10.1039/c4ra06568a

Nwadiogbu, J.O., Ajiwe, V.I.E., Okoye, P.A.C., 2016. Removal of crude oil from aqueous medium by sorption on hydrophobic corncobs: Equilibrium and kinetic studies. J. Taibah Univ. Sci. 10, 56–63. https://doi.org/10.1016/j.jtusci.2015.03.014

Oddershede, J., Nielsen, K., Stahl, K., 2007. Using X-ray powder diffraction and principal component analysis to determine structural properties for bulk samples of multiwall carbon nanotubes. Zeitschrift fur Krist. 222, 186–192. https://doi.org/10.1524/zkri.2007.222.3-4.186

Olalekan, A.P., Dada, A.O., Adesina, O.A., 2014. Review: Silica aerogel as a viable absorbent for oil spill remediation. J. Encapsulation Adsorpt. Sci. 4, 122–131.

Ornitz, B.E., Champ, M.A., 2002. Oil spills first principles: Prevention and best response, Elsevier. Elsevier.

Ovejero, G., Sotelo, J.L., Romero, M.D., Rodríguez, A., Ocaña, M.A., Rodríguez, G., García, J., 2006. Multiwalled carbon nanotubes for liquid-phase oxidation. functionalization, characterization, and catalytic activity. Ind. Eng. Chem. Res. 45, 2206–2212. https://doi.org/10.1021/ie051079p

Peixoto, D.P.B., Cabral de Menezes, S.M., Pais da Silva, M.I., 2003. Influence of different processes of dealumination on acid properties of an H-ferrierite zeolite. Mater. Lett. 57, 3933–3942. https://doi.org/10.1016/S0167-577X(03)00243-X

Perraki, T., Orfanoudaki, A., 2004. Mineralogical study of zeolites from Pentalofos area, Thrace, Greece. Appl. Clay Sci. 25, 9–16. https://doi.org/10.1016/S0169-1317(03)00156-X

Peterson, C.H., Rice, S.D., Short, J.W., Esler, D., Bodkin, J.L., Ballachey, B.E., Irons, D.B., 2003. Long-term ecosystem response to the Exxon Valdez oil spill. Science (80-.). 302, 2082–2086. https://doi.org/10.1126/science.1084282

Pham, V.H., Dickerson, J.H., 2014. Superhydrophobic silanized melamine sponges as high efficiency oil absorbent materials. Appl. Mater. interfaces 6, 14181–14188. https://doi.org/10.1021/am503503m

Phan, T.T.N., Nikoloski, A.N., Bahri, P.A., Li, D., 2019. Enhanced removal of organic using $LaFeO_3$-integrated modified natural zeolites via heterogeneous visible light photo-Fenton degradation. J. Environ. Manage. 233, 471–480. https://doi.org/10.1016/j.jenvman.2018.12.051

Pichat, P., Beaumont, R., Barthomeuf, D., 1974. Infra-red structural study of aluminiumdeficient Y zeolites. J. Chem. Soc. Faraday Trans. 1 Phys. Chem. Condens. Phases 70, 1402–1407. https://doi.org/10.1039/F19747001402

Pourzamani, H., Hajizadeh, Y., Fadaei, S., 2015. Efficiency enhancement of multi-walled carbon nanotubes by ozone for benzene removal from aqueous solution. Int. J. Environ. Health Eng. 4, 29. https://doi.org/10.4103/2277-9183.163972

Radetić, M.M., Jocić, D.M., Jovančić, P.M., Petrović, Z.L., Thomas, H.F., 2003. Recycled wool-based nonwoven material as an oil sorbent. Environ. Sci. Technol. 37, 1008–1012. https://doi.org/10.1021/es0201303

Rajakovi, V., Rajakovi, L., 2008. Governing factors for motor oil removal from water with different sorption materials. J. Hazard. Mater. 154, 558–563. https://doi.org/10.1016/j.jhazmat.2007.10.066

Rebelo, S.L.H., Guedes, A., Szefczyk, M.E., Pereira, A.M., Araújo, J.P., Freire, C., 2016. Progresses on the Raman spectra analysis of covalently functionalized multiwall carbon nanotubes: unraveling disorder on graphitic materials. Phys. Chem. Chem. Phys. 18, 12784–12796. https://doi.org/10.1039/C5CP06519D

Reeve, P.J., Fallowfield, H.J., 2018. Natural and surfactant modified zeolites: A review of their applications for water remediation with a focus on surfactant desorption and toxicity towards microorganisms. J. Environ. Manage. 205, 253–261. https://doi.org/10.1016/j.jenvman.2017.09.077

Reichenbächer, M., Einax, J.W., 2011. Challenges in analytical quality assurance. Springer Berlin Heidelberg, Berlin, Heidelberg. https://doi.org/10.1007/978-3-642-16595-5

Roberge, D.M., Hausmann, H., Hölderich, W.F., 2002. Dealumination of zeolite beta by acid leaching: A new insight with two-dimensional multi-quantum and cross polarization ^{27}Al MAS NMR. Phys. Chem. Chem. Phys. 4, 3128–3135. https://doi.org/10.1039/b110679c

Saifuddin, N., Raziah, A.Z., Junizah, A.R., 2012. Carbon nanotubes: a review on structure and their interaction with proteins. J. Chem. 2013, 1–18. https://doi.org/10.1155/2013/676815

Sakthivel, T., Reid, D.L., Goldstein, I., Hench, L., Seal, S., 2013. Hydrophobic high surface area zeolites derived from fly ash for oil spill remediation. Environ. Sci. Technol. 47, 5843–5850. https://doi.org/10.1021/es3048174

Salem, N.M., Ahmad, R.A., Awwad, A.M., 2010. Chemical modification of zeolitic tuff for removal of Hg(II) from water. Environ. Res. J. 4, 286–290. https://doi.org/10.3923/erj.2010.286.290

Salih, A.M., 2018. The purification of industrial wastewater to remove heavy metals and investigation into the use of zeolite as a remediation tool. Dr. Diss. Univ. Wolverhampt.

Samadishadlou, M., Farshbaf, M., Annabi, N., Kavetskyy, T., Khalilov, R., Saghfi, S., Akbarzadeh, A., Mousavi, S., 2018. Magnetic carbon nanotubes: Preparation, physical properties, and applications in biomedicine. Artif. Cells, Nanomedicine, Biotechnol. 46, 1314–1330. https://doi.org/10.1080/21691401.2017.1389746

Sepehri, A., Sarrafzadeh, M.H., 2018. Effect of nitrifiers community on fouling mitigation and nitrification efficiency in a membrane bioreactor. Chem. Eng. Process. - Process Intensif. 128, 10–18. https://doi.org/10.1016/j.cep.2018.04.006

Shang, Y., Si, Y., Raza, A., Yang, L., Mao, X., Ding, B., Yu, J., 2012. An in situ polymerization approach for the synthesis of superhydrophobic and superoleophilic nanofibrous membranes for oil-water separation. Nanoscale 4, 7847–7854. https://doi.org/10.1039/c2nr33063f

Shaw, R., Sharma, R., Tiwari, S., Tiwari, S.K., 2016. Surface engineered zeolite: An active interface for rapid adsorption and degradation of toxic contaminants in water. ACS Appl. Mater. Interfaces 8, 12520–12527. https://doi.org/10.1021/acsami.6b01754

Simonin, J.P., 2016. On the comparison of pseudo-first order and pseudo-second order rate laws in the modeling of adsorption kinetics. Chem. Eng. J. 300, 254–263. https://doi.org/10.1016/j.cej.2016.04.079

Sing, K, S.W., Evertt, D.H., Haul, R.A.W., Moscou, L., Pierotti, R.A., Rouquerol, J., Simieniewska, T., 1985. Reporting physisorption data for gas/solid systems with special reference to the determination of surface area and porosity. Pure Appl. Chem. 57, 603–619.

Site, A.D., 2000. Factors affecting sorption of organic compounds in natural sorbent/water systems and sorption coefficients for selected pollutants. J. Phys. Chem. Ref. Data 30, 2001. https://doi.org/10.1063/1.1347984

Sivagami, K., Anand, D., Divyapriya, G., Nambi, I., 2019. Treatment of petroleum oil spill sludge using the combined ultrasound and Fenton oxidation process. Ultrason. Sonochem. 51, 340–349. https://doi.org/10.1016/j.ultsonch.2018.09.007

Sultanov, F.R., Bakbolat, B., Mansurov, Z.A., Azizov, Z.M., Pei, S.S., Ebrahim, R., 2017. Spongy structures coated with carbon nanomaterials for efficient oil/water separation. Eurasian Chem. J. 19, 127–132. https://doi.org/10.18321/ectj286

Sun, H., La, P., Zhu, Z., 2014. Hydrophobic carbon nanotubes for removal of oils and organics from water. J Mater Sci 49, 6855–6861. https://doi.org/10.1007/s10853-014-8387-9

Suresh Kumar, P., Prot, T., Korving, L., Keesman, K.J., Dugulan, I., van Loosdrecht, M.C.M., Witkamp, G.J., 2017. Effect of pore size distribution on iron oxide coated granular activated carbons for phosphate adsorption – Importance of mesopores. Chem. Eng. J. 326, 231–239. https://doi.org/10.1016/j.cej.2017.05.147

Swenson, H., Stadie, N.P., 2019. Langmuir's theory of adsorption: A centennial review. Langmuir 35, 5409–5426. https://doi.org/10.1021/acs.langmuir.9b00154

Syuhada, N., Thani, M., Mohd Ghazi, R., Ismail, N., 2017. Response surface methodology optimization of oil removal using banana peel as biosorbent. Malaysian J. Anal. Sci. 21, 1101–1110. https://doi.org/10.17576/mjas-2017-2105-12

Teas, C., Kalligeros, S., Zanikos, F., Stournas, S., Lois, E., Anastopoulos, G., 2001. Investigation of the effectiveness of absorbent materials in oil spills clean up. Desalination 140, 259–264. https://doi.org/10.1016/S0011-9164(01)00375-7

Tic, W., 2015. Characteristics of adsorbents used to remove petroleum contaminants from soil and wastewater. Przem. Chem. 1, 79–84. https://doi.org/10.15199/62.2015.3.7

Tong, K., Zhang, Y., Liu, G., Ye, Z., Chu, P.K., 2013. Treatment of heavy oil wastewater by a conventional activated sludge process coupled with an immobilized biological filter. Int. Biodeterior. Biodegrad. 84, 65–71. https://doi.org/10.1016/j.ibiod.2013.06.002

Toyoda, M., Inagaki, M., 2000. Heavy oil sorption using exfoliated graphite new application of exfoliated graphite to protect heavy oil pollution. Carbon N. Y. 38, 199–210. https://doi.org/10.1016/S0008-6223(99)00174-8

Tu, W., Lin, Y., Bai, R., 2016. Enhanced performance in phenol removal from aqueous solutions by a buoyant composite photocatalyst prepared with a two-layered configuration on polypropylene substrate. J. Environ. Chem. Eng. 4, 230–239. https://doi.org/10.1016/j.jece.2015.10.034

U.S. Geological Survey, 2019. Mineral commodity summaries 2019, U.S. Geological Survey. Reston, Virginia. https://doi.org/10.1007/978-3-540-47108-0-4

Upadhyayula, V.K.K., Deng, S., Mitchell, M.C., Smith, G.B., 2009. Science of the total environment application of carbon nanotube technology for removal of contaminants in drinking water: A review. Sci. Total Environ. 408, 1–13. https://doi.org/10.1016/j.scitotenv.2009.09.027

Van Steen, E., Callanan, L., Claeys, M., 2004. Recent advances in the science and technology of zeolites and related materials, in: Proceedings of the 14 International Zeolite Conference. Elsevier, Cape Town, South Africa, pp. 1370–1374.

Vandamme, T.F., 2002. Microemulsions as ocular drug delivery systems: Recent developments and future challenges. Prog. Retin. Eye Res. 21, 15–34. https://doi.org/10.1016/S1350-9462(01)00017-9

Vidal, C.B., Raulino, G.S.C., Barros, A.L., Lima, A.C.A., Ribeiro, J.P., Pires, M.J.R., Nascimento, R.F., 2012. BTEX removal from aqueous solutions by HDTMA-modified Y zeolite. J. Environ. Manage. 112, 178–185. https://doi.org/10.1016/j.jenvman.2012.07.026

Wang, C.F., Lin, S.J., 2013. Robust superhydrophobic/superoleophilic sponge for effective continuous absorption and expulsion of oil pollutants from Water. Appl. Mater. Interfaces 5, 8861–8864. https://doi.org/10.1021/am403266v

Wang, J., Chen, S., Quan, X., Yu, H., 2018. Fluorine-doped carbon nanotubes as an efficient metal-free catalyst for destruction of organic pollutants in catalytic ozonation. Chemosphere 190, 135–143. https://doi.org/10.1016/j.chemosphere.2017.09.119

Wang, J., Liu, S., Chen, C., Zou, Y., Hu, H., Cai, Q., Yao, S., 2013. Natural cotton fibers as adsorbent for solid-phase extraction of polycyclic aromatic hydrocarbons in water samples. Analyst 139, 3593–3599. https://doi.org/10.1039/c4an00195h

Wang, J., Yin, J., Ge, L., Zheng, J., 2010. Using flotation to separate oil spill contaminated beach sands. J. Environ. Eng. 136, 147–151. https://doi.org/10.1061/(ASCE)EE.1943-7870.0000117

Wang, S., Peng, Y., 2010. Natural zeolites as effective adsorbents in water and wastewater treatment. Chem. Eng. J. 156, 11–24. https://doi.org/10.1016/j.cej.2009.10.029

Wang, Y.T., Chen, H., Wang, D.J., Bai, L.J., Xu, H., Wang, W.X., 2016. Preparation of corn stalk-based adsorbents and their specific application in metal ions adsorption. Chem. Pap. 70, 1171–1184. https://doi.org/10.1515/chempap-2016-0064

Weitkamp, J., 2000. Zeolites and catalysis. Solid State Ionics 131, 175–188.

Weitkamp, J., Puppe, L., 1999. Catalysis and Zeolites. Springer Heidelberg Dordrecht. https://doi.org/10.1007/978-3-662-03764-5

Weitkamp, J., Sakuth, M., Chen, C.-Y., Ernst, S., 2004. Dealumination of zeolite beta using $(NH_4)_2SiF_6$and $SiCl_4$. J. Chem. Soc. Chem. Commun. 6, 1908. https://doi.org/10.1039/c39890001908

WHO, 2008. Guidelines for drinking-water quality, WHO chronicle. Geneva. https://doi.org/10.1016/S1462-0758(00)00006-6

Wu, C., 2007. Adsorption of reactive dye onto carbon nanotubes: Equilibrium, kinetics and thermodynamics 144, 93–100. https://doi.org/10.1016/j.jhazmat.2006.09.083

Wu, H.C., Chang, X., Liu, L., Zhao, F., Zhao, Y., 2010. Chemistry of carbon nanotubes in biomedical applications. J. Mater. Chem. 20, 1036–1052. https://doi.org/10.1039/b911099m

Xiao, Y., Azaiez, J., Hill, J.M., 2018. Erroneous application of pseudo-second-order adsorption kinetics model: Ignored assumptions and spurious correlations. Ind. Eng. Chem. Res. 57, 2705–2709. https://doi.org/10.1021/acs.iecr.7b04724

Yasin, S.M., Zurquiah, N.A., Sahawneh, J., Madanat, M., 2015. Mineral status and future opportunity: Zeolitic tuff, Natural Resources Authority. Amman, Jordan.

Yonli, A.H., Batonneau-Gener, I., Koulidiati, J., 2012. Adsorptive removal of α-endosulfan from water by hydrophobic zeolites. An isothermal study. J. Hazard. Mater. 203–204, 357–362. https://doi.org/10.1016/j.jhazmat.2011.12.042

Yörükoğullar, E., Yilmaz, G., Dikmen, S., 2010. Thermal treatment of zeolitic tuff. J. Therm. Anal. Calorim. 100, 925–928. https://doi.org/10.1007/s10973-009-0503-8

Yousef, R.I., Tutunji, M.F., Derwish, G.A.W., Musleh, S.M., 1999. Chemical and structural properties of Jordanian zeolitic tuffs and their admixtures with urea and thiourea: Potential scavengers for phenolics in aqueous medium. J. Colloid Interface Sci. 216, 348–359. https://doi.org/10.1006/jcis.1999.6334

Yusa, H., Watanuki, T., 2005. X-ray diffraction of multiwalled carbon nanotube under high pressure: Structural durability on static compression. Carbon N. Y. 43, 519–523. https://doi.org/10.1016/j.carbon.2004.10.011

Zhang, C., Han, L., Shi, X., 2015. Modified assessment methodology for mechanical recovery capacity for oil spill response at sea. Aquat. Procedia 3, 29–34. https://doi.org/10.1016/j.aqpro.2015.02.224

Zhu, K., Shang, Y.Y., Sun, P.Z., Li, Z., Li, X.M., Wei, J.Q., Wang, K.L., 2013. Oil spill cleanup from sea water by carbon nanotube sponges. Front. Mater. Sci. 7, 170–176. https://doi.org/10.1007/s11706-013-0200-1

Zhu, R., Zhou, Q., Zhu, J., Xi, Y., He, H., 2015. Organo-clays as sorbents of hydrophobic organic contaminants: Sorptive characteristics and approaches to enhancing sorption capacity. Clays Clay Miner. 63, 199–221. https://doi.org/10.1346/CCMN.2015.0630304

Zou, J., Liu, J., Karakoti, A.S., Kumar, A., Joung, D., Li, Q., Khondaker, S.I., Seal, S., Zhai, L., 2010. Ultralight multiwalled carbon nanotube aerogel. ACS Nano 4, 7293–7302. https://doi.org/10.1021/nn102246a

Appendices

Appendix A

Title change in toluene removal efficiency

Table 21: The change in toluene removal efficiency of over µEMWCNTs in the function of contact time

Time	RE. %	c_f (mg/l)	q_t	t/q	$t^{0.5}$	$\ln(q_e-q_t)$
0	0	500	0	0	0	
10	54.23	228.85	2.71	3.68	3.16	4.56
20	79	105	3.95	5.06	4.47	4.55
30	90	50	4.5	6.66	5.47	4.54
40	94	30	4.7	8.51	6.32	4.54
50	96.22	18.9	4.81	10.39	7.07	4.54
60	**98.89**	**5.55**	**4.94**	12.13	7.74	4.54
90	98.94	5.3	4.94	18.19	9.48	4.54
120	98.95	5.25	4.94	24.25	10.95	4.54

Table 22: The change in toluene removal efficiency of over MWCNTs in the function of contact time

Time	RE. %	cf (mg/l)	qt	t/q	t0.5	ln(qe-qt)
0.00	0.00	500.00	0.00	0.00	0.00	1.49
10.00	28.00	360.00	1.40	7.14	3.16	1.11
20.00	58.00	210.00	2.90	6.90	4.47	0.43
30.00	77.00	115.00	3.85	7.79	5.48	-0.52
40.00	79.00	105.00	3.95	10.13	6.32	-0.70
50.00	80.10	99.50	4.01	12.48	7.07	-0.82
60.00	**80.90**	**95.50**	**4.05**	14.83	7.75	-0.92
90.00	80.90	95.50	4.05	22.25	9.49	-0.92
120.00	88.89	55.55	4.44	27.00	10.95	-

Appendix B

Calculations of microemulsion amount attached on each adsorbent

Table 23: Densities of microemulsion components

Material	v%	Density g/cm^3
Coconut oil	10	0.925
Isoamyl alcohol	40	0.81
n-octane	25	0.703
Water	25	0.998

The density of the microemulsion mixture is given by the following equation:

$$\rho = \frac{\rho_1 v_1 + \rho_2 v_2 + \rho_3 v_3 + \cdots}{v_1 + v_2 + v_3 + \cdots}$$

Where v_1, v_2, v_3 … represent the volumes of substances of densities ρ_1, ρ_2, ρ_3 in the mixture. The calculated density for microemulsion mixture was found as follow:

ρ of microemulsion=0.84175 g/cm^3

B.1 µEMWCNTS MICROEMULSION MASS CALCULATIONS

Density of MWCNTs=1.4 g/cm^3

Occupied volume after microemulsion= 0.0069 cm^3/g, per gram = 0.0069 cm^3. For 1 g adsorbent, the volume of attached hydrocarbon chain from microemulsion is 0.00116 m^3

$$mass = density \times volume$$

$$mass = 0.84175 \frac{\text{g}}{cm^3} \times 0.0069\ cm^3$$

Mass=0.0058 g

B.1 µETZT MICROEMULSION MASS CALCULATIONS

Occupied volume after microemulsion= 0.0100 cm^3/g, per 1 gram of adsorbent = 0.0100 cm^3

$$mass = density \times volume$$

$$mass = 0.84175 \frac{\mathrm{g}}{cm^3} \times 0.0100 cm^3$$

Mass=0.0084 g